

Rowan University

Rowan Digital Works

Theses and Dissertations

6-30-2022

ELECTRO-MECHANICAL DATA FUSION FOR HEART HEALTH MONITORING

Kemal Yakut
Rowan University

Follow this and additional works at: <https://rdw.rowan.edu/etd>



Part of the [Biomedical Engineering and Bioengineering Commons](#), and the [Mechanical Engineering Commons](#)

Recommended Citation

Yakut, Kemal, "ELECTRO-MECHANICAL DATA FUSION FOR HEART HEALTH MONITORING" (2022). *Theses and Dissertations*. 3039.

<https://rdw.rowan.edu/etd/3039>

This Thesis is brought to you for free and open access by Rowan Digital Works. It has been accepted for inclusion in Theses and Dissertations by an authorized administrator of Rowan Digital Works. For more information, please contact graduateresearch@rowan.edu.

**ELECTRO-MECHANICAL DATA FUSION FOR HEART HEALTH
MONITORING**

by

Kemal Yakut

A Thesis

Submitted to the
Department of Mechanical Engineering
College of Engineering
In partial fulfillment of the requirement
For the degree of
Master of Science in Mechanical Engineering
at
Rowan University
May 26, 2022

Thesis Chairs:

Wei Xue, Ph.D., Associate Professor, Department of Mechanical Engineering
Francis Haas, Ph.D., Assistant Professor, Department of Mechanical Engineering

Committee Members:

Mitja Trkov, Ph.D., Assistant Professor, Department of Mechanical Engineering
Behrad Koohbor, Ph.D., Assistant Professor, Department of Mechanical Engineering

© 2022 Kemal Yakut

Dedications

This thesis is dedicated to my parents, Mustafa and Mehtap Yakut. I could not have done this without their support.

Acknowledgments

I would like to thank my advisors Dr. Wei and Dr. Haas who have made me feel at home since the first day I started this project. They always supported me and showed me the right way to be successful. I will never forget them as they built a family atmosphere rather than a professor-student relationship and made me feel like the luckiest student at Rowan University. Also, I would like to thank the committee members Mitja Trkov, Ph.D., Behrad Koohbor, Ph.D. I also would like to thank Dr. Robert (Bob) Hirsh for being the brain of this project.

I also would like to thank Xinghui Zhao, Ph.D., Tyler Petty, and Joseph Boothby at Washington State University Vancouver for their collaboration with us. I also would like to thank Rowan University Camden Health Research Initiative for being sponsor of this project.

I would also like to thank undergraduate students Elizabeth Lee, Jessica Rodgers, Jacob Taylor, Brian Berry, and Alex Herrman, who contributed to this project and helped me develop the project.

Last but not least, I would love to thank Grad Squad (Nabil Jamhour, Nicholas Pagliocca, Jacob Mahon, Jordan Cook, Rhandy Paladines, Kazi Zahir Uddin, Vincent Adeniyi, Ibnaj Anamika, Chadi Ellouzi, Mahmut Gemici, and Kaan Erdogan) for their help for this project and their support.

Abstract

Kemal Yakut

ELECTRO-MECHANICAL DATA FUSION FOR HEART HEALTH MONITORING
2021-2022

Wei Xue, Ph.D. and Francis M. Haas, Ph.D.
Master of Science in Mechanical Engineering

Heart disease is a major public health problem and one of the leading causes of death worldwide. Therefore, cardiac monitoring is of great importance for the early detection and prevention of adverse conditions. Recently, there has been extensive research interest in long-term, continuous, and non-invasive cardiac monitoring using wearable technology. Here we introduce a wearable device for monitoring heart health. This prototype consists of three sensors to monitor electrocardiogram (ECG), phonocardiogram (PCG), and seismocardiogram (SCG) signals, integrated with a microcontroller module with Bluetooth wireless connectivity. We also created a custom printed circuit board (PCB) to integrate all the sensors into a compact design. Then, a flexible housing for the electronic components was 3D printed using thermoplastic polyurethane (TPU). In addition, we developed peak detection algorithms and filtering programs to analyze the recorded cardiac signals. Our preliminary results show that the device can record all three signals in real-time. Initial results for signal interpretation come from a recurrent neural network (RNN) based machine learning algorithm, Long Short-Term Memory (LSTM), which is used to monitor and identify key features in the ECG data. The next phase of our research will include cross-examination of all three sensor signals, development of machine learning algorithms for PCG and SCG signals, and continuous improvement of the wearable device.

Table of Contents

Abstract	v
List of Figures	ix
List of Tables	xiii
Chapter 1: Introduction	1
1.1 Heart Diseases and Heart Health Monitoring	1
1.2 Heart and Blood Flow	2
1.2.1 Heart as a Pump	5
1.2.2 Cardiac Cycle	6
1.2.3 Conduction System	7
1.3 Electrocardiogram (ECG)	8
1.3.1 ECG Electrodes	8
1.3.2 Waveform	9
1.3.3 Segments and Intervals	14
1.4 Phonocardiography (PCG)	16
1.4.1 Heart Sounds	17
1.4.2 Murmurs	19
1.5 Seismocardiography (SCG)	19
1.6 Signal Correlation	22
1.7 Wearable Devices in Heart Monitoring (SCG)	23
1.8 Applications	25
1.9 Motivation and Objectives	27
1.10 Thesis Layout	29

Table of Contents (Continued)

Chapter 2: System Design.....	30
2.1 Previous Work and Hardware Improvement	30
2.2 Sensor Module	36
2.3 Microcontroller Module.....	36
2.4 Artificial Intelligence (AI) Processing Module	38
2.5 Printed Circuit Board (PCB) Design.....	38
2.6 Stethoscope and Housing.....	40
Chapter 3: Data Acquisition.....	44
3.1 Device Programming	44
3.1.1 Arduino Programming for the Device	44
3.1.2 LabVIEW Programming for the Device	46
3.2 Device Placement.....	47
3.3 Real Time Monitoring.....	49
3.3.1 Real-Time Monitoring Using the Arduino IDE Platform.....	49
3.3.2 Real-Time Monitoring Using LabVIEW	50
3.4 Phone Application.....	52
3.5 Data Harvesting from SD Card to Spreadsheet	53
Chapter 4: Signal Processing	55
4.1 Fast Fourier Transform (FFT).....	56
4.2 Filter	60
4.2.1 Low-Pass Filter	61
4.2.2 High-Pass Filter	62

Table of Contents (Continued)

4.2.3 Band-Pass Filter	63
4.2.4 Real-Time Filtering Using LabVIEW	64
4.3 MATLAB Program for Signal Processing.....	67
4.3.1 Signal Filtering Using MATLAB	73
4.3.2 Peak Detection and Heart Rate Calculation using MATLAB	78
Chapter 5: Device Performance and Machine Learning	85
5.1 Device Performance.....	85
5.2 Training LSTM.....	91
5.3 System Evaluation	94
Chapter 6: Conclusion.....	96
6.1 Thesis Summary.....	96
6.2 Future Work	99
References.....	101
Appendix A: Arduino Code for ESP32	108
Appendix B: MATLAB Code for Filtering	113

List of Figures

Figure	Page
Figure 1. Blood Flow in the Heart	4
Figure 2. Alternative Scheme Form for the Heart as a Mechanical Pumping System	6
Figure 3. Electrodes are Connected to the Leads of the ECG	9
Figure 4. Positive and Negative Complex of Depolarization	10
Figure 5. Schematic Signal Waveform for Electrocardiogram (ECG) Showing Important Fiducial Points Used in ECG Analysis	11
Figure 6. (A) Detailed Illustration of the P Wave in a Typical ECG Signal, (B) Normal and Abnormal P Waves Notched, Peaked (pointed), and Inverted (negative), adapted from [7]	12
Figure 7. U Wave of Schematic ECG Signal.....	14
Figure 8. Components of the Schematic ECG Signal with Critical Peaks Marked	14
Figure 9. Components of the Schematic PCG Signal	17
Figure 10. Recommended SCG Sensor (accelerometer) Position for Measurement of Chest Wall Motion.....	21
Figure 11. Schematic SCG Signal with Some Important Events Marked	22
Figure 12. Schematic, Concurrent Waveforms for ECG, PCG, and SCG Signals with Key Features Labeled	23
Figure 13. The Previous Prototype Including (A) Assembled Three-decker(right) (B) Individual Tiers(left) (C)MEMS Microphone Testing Setup	31
Figure 14. Initial Prototype Update with Modifications Including SD Card Module, Bluetooth Module, Arduino Nano, and PCB	32
Figure 15. Last Prototype Update with Modifications Including Accelerometer, Stethoscope, ESP32 Microcontroller, Sen0213 ECG sensor, and Custom PCB	34
Figure 16. Simplified Block Diagram of the Prototype Wearable Heart Health Monitoring System.....	35

List of Figures (Continued)

Figure 17. Schematic Wiring Design on Eagle CAD for ESP32 and Sensors Connections.....	39
Figure 18. PCB Design Includes a) Wire Connection of the Board b) Top Look c) Bottom Look	40
Figure 19. Stethoscope Designs Made with Different Materials.....	41
Figure 20. Housing Designs Made with Different Materials.....	43
Figure 21. Schematic Design for Using ESP32 Microprocessor with 3 Sensors on LabVIEW	47
Figure 22. ECG Lead-Electrode Connection	48
Figure 23. ECG Signal Monitoring on Arduino Serial Plotter	50
Figure 24. Real-Time PCG Signal Monitoring on LabVIEW	51
Figure 25. Real-time Monitoring Using the RemoteXY Phone Application.....	53
Figure 26. Transferred Raw Data from the SD Card to Excel Spreadsheet	54
Figure 27. Schematic of a) Signal in the Time Domain and b) Signal in the Frequency Domain Used to Explain FFT	56
Figure 28. Fast Fourier Transform (FFT) Set up on LabVIEW	58
Figure 29. Raw ECG Signal in Time Domain and Frequency Domain.....	59
Figure 30. Raw PCG Signal in Time Domain	59
Figure 31. PCG Signal in Frequency Domain	60
Figure 32. Schematic of Noise Isolation from the Signal.....	61
Figure 33. Schematic of a Low-Pass Filter.....	62
Figure 34. Schematic of a High-Pass Filter	63
Figure 35. Schematic of a Band-Pass Filter.....	64
Figure 36. Block Diagram for the Signal Filtering Process.....	65

List of Figures (Continued)

Figure 37. Filtered ECG Signals Acquired in Real Time Using a Band-pass Filter Using Different Cutoff Frequency Ranges.....	66
Figure 38. PCG Signal is Filtered in Real-Time by Using a Band-Pass Filter Using Different Cutoff Frequency Ranges Selected Regarding Figure 31	67
Figure 39. Step 1 for Preparing Filtering Code.....	68
Figure 40. Step 2 for Preparing Filtering Code.....	69
Figure 41. Step 9 for Preparing Filtering on MATLAB	71
Figure 42. Step 10 for Preparing Filtering on MATLAB	72
Figure 43. Original ECG Signal and 0.2-36 Hz Band-Pass Filtered Form.....	74
Figure 44. Zoomed in Version of Original ECG Signal and 0.2-36 Hz Band-Pass Filtered Form.....	74
Figure 45. Zoomed in Version of the Original ECG Signal and 0.2-36 Hz Band-Pass Filtered Form	75
Figure 46. Original PCG Signal and 25-35 Hz Band-Pass Filtered Form	76
Figure 47. Original PCG Signal and 10-45 Hz Band-Pass Filtered Form.....	77
Figure 48. Original PCG Signal and 20-40 Hz Band-Pass Filtered Form.....	77
Figure 49. Original ECG Signal Obtained from Subject 2	80
Figure 50. FFT Filtered ECG Signal Obtained from Subject 2	80
Figure 51. Steps of Detecting R Peaks from the ECG Signal Obtained from Subject 2.....	81
Figure 52. Detected R Peaks are Placed on the Original ECG Signal Obtained from Subject 2.....	81
Figure 53. Original ECG Signal Obtained from Subject 1	82
Figure 54. FFT Filtered ECG Signal Obtained from Subject 1	83
Figure 55. Steps of Detecting R Peaks from the ECG Signal Obtained from Subject 1.....	84

List of Figures (Continued)

Figure 56. R Peaks are Properly Placed on the Original ECG Signal Obtained from Subject 1.....	84
Figure 57. Simultaneous ECG, PCG, and SCG Signals were Recorded by the Prototype Heart Health Monitor.....	86
Figure 58. Representative 6 Seconds of 10 min Recording of ECG Signal	87
Figure 59. Representative 6 Seconds of 10 min Recording of PCG Signal	88
Figure 60. Representative 6 Seconds of 10 min Recording of SCG Signal	88
Figure 61. Correlation Between the ECG and PCG Signals.....	89
Figure 62. Correlation Between the ECG and SCG Signals.....	90
Figure 63. Correlation Between the ECG, PCG, and SCG Signals.....	90
Figure 64. ROC Curve and Precision-Recall Curve of The LSTM Model for Classifying Normal and Abnormal Signals.....	93

List of Tables

Table	Page
Table 1. Cost of The Prototype	37
Table 2. Labels in Training Dataset, from [84]	91
Table 3. Detected Conditions on Data Collected by the System	94

Chapter 1

Introduction

1.1 Heart Diseases and Heart Health Monitoring

Heart disease is the leading cause of death worldwide. For example, someone in the U.S. dies of cardiovascular disease (CVD), on average, every 36 seconds, or about 2,400 U.S. deaths from CVD each day [1]. Associated costs run into the hundreds of billions of dollars – between 2017 and 2018, the U.S. economy spent almost \$378 billion on the diagnosis and treatment of heart disease [2]. Among heart conditions, arrhythmias, myocardial infarctions (heart attacks), and cardiomyopathies are the most common. These conditions often exhibit biophysical signals that can be detected before acute, irreversible damage is sustained by the heart or before more extensive damage is incurred. These and many other cardiac conditions can benefit from long-term heart monitoring. However, standard non-invasive electrocardiogram (ECG) monitoring systems with bedside monitors are large, heavy, and expensive. This makes home monitoring difficult, resulting in cardiac monitoring mostly limited to costly clinical settings. Accordingly, there has been extensive interest in developing wearable ECG-based health monitoring systems to detect cardiac conditions [3].

While electrocardiography is widely used to detect heart problems, it is unable to directly observe the mechanical performance of the heart and its proximate vasculature. Instead, the mechanical behaviors of the heart can be non-invasively monitored by acoustic (phonocardiogram, PCG) or vibratory (seismocardiogram, SCG) signals. Therefore, PCG has been used by physicians for decades to detect heart murmurs [4], while SCG can

complement ECG to provide a more accurate diagnostic for long-term post-ischemic survival than ECG alone [5].

Herein, in this thesis, we describe a rechargeable, compact, and wearable heart health monitor that acquires real-time ECG, PCG, and SCG signals from the human body. The recorded information can be transferred wirelessly to the user's phone or computer, where a machine learning model can be used to monitor biophysical data and identify features such as abnormal heart rhythms. In other words, this thesis describes the design, development, and testing of a mobile health (M-health) platform for heart health surveillance. The relatively low cost of this device may permit home monitoring in many cases.

1.2 Heart and Blood Flow

The heart is one of the most critical organs in the human body. The size of the heart is approximately the one's closed fist [6]. The heart has four chambers: right and left ventricles (lower chambers), and right and left atriums (upper chambers). Chambers are divided by a thin wall called the septum. There are four valves in total, with two of them located between the atria and ventricles and the other two valves between the ventricles and vessels. These valves help the blood to flow in one direction and allow unidirectional circulation inside the body. Figure 1 shows the main structure of the heart as well as the blood flow through the heart [6].

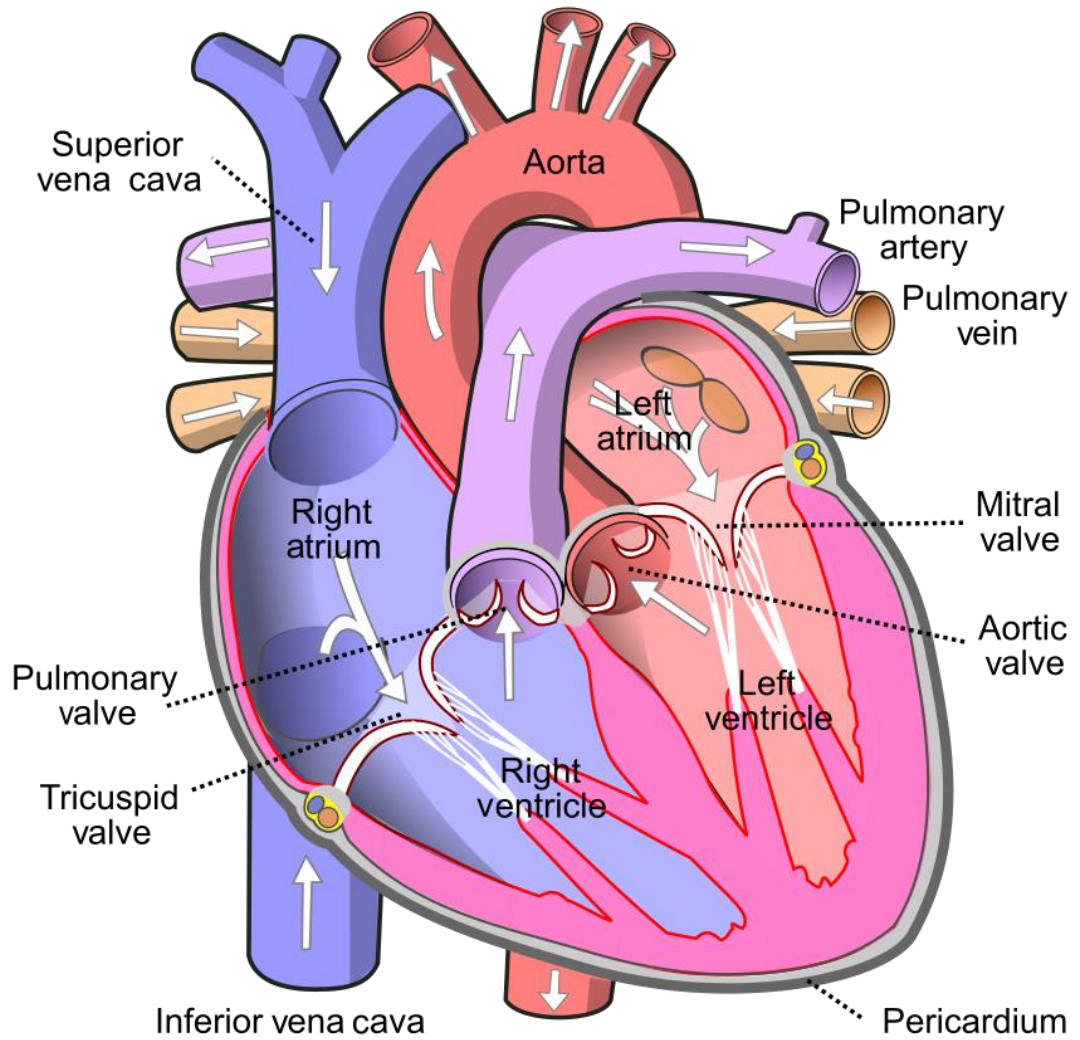
Deoxygenated blood from the two large veins flows to the right atrium. The tricuspid valve (located between the right atrium and right ventricle) allows the blood to move between the right atrium to the right ventricle. Once the right ventricle receives the blood,

it contracts to increase the blood pressure, and the tricuspid valve closes because of the higher internal pressure. When the tricuspid valve is closed, the blood can only flow through the pulmonary valve [7]. As a result, the blood leaves the right ventricle and moves to the pulmonary trunk and then to the lungs. The blood absorbs the oxygen in the lungs and releases its carbon dioxide. The oxygenated blood then flows into the left atrium through the pulmonary veins.

Next, the left atrium contracts and the blood moves through the mitral valve and then into the left ventricle. Then the left ventricle contracts and the mitral valve closes. Afterward, the blood moves through the aortic valve and then into the aorta. The aorta is the largest artery in the body, and it extends down to the entire body.

Figure 1

Blood Flow in the Heart [8]



Note. The deoxygenated blood flows into the right atrium. Then the blood is pumped into the right ventricle where it is then delivered to the lungs. After reoxygenation as blood returns to the left atrium. Post-reoxygenation flows into the left ventricle and the left ventricle pumps blood to the rest of the body.

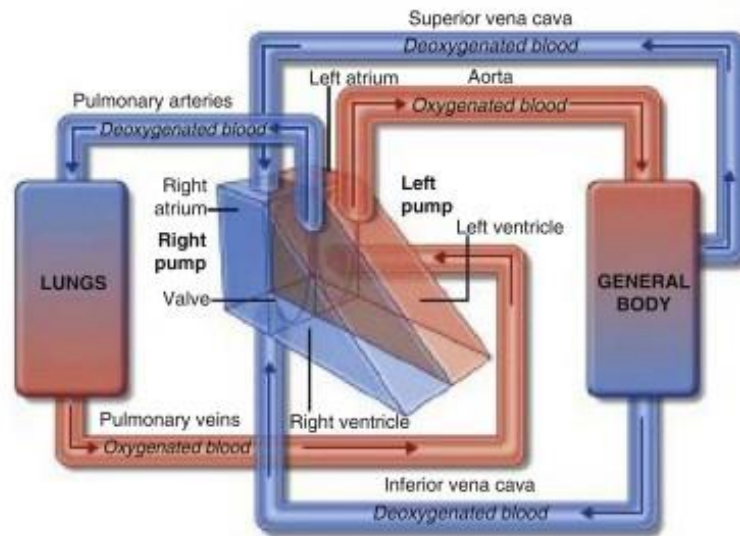
1.2.1 Heart as a Pump

As mentioned above, the right and left sides of the heart are separated by a wall called a septum. There are two septa in the heart, with the interatrial septum separating the right and left atria, and the interventricular septum separating the right and left ventricles [7]. This wall separates the heart into two functional pumps. The right atrium and ventricle are one half, and the left atrium and ventricle are the other half.

As is demonstrated in Figure 2, the right side of the heart pumps unoxygenated blood from the body through the lungs to release carbon dioxide and absorb oxygen. Then oxygenated blood moves through the left side of the heart, in the process called pulmonary circulation. Afterward, the left side of the heart pumps the oxygenated blood out to the entire body. In systemic circulation, the blood carries nutrients and oxygen through arteries and arterioles before delivering it to cells. Also, carbon dioxide and waste are exchanged. The deoxygenated blood then flows over the superior vena and inferior vena before arriving at the right side of the heart. Usually, blood pressure measured on the right atrium and right ventricle (right side of the heart) is lower than the pressure on the left side [9].

Figure 2

Alternative Scheme Form for the Heart as a Mechanical Pumping System [9]



1.2.2 Cardiac Cycle

The cardiac cycle is a pumping process that includes all the events associated with the blood flow through the heart. It has two phases, systole and diastole, for each chamber. Systole is the period in which the chamber contracts and the blood is ejected. Diastole is the period of muscle relaxation during which the chambers are allowed to expand and fill with more blood. The cardiac cycle depends on the ability of the cardiac muscle to contract and on the condition of the heart's conduction system. The efficiency of the heart may be affected by abnormalities of the cardiac muscle, the valve, or the conduction system. The pressure of each chamber of the heart rises in systole and falls in diastole. The valves of the heart help the blood to flow in the proper direction. As previously mentioned, the blood flows from one chamber to another, driven by the blood pressure, from higher to lower pressure [6, 7].

1.2.3 Conduction System

Special electrical cells in the heart are arranged in a system of pathways called the conduction system. The cardiac conduction system is a network of nodes and specialized conducting cells that control and trigger heart muscle activity. In a normal heart, the cells of the conduction system are interconnected. The conduction system consists of the sinoatrial node, atrioventricular node, atrioventricular bundle, and Purkinje fibers.

1.2.3.1 Sinoatrial Node. The sinoatrial node (SA) is a conducting tissue that is located in a place where the superior vena cava and the right atrium meet. The right atrium contraction begins and ends earlier than the left atrium because the SA is located in the right atrium [10]. The length of the SA node in an adult is usually 10-20 mm and the thickness is around 2-3 mm [11]. Two main types of cells exist in the SA node: the first one is round and small with some myofibrils, and the second one is elongated and thin. The round cells are known as pacemaker cells and the elongated cells are known as responsible for conducting the electrical impulse. Although the SA node is the heart's smallest electrical tissue, it is normally the primary pacemaker. The electrical impulse that begins in the SA node causes the heart to beat normally [12].

1.2.3.2 Atrioventricular Node. The atrioventricular (AV) node is a small structure located in the interatrial septum, close to the attachment of the septal cusp of the tricuspid valve, and near the coronary sinus. This specific place is called Koch Triangle[13]. The AV node is quite small (~1 mm × 3 mm × 5 mm). The depolarization and repolarization of cell membranes result from the movement of ions across cell membranes. The AV node is a vital part of the cardiac conduction system responsible for transmitting impulses from the sinoatrial (SA) node to the ventricles of the heart. An important feature of the AV node is

its ability to slightly delay electrical signals, thereby coordinating the contraction of the atria first and the ventricles second. Thus, the AV node regulates myocyte mechanical activity.[9].

1.3 Electrocardiogram (ECG)

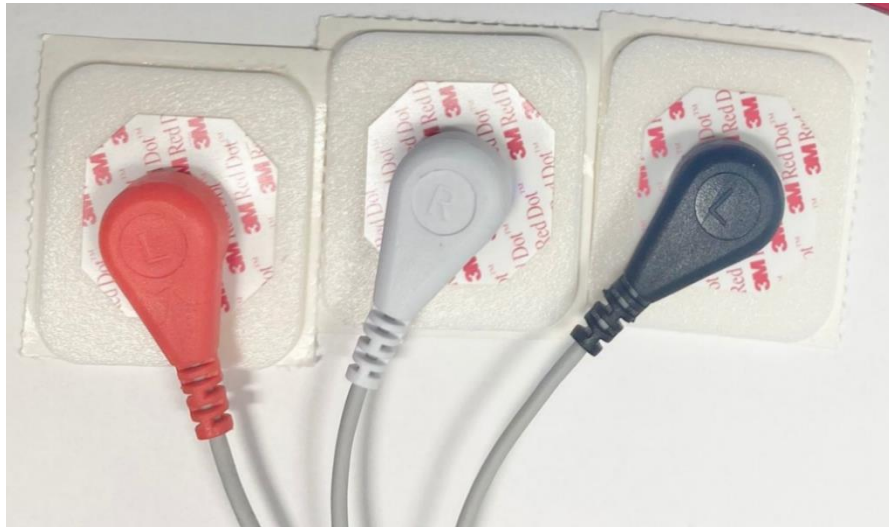
Electrocardiogram (ECG) is a graphical display of the heart's electrical activity. It was introduced by William Einthoven in the 1900s [7]. ECG is a cheap and usually repeatable test. It is commonly used for monitoring a patient's heart rate and cardiac rhythm, evaluating pacemaker functions, monitoring the response of medications, assessing the effects of a disease on heart functions, and more.

1.3.1 ECG Electrodes

ECG electrodes are adhesive pads with a conductive substance in the center. These electrodes can be applied to a specific position on the patient's chest wall to view the electrical activity of the heart from different angles. As depicted in Figure 3, the electrodes are connected to the leads of the ECG module. They are used to monitor skin surface voltage changes. Once the electrodes are attached to the skin, the ECG monitoring machine functions as a voltmeter where it detects and records voltage changes during the depolarization and repolarization events. Before applying these electrodes, dead cells and oil must be removed from the patient's skin. The ECG electrodes are usually gel-based with a sticky surface. Before they are applied to the skin, patients are usually recommended to shave or cut their chest hair to minimize negative effects on the skin.

Figure 3

Electrodes are Connected to the Leads of the ECG

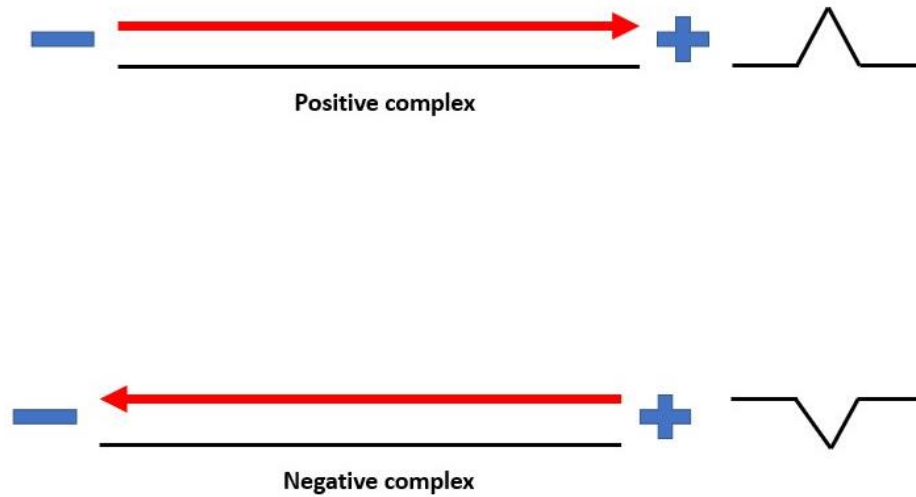


1.3.2 Waveform

When electrical activity is not detected from the heart, a straight line is monitored by the ECG monitor. This line is called the baseline. Common waves are rounded curves or straight lines that leave or return to baseline. As Figure 4 demonstrates, if the wave of depolarization moves toward the positive electrode, the waveform will be upward and is called positive deflection. If the wave of depolarization moves away from the positive electrode, the waveform will be downward, which is called negative deflection. A standard ECG is made up of a group of waves that reflect specific electrical events in the heart. These waves are named alphabetically to be easily recognizable, and each wave is designated by one letter P, Q, R, S, or T. Figure 5 illustrates a typical waveform for one ECG signal cycle.

Figure 4

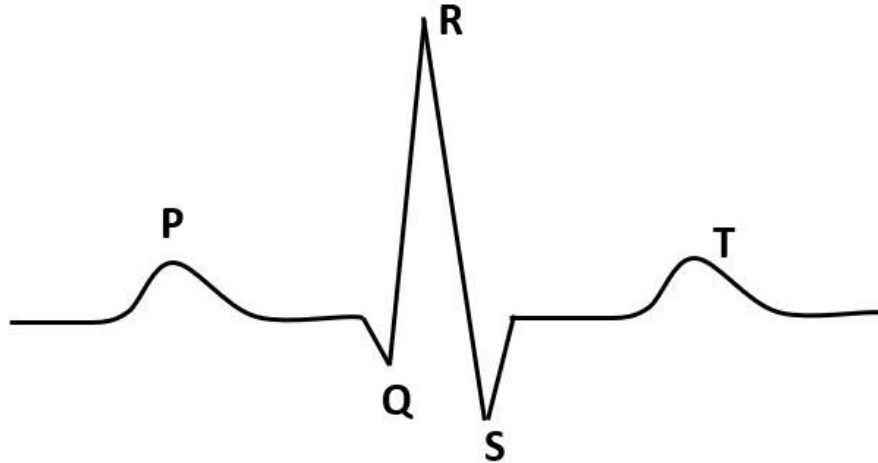
Positive and Negative Complex of Depolarization



Note. If the depolarization wave propagates towards the positive pole of that lead, a positive complex is seen (Above). If the depolarization wave propagates towards the negative pole of the lead (away from the positive pole), a negative complex is seen (Bottom).

Figure 5

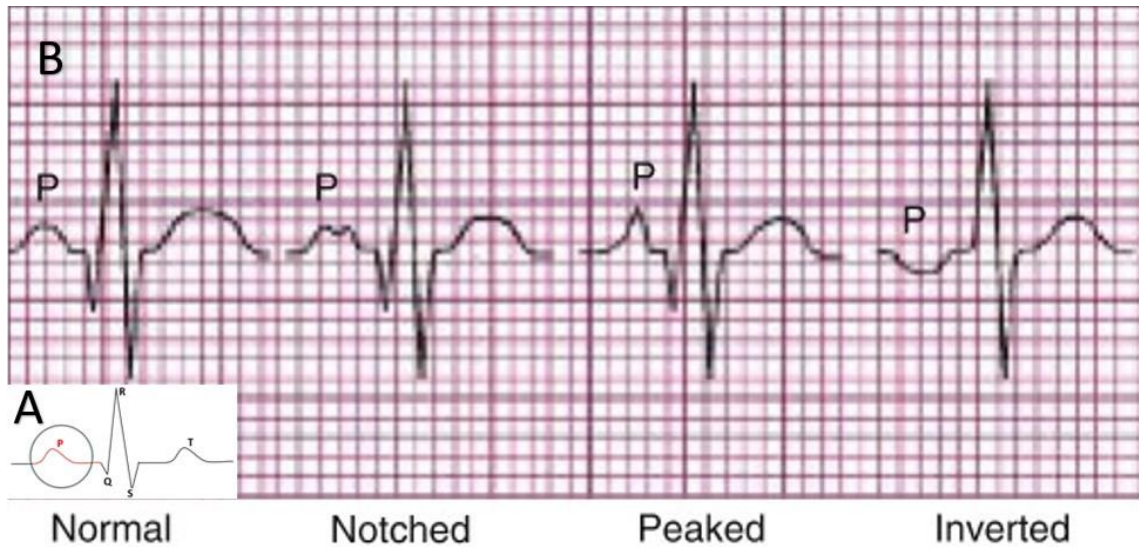
Schematic Signal Waveform for Electrocardiogram (ECG) Showing Important Fiducial Points Used in ECG Analysis



1.3.2.1 P Wave. The P wave is the first waveform in the cardiac cycle. This wave is smooth and rounded. The amplitude of the P wave is usually no more than 2.5 mV, and its duration is no more than 0.12 seconds. The P wave represents the electrical activation of the right and left atrial depolarization [14]. The first half of the P wave corresponds to the depolarization of the right atrium, and the second half corresponds to the left atrium depolarization [15]. The atrium contracts right after the P wave begins. Next, the atrium begins to repolarize at the same time as the ventricle depolarizes. However, it is not possible to see the waveform for this atrium repolarization event on the ECG because it is small and buried in the QRS complex. As shown in Figure 6, abnormal P waves such as notched, peaked, or inverted can be used to identify heart failure, valvular disease, or chronic heart problems [16].

Figure 6

(A) Detailed Illustration of the P Wave in a Typical ECG Signal, (B) Normal and Abnormal P Waves: Notched, Peaked (pointed), and Inverted (negative), adapted from [7]



1.3.2.2 QRS Complex. The QRS complex occurs right after the P wave. The QRS complex consists of the Q, R, and S waves and it is the electrical impulse through the ventricles. In other words, it represents the activation of ventricular depolarization. Right after the electrical impulse arrives in the ventricles, the ventricles contract and pump blood around the body. The QRS complex is higher in amplitude than the P wave. It is because the ventricles are larger than the atria. The depolarization of ventricles uses more muscle mass than the depolarization of the atria.

The Q wave is the first deflection, occurring right after the P wave, and it is down from the baseline. It is always a negative waveform, which represents the depolarization of the interventricular septum. The large triangular R wave occurs right after the Q wave. The R wave is always positive, in other words, it is always upwards. Right after the R wave, the S wave appears. The S wave is always downwards (or negative). The R and S waves represent

the depolarization of the right and left ventricles, respectively [16, 17].

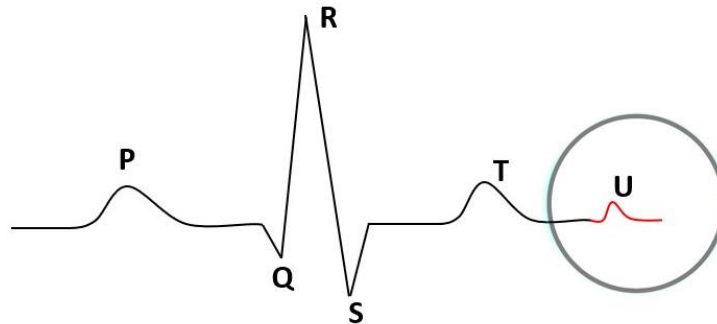
The amplitude of the QRS complex can be affected by age, gender, race, ECG lead placements, electrodes, and skin surface [18]. Abnormalities of the QRS complexes are very important as they often indicate underlying diseases. For example, the duration of the QRS complex is usually 0.075-0.11 seconds in a healthy adult under low stress condition. If the duration is greater than 0.11 seconds, the QRS complex can be identified as abnormal [19].

1.3.2.3 T Wave. The T wave always occurs directly after the QRS complex. It is usually small, rounded, and slightly asymmetric, representing the repolarization of the right and left ventricles. Additionally, the size of the wave can be changed due to the connection and quality of the ECG leads [10]. If the leads contain dust or liquid, the T wave appearance can change due to monitoring error. However, when the monitoring system is accurate, the abnormalities in T waves can help physicians to identify some diseases. For example, the T wave always moves in the same direction as the QRS complex. If the QRS complex points upward from the baseline and the T wave points downward from the baseline, a heart abnormality is present. A lower T wave amplitude is also a potential indicator of hypokalemia or hypomagnesemia [20].

1.3.2.4 U Wave. The U wave is usually small and follows the T wave of ventricular repolarization (see Figure 7). It usually appears when monitoring a slower heartbeat, representing the late repolarization of the Purkinje fibers. Abnormally large U waves or inverted U waves almost always indicate diseases such as hypertension, coronary disease, valve disease, cardiomyopathy, or hypokalemia [21]. Although the U wave can be an important metric, it is not found in many ECG recordings because of its small amplitude. For this reason, the U wave will not be studied in this thesis.

Figure 7

U Wave of Schematic ECG Signal

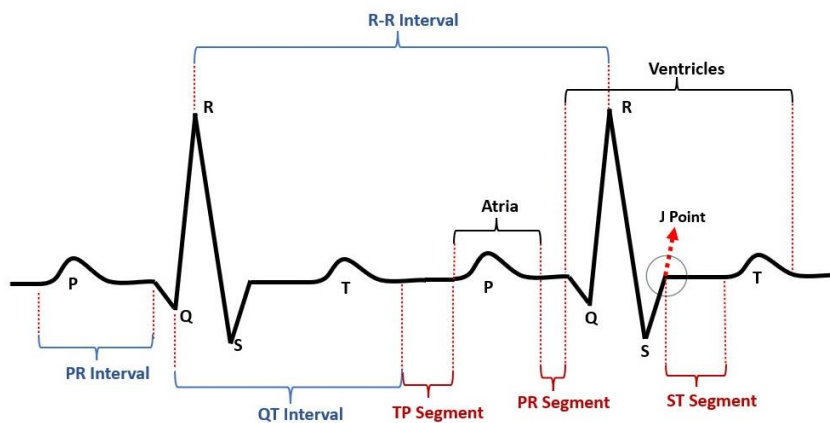


1.3.3 Segments and Intervals

A segment is a baseline that connects two waves. Segments are always measured between waves but never include the waves. Intervals are periods of time including waves, segments, and complex. Figure 8 describes the components of common segments and intervals of the ECG signal.

Figure 8

Components of the Schematic ECG Signal with Critical Peaks Marked



1.3.3.1 PR Segment. PR segment is the horizontal line between the end of the P wave and the beginning of the QRS complex. It is also called as PQ segment. It is isoelectric and represents the electrical impulse from the AV node. If there is a delay during the PR segment, it is more likely the result of slow conduction in the AV node [19]. The PR segment ends right before the QRS complex starts [15].

1.3.3.2 TP Segment. TP segment connects the end of the T wave and the beginning of the P wave. This segment presents only if the U wave is not present. As previously mentioned, the impact of the U wave is negligible and is omitted from considerations in this thesis. At a normal heart rate, the TP segment is usually isoelectric. When the heart rate is rapid, the TP segment is unrecognizable.

1.3.3.3 ST Segment. ST segment is between the T and the QRS complex. It represents the early repolarization of the ventricles. ST segment should be isoelectric, but some displacements may happen depending on age, race, gender, or lead connection. The point between the ST segment and the QRS complex is called the J point. Any displacement of the ST segment or the J point from the baseline can help doctors identify some heart diseases. For example, myocardial ischemia, ventricular aneurysm, and pericarditis can be the reason for the deviation or elevation of the ST segment from the baseline [20].

1.3.3.4 RR Interval. RR interval starts at the peak of the one R wave and ends at the peak of the next R peak. It represents the time between the two QRS complexes. This measurement is used to determine heart rate and the regularity of the cardiac rhythm [22, 23].

1.3.3.5 PR Interval. PR interval begins at the beginning of the P wave and ends at the beginning of the QRS complex. It is also known as the PQ interval. This interval represents the time it takes for the cardiac impulse to reach the ventricles. The PR interval usually takes 0.12-0.20 seconds in healthy adults. The heart rhythm and the interval time are inversely proportional. If the heart rhythm increases, the PR interval time will decrease [7].

1.3.3.6 QT Interval. QT interval represents the duration from depolarization to repolarization of the ventricles. It starts at the beginning of the QRS complex and ends at the end of the T wave. The duration of the QT interval can be different with age, race, gender, and heart rate. An inverse relationship between the QT interval and heart rhythm exists, where the QT interval shortens as the heart rhythm accelerates. There are multiple formulas to calculate the correct QT interval. Bazett's formula [24] is one of the most common formulas, where the corrected QT interval is found by dividing the QT interval by the square root of the RR interval. All units must be based on second intervals during this calculation. Some diseases can also change the duration of the QT interval. For example, usually if the corrected QT interval is more than 450 milliseconds, it might be attributed to ventricular arrhythmias, where the lower chambers of the heart flutter rather than consistently pumping [25]. Medications, myocardial ischemia, neurologic events, or hypokalemia can increase the QT interval [19].

1.4 Phonocardiography (PCG)

Phonocardiography is a technique that is used for heart sound recording. Phonocardiogram is a recording of a heart sound's intensity over time [26]. It evolved from auscultation and provided a record of the vibration of the chest wall originating from the

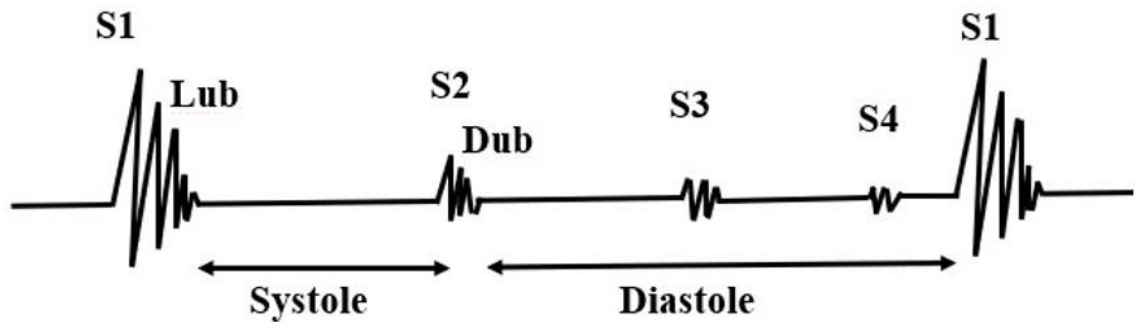
heart.

1.4.1 Heart Sounds

Acceleration and deceleration of the blood in the heart chambers results in sounds and murmurs. The closures of the valves are believed to be major contributors to heart sounds [27]. These sounds radiate to the surface, and they can be detected by a stethoscope. Two major heart sounds happen during the one complete cardiac cycle. It is also called as Lub-Dub [28, 29] and it demonstrates the two components in a heart signal. Figure 9 demonstrates the typical components of the PCG signal.

Figure 9

Components of the Schematic PCG Signal



The first sound is Lub, which is also known as S1 in the medical community and can be divided into four components. The first component of the S1 occurs when the blood accelerates in the ventricle. The frequency of the first component is very low because ventricles are relaxed, and the acceleration of the blood is low. The movement of the blood closes the atrioventricular valves before the ventricular pressure rises [30]. The second

component of the S1 begins with abrupt tension of the closed AV valves, decelerating the moving blood. The frequency of these vibrations is greater than the first component. The third component of the S1 occurs during ventricular contraction. The pressure rises in the ventricle and the blood moves toward the semilunar valves. The frequency of this vibration is similar to the second component. The last or the fourth component represents the vibration caused by the turbulence in the blood flowing through the aorta and pulmonary artery [30]. The S1 sounds last for a period of 100-200 ms with a frequency range of 10-200 Hz [31].

The second heart sound is Dub, which is also known as S2 in the medical community. It is associated with the vibrations of the closed aortic and pulmonary valves. Although the primary vibration occurs in the arteries, it is also transmitted to the ventricles and atria by the movement of the blood [30]. Its occurrence coincides with the end of the T wave of the ECG.

The normal heart sounds S1 and S2 define systole and diastole periods, respectively, and form the basis for analyzing all cardiac auscultations. The S1 sound occurs due to the closing of the atrioventricular valves and the S2 sound occurs due to the closing of the semilunar valves [32].

There are two other sounds S3 and S4 which are both caused by the sound of blood entering the chambers of the heart. In some cases, an S3 sound corresponds to the rapid filling of the ventricle. It usually occurs right after S2. The S4 sound is associated with late diastolic filling, and it usually occurs right after S3 or right before the next S1. If S3 is audible, it is often associated with an innocent murmur in young people or children. The S3 sound should not be heard from patients older than age 35; if it occurs, however, it is considered an abnormal heart sound. In addition, S4 is always considered an abnormal heart

sound [31].

1.4.2 Murmurs

The intervals between S1 and S2, and then S2 and S1 of the next cardiac cycle, are usually silent. Certain cardiovascular defects and diseases cause murmurs that occur in these intervals. As blood flows through the cardiac vessels, it may change its direction and speed, which can cause murmurs. Murmurs have high-frequency noises when the blood velocity becomes high in the presence of an irregularity through the blood flow. When a specific murmur indicates heart disease, it is called a pathologic murmur [33].

1.5 Seismocardiography (SCG)

Seismocardiography is a non-invasive method of measuring the mechanical vibration of the chest caused by the heartbeat [34]. The chest surface vibrations are usually measured by an accelerometer or a piezoelectric sensor. Seismocardiography was initially introduced by Eliot et al. in 1957 [35] and the signal was first observed and described by Bozhenko in 1961 [36]. He used this method in his study of space flights to monitor the health conditions of cosmonauts. Although it was an important method to monitor cardiovascular events, its influence was negligible outside of Russia until the 1990s. The first modern use of SCG in a clinical setting was reported by Zanetti in 1991 [37]. Later, the progress in microelectromechanical systems (MEMS) technology produced lighter, smaller, lower-cost, more effective, and more sensitive accelerometers. This made SCG one of the feasible methods for cardiac monitoring [38]. Several wearable systems for seismocardiogram assessment in daily life conditions have been reported and implemented in clinical applications. Specifically, in 1992, SCG was used with ECG in the diagnosis of artery

disease [39]. Also more recently, Inan et. al. developed a seismocardiogram with artificial intelligence (AI) algorithms that could be used to assess the patient's clinical status [40].

Figure 10 illustrates the position of the accelerometer and its 3-axis for chest vibration sensing. SCG is recorded by using a 1-axis or 3-axis accelerometer on the sternum. Usually, one sensor is enough to measure the SCG signals. If the sensor is placed closer to the heart, it gives a better representation of the vibrations of the heartbeat signals. J. Zanetti used a 1D accelerometer to introduce SCG, which was utilized to collect only the Z-axis acceleration [37]. 3-axis accelerometers can also be used for SCG sensing as they can collect the X-axis, Y-axis, and Z-axis accelerations of the heart. The maximum force generated by the heart is typically in the Z direction in all conditions such as laying down, or standing due to the accelerometer position, because of that, Z-axis is the main acceleration direction and the focus of most of the research studies on SCG monitoring [41]. Though gravity affects the magnitude of acceleration, it can be easily separated from the relatively high frequency cardiac motions captured by the SCG. Important cardiac events can be detected as peaks observed in the SCG signal. Figure 11 shows the main peaks in an SCG signal that is divided into two groups: (1) during the systolic cycle mitral valve closing (MC), isovolumic moment (IM), aortic valve opening (AO), and rapid ejection (RE) and (2) during the diastolic cycle aortic valve closing (AC), mitral valve opening (MO), and rapid filling (RF) [37].

Figure 10

Recommended SCG Sensor (accelerometer) Position for Measurement of Chest Wall Motion

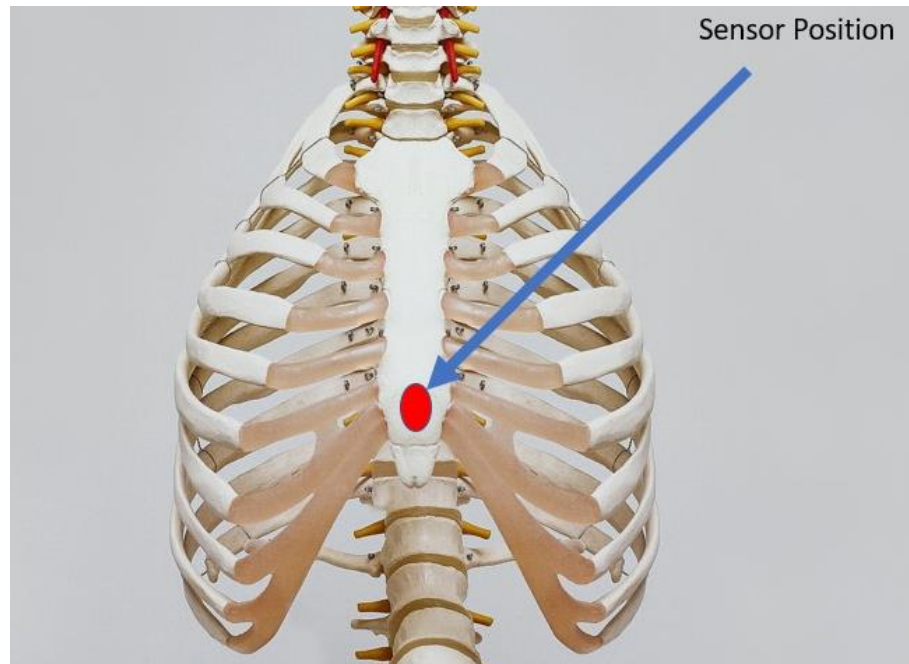
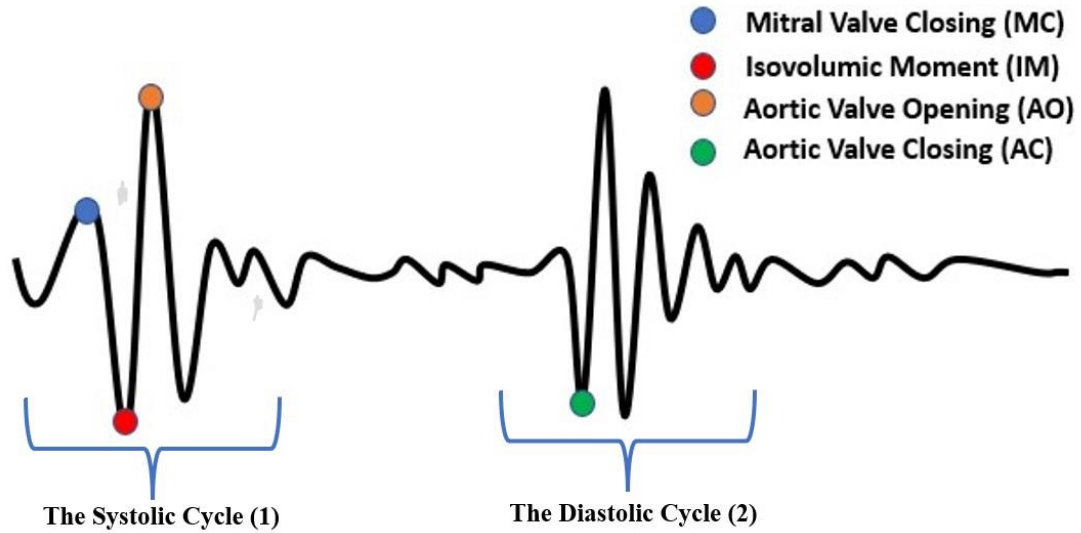


Figure 11

Schematic SCG Signal with Some Important Events Marked



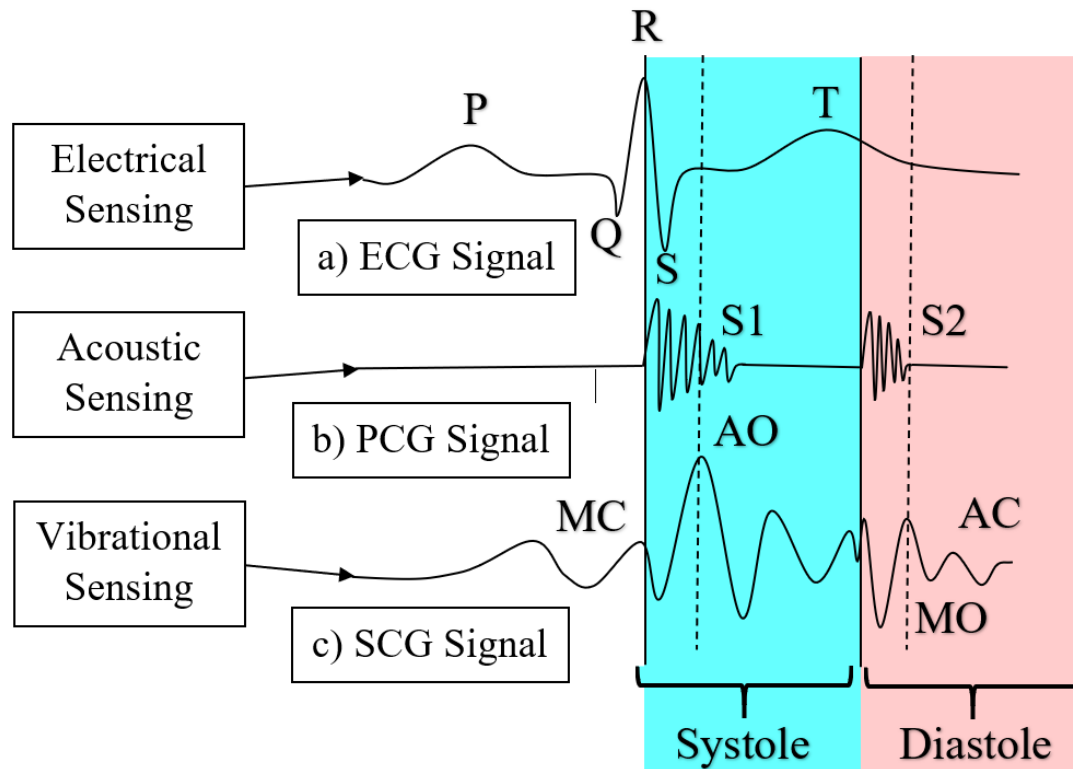
1.6 Signal Correlation

ECG is produced by the electrical activities of the heart, while PCG and SCG are produced by the mechanical activities of the heart. These three signals are produced in a full heartbeat, each with a different waveform containing similar information about important cardiac events. Figure 12 represents the cycle and correlation of ECG, PCG, and SCG signals with the main events marked. The S1 wave of the PCG signal occurs simultaneously with the MC wave of the SCG signal and directly after the R peak of the ECG signal. The MC wave of the SCG signal and the S1 wave (first sound of the heart) of the PCG signal represent the closure of the mitral valve [30, 37]. Also, the QRS peak of the ECG represents ventricular depolarization. Since the timing of these important cardiac events is closely grouped, the relationship between the signals is also a significant parameter. Furthermore,

the beginning of the S2 wave occurs with the AC peak of the SCG signal and directly after the T peak of the ECG signal. The S2 wave (second sound of the heart) of the PCG signal and the AC wave of the SCG signal represent the aortic valve closing. Furthermore, the T wave represents the repolarization of the right and left ventricles. These important cardiac events help to understand the correlation between ECG, SCG, and PCG signals. In chapter 5, we will discuss and show the correlation between these three signals from the collected data from different volunteers.

Figure 12

Schematic, Concurrent Waveforms for ECG, PCG, and SCG Signals with Key Features Labeled



1.7 Wearable Devices in Health Monitoring

The development of MEMS technology in the past two decades has affected the health sector. With the new MEMS technology and other advancements in materials and devices, the overall sizes of the devices used in healthcare applications have been significantly reduced [42]. These advances not only make devices more accessible and reliable, but they are also more affordable, enabling long-term monitoring of patients' daily lives [43]. Many companies and researchers are working to make these devices more wearable for use in healthcare applications [44-46]. These wearable devices have been used in many applications for psychological diseases such as Parkinson's disease and Alzheimer's disease, as well as physical diseases such as cardiovascular diseases, hypertension, and muscle disorders [47]. Wearables come in a variety of formats, including skin-based, textile-based, tattoo-based, clothing-based, and jewelry-based. In a broad sense, the new trend in healthcare monitoring requires the device to have a minimum size and weight, functional and power autonomy, and be easy to use and comfortable to wear [48].

Wearable devices have the potential to be an integral part of today's healthcare systems, as they can offer alternatives and solutions to a variety of medical and social needs. Not only can it help improve the quality of life and healthcare providers of people with chronic illness and disability, but it can also help financially by reducing healthcare costs in hospital admissions through prevention or the provision of appropriate measures [49]. In the United States alone, 6 of 10 adults have diabetes, asthma, and chronic conditions such as heart disease and Alzheimer's disease. 90% of the \$3.8 trillion in annual healthcare spending in the United States goes to people living with chronic and psychiatric conditions. It is clear that chronic diseases place significant medical and economic burdens on the population in

the United States. Preventing chronic diseases or managing symptoms when prevention is not possible can reduce these costs [50, 51].

Typical devices are usually built around a central processor combined with the use of microelectronics and mechanical functions. These devices enable physiological monitoring, data storage, data processing, and other functions by using recorded health data from sensors. Most wearable devices have three key components: a data input mechanism, a processing unit, and a data output mechanism. The input mechanism deals with the collection of data from the patient using sensors, data entered directly by the patient, or data transfers. The processing unit is responsible for generating appropriate feedback by processing the incoming information in real-time. These feedbacks are presented to the user as monitoring, informing, alerting, and decision support functions [48]. The output mechanism usually provides visual, audio, or telemetric services through computers or smartphones.

Wearable devices have been on the market for a long time. One of the most used and known noninvasive devices is the Holter monitor [52, 53]. Holter monitor is a wearable electrocardiogram device and has been used in the detection of heart diseases for many years. ECG signals up to 24 hours can be recorded on magnetic tape. The system is sensitive enough to detect a variety of cardiac arrhythmias, as well as conduction pattern changes, ST segment, and T wave anomalies [49]. Holter monitoring plays an important role in the assessment of various symptoms that may be associated with abnormal heartbeats, such as dizziness, fainting, chest pain, and palpitations. In addition, Holter monitoring provides useful information for pacemaker function, diagnosis of transient myocardial ischemia and evaluation of antiarrhythmic drug treatment [48, 49].

1.8 Applications

For more accurate diagnosis of heart diseases, numerous companies and researchers are doing extensive research in order to reduce deaths from heart diseases, increase the chance of early diagnosis, and minimize the money spent on treatment. Researchers are trying to diagnose heart diseases using methods such as electrocardiogram, seismocardiogram, phonocardiogram, photoplethysmography (PPG), and blood pressure measurement. A number of researchers have produced wearable devices using a single method, while others have produced multisensory wearable devices that can produce more effective results by combining these methods.

In 2020, Ozkan et al. developed a wearable Tele-ECG and heart rate monitoring system [54]. Their work features a reconstructed flexible single with textile electrodes (TEs), textile threads, snap closures, Velcro, sponges, and an ECG circuit. They developed Bluetooth low energy (BLE) communication, smartphone application, server, and webpage for remote monitoring of heart signals and integrated these functions with the device. Although the device they have produced is large, it is very successful for ECG monitoring and can detect heart rhythm successfully.

In 2021 Lo Presti et al. introduced a multipoint heart rate monitoring system based on fiber-optic technology [55]. In the system they used, they acquired the ECG and SCG signals with awareness and investigated the relationships between the signals. They place the fiber optic system they have developed for SCG on the t-shirt. Later, the t-shirt is worn by the user and they collect data while the user is in the laying down position. They simultaneously record ECG signals from the same user and work on the correlation between SCG and ECG. In addition to these, they also detect the heart rhythm. This fiber optic system

they have made gives successful results to measure heart rhythm using ECG and SCG methods.

In 2020 Rienzo et al. presented a multi-sensor wireless platform for cardiovascular monitoring in telemedicine [56]. They have designed a device that can record three different signals together, about 2-3 quarters in size. The device they use can monitor ECG, PPG, and SCG signals simultaneously. They also provide data security thanks to the SD card in the device. The device consists of two ECG leads and contains a PPG sensor. They use a USB as a hub and start their devices on that hub. Then, after the communication between the computer and the device is set, they perform real-time monitoring over the computer. Although the device is suitable for data recording by being worn on certain parts of the body, when used together for three signals, it is worn on the chest area.

In 2020 Cotur et al. reported a different method to collect the PCG signal. Using the microphone in combination with a flexible and mechanically strong low-cost soft composite made of silicone polymers and water, they monitored sounds coming from the hearts of humans or animals [57]. First, a mold is formed from silicone, then water is filled into this mold. Later, this mold is covered with another silicone reinforcement to prevent water leakage. Then, a microphone is placed on the outside of this water-filled silicon system. Finally, it is placed on the user's chest with the help of a belt. With this system, they can successfully receive the PCG signal.

1.9 Motivation and Objectives

Deaths from heart disease are the leading cause of death not only in the United States but worldwide. With the increase in the world population, the number of deaths from heart

diseases is also increasing significantly [1]. Countries spend billions of dollars on the diagnosis and treatment of heart diseases as well as lives lost [2]. Early diagnosis of cardiovascular diseases plays a key role in saving the patient's life. That's why companies are developing devices, drugs, and technologies that can prevent death from heart disease. Many companies have made wearable electrocardiogram devices that will provide long-term monitoring. This technological development has seriously affected the health sector and has saved the lives of many patients. Although ECG is the most common and important method for diagnosing cardiovascular disease, it is still insufficient to detect CVD with high accuracy [3].

With each beat cycle, the heart generates acoustic, vibration, and electrical signals, as scientists have shown in previous studies [7, 26, 36, 37, 58]. Previously, companies and researchers have created wearable devices that include ECG, combined ECG / PCG and combined ECG / SCG [58-61]. By looking at these simultaneously recorded signals, we can obtain important findings in diagnosing heart problems. We can create datasets using the data collected from healthy and sick people, and we can provide an early diagnosis by developing a machine-learning algorithm to learn the patterns of sick patients. In this thesis, we describe a rechargeable, compact, and wearable heart health monitor that measures ECG, PCG, and SCG signals from the human body in real-time. The recorded data can be wirelessly sent to the user's phone or computer, where a machine learning model can be used to monitor biophysical data and identify abnormalities such as abnormal cardiac rhythms. In other words, this study describes the mobile health (M-health) platform for monitoring heart health. The relatively inexpensive cost of this device may permit home monitoring in many cases.

1.10 Thesis Layout

In the next chapter, we give information about the previous design, hardware and software improvements, PCB design, as well as the stethoscope, and housing designs. Chapter 3 mostly covers data acquisition, device programming, real-time monitoring on different platforms, device placement on the chest, and phone application. Chapter 4 contains the signal processing process of the raw data, different signal filtering processes using different platforms, and peak detection for ECG signals. Device performance and machine learning are detailed in Chapter 5, as well as the correlation between ECG, PCG, and SCG signals from healthy individuals. The paper is concluded in Chapter 6, which contains a summary of all work completed to this point, as well as the future works and goals of this research as it continues into the future.

Chapter 2

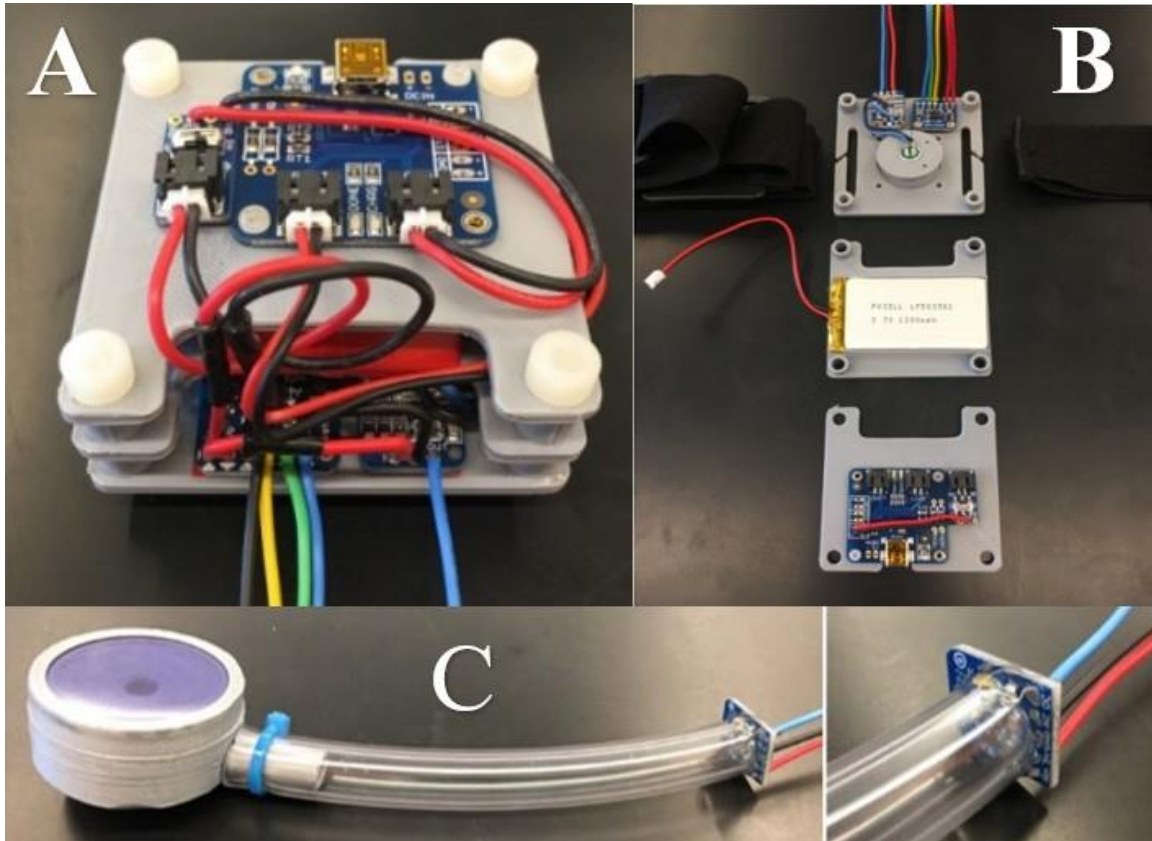
System Design

2.1 Previous Work and Hardware Improvement

The current design is based on an earlier prototype developed in 2019 in which three signals were received. This device, which consists of three different layers, is placed on the chest area with the help of a strap (Figure.13A). A microphone and an accelerometer are in the first layer, a battery and an ECG sensor are located in the second layer, and a battery control unit is in the third layer (Figure.13B). The previous student working on this project combined the microphone with a tube and a stethoscope to receive the PCG signal with better quality (Figure.13C). A microcontroller module Arduino Uno is used as the processor and is located in a separate place from the prototype. Although this device was wearable, it was quite large and not very comfortable for long-term use. In addition, this design did not allow any backup data collection as it did not have an SD card module. Since Bluetooth or Wi-Fi was not used, the device was not suitable for remote information transfer, instead, the received data was transferred from the device to a computer using a cable.

Figure 13

The Previous Prototype Including (A) Assembled Three-decker(right) (B) Individual Tiers(left) (C)MEMS Microphone Testing Setup

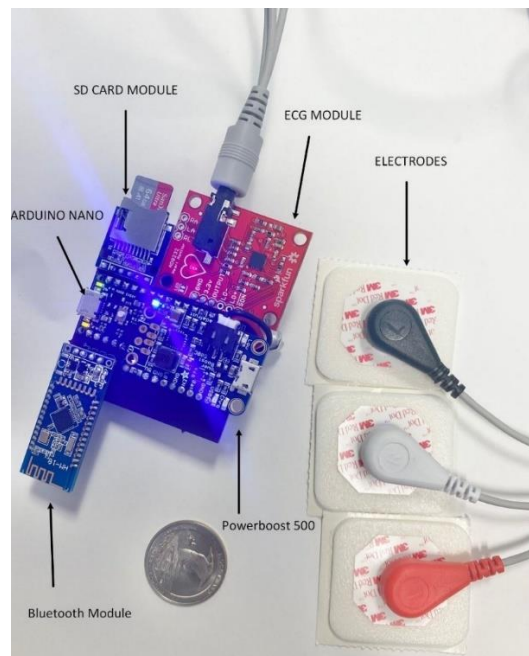


While previous work was sufficient to collect data, some aspects needed improvement. The microprocessor was far from the prototype and the device was not suitable for remote information transfer. Initially, we planned to reduce the size of the device, integrate the microprocessor into the device, and at the same time, give the device wireless communication capability. Accordingly, we made changes on the device and developed different designs, Figure 14 shows a small-sized design including a microprocessor was made on the prototype. Instead of the first microcontroller Arduino Uno, the smaller size Arduino Nano with the same clock speed was used in the new design.

HM-10 Bluetooth module was used for remote data transfer. Later, the custom PCB was designed to make the device more compact. In addition, an SD card module was added to the device for the security and sustainability of the collected data. Using the new design, all components could be placed on a single layer. The Bluetooth module, Arduino Uno, ECG sensor, and SD card module were placed on the upper part of this layer, while the battery system, microphone, and accelerometer were placed on the lower layer. A serious improvement has been achieved in the device in terms of size and function.

Figure 14

Initial Prototype Update with Modifications Including SD Card Module, Bluetooth Module, Arduino Nano, and PCB



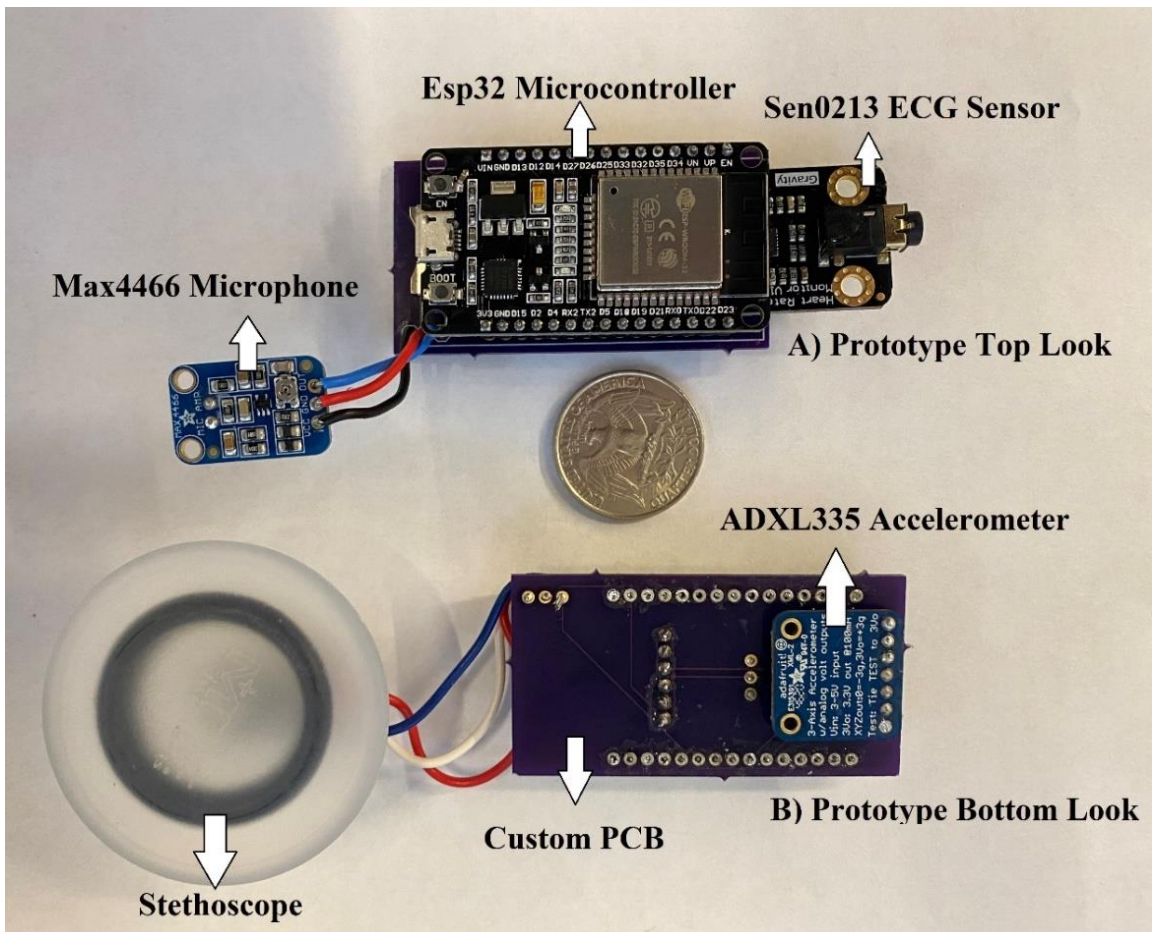
Although the first device designed could give the desired result in line with the tests and collected data, it still suffers from the low speed of the microcontroller, the low quality of the sensors used, and the low Bluetooth speed. As shown in Figure 15, the device size has been greatly reduced and made more efficient. As a result, a second design is implemented to overcome these issues. Instead of the Arduino Nano microcontroller (16 MHZ clock speed and 10-bit ADC resolution), the ESP32 microcontroller (240 MHZ clock speed with 32-bit ADC resolution) is selected as it is suitable for programming in the Arduino IDE platform. The ESP32 not only has a higher clock speed but also has an internal battery charger as well as Wi-Fi and Bluetooth modules [62].

In addition to replacing the microprocessor, some changes were also made to the sensors. The AD8232 development board was able to obtain a medium quality ECG signal, but it was very sensitive. Furthermore, it has caused problems in collecting quality signals in long-term recordings. Therefore, the Sen0312 development board (DFROBOT) was then used with the AD8232 chip to improve both measurement accuracy and device design. The Sen0312 is more compact, uses modern components and has wider filtering capabilities. Using the new development board, better quality and cleaner ECG signals are obtained. Also, the initial microphone used was sufficient for PCG signal recordings and for this reason, no changes were made. Since the stethoscope used was large, inefficient, and needed a tube for amplification, it was replaced with a new specially designed stethoscope. In addition, although the initial accelerometer (ADXL335) gave the desired information with filtering, the received data still contained significant noises and the overall device was not sensitive enough. MPU6050, which is much more sensitive and offers different range of gravitational acceleration (g) measurements, was selected over the

ADXL335 used in the previous study [63-65]. In addition, a more compact PCB was designed to house all the modules (Figure 17.).

Figure 15

Last Prototype Update with Modifications Including Accelerometer, Stethoscope, ESP32 Microcontroller, Sen0213 ECG sensor, and Custom PCB



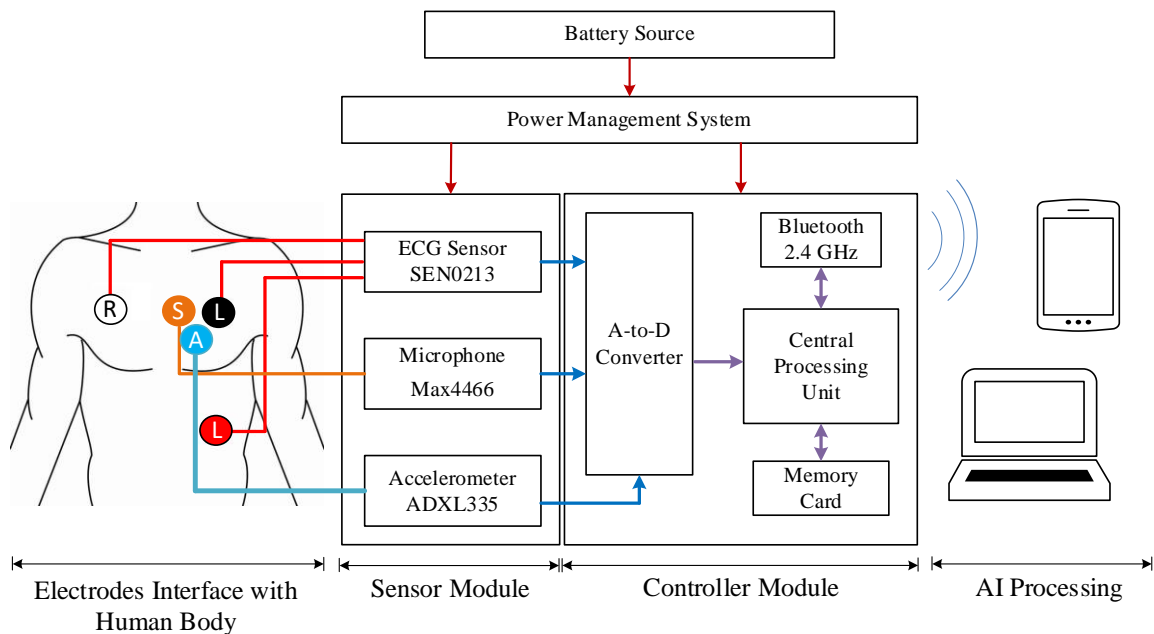
Note. a) prototype top look b) prototype bottom look.

To detect all three signals simultaneously, a wearable heart monitoring system is designed, as represented by the block diagram shown in Figure 16. ECG measurement is performed by three Ag/AgCl electrodes in a grounded lead configuration. The conductive

gel on the electrodes reduces the noise and skin-electrode contact impedance, hence improving the signal quality. Furthermore, a stethoscope (Orange - S) and a 3-axis accelerometer (Blue - A) are placed on the sternum to measure the PCG and SCG signals, respectively. The signals acquired from the human body are processed in the sensor module. The analog data collected in the sensor module is transferred to the analog-to-digital converter (ADC) in the microcontroller and converted into digital form there. Then, the data is simultaneously recorded on the memory card via the processing unit and transferred to the computer and phone with the help of a Bluetooth connection or a cable connection.

Figure 16

Simplified Block Diagram of the Prototype Wearable Heart Health Monitoring System



Note. White R (right anterior) – Orange S (stethoscope) – Black L (under the left clavicle, mid-clavicular line within the rib cage frame) – Red L (the lower left abdomen within the rib cage frame) – Blue A (accelerometer)

2.2 Sensor Module

The ECG signals acquired from the body are processed using a SEN0213 development board (DFROBOT). An AD8232 chip is included on the custom-designed PCB. The chip contains an active bandpass filter that removes the DC offset as well as high-frequency noises from the measured ECG signals, including power line interference (50-60 Hz) and EMG noise (100-500 Hz) [66]. In addition to the gain provided by the active filter, an operational amplifier with a gain of $11\times$ is also used, resulting in an overall system gain of $1100\times$ [67]. To save power, the development board contains a lead-off detection circuit, which enables the device to perform the processing only when the ECG leads are connected. The sensor module also contains an electrostatic capacitor-based microphone interfaced with a stethoscope to measure PCG signals. The signals acquired by the microphone are amplified by using a Maxim Max4466 amplifier; this op-amp provides an adjustable amplification gain from $25\times$ to $125\times$. The sensor module also contains an MPU6050 3-axis accelerometer, which is used to measure the acceleration of the chest wall caused by cardiac vibrations.

2.3 Microcontroller Module

The controller module consists of an ESP32 Dev Kit V1 development board featuring a dual-core, 32-bit ESP-WROOM-32 chipset, supporting a clock frequency of up to 240 MHz and a 32-bit ADC. Once the signals are recorded by the individual sensor modules, they are processed through the ADC before being acquired by the controller. The controller module also provides wireless connectivity. Bluetooth, BLE and Wi-Fi are integrated into the ESP32 chip, enabling the establishment of a wireless connection with a smartphone or a computer. Furthermore, the signal data can be saved in a micro-SD card which can be

used as a backup in case the wireless communication is interrupted. In this project, we have used the Blynk and Remote XY platforms for creating applications. These applications are compatible with Android, iOS phones, and personal computers.

Table 1

Cost of The Prototype

Cost Breakdown of Components		
Part	Part Number	Price
Accelerometer	MPU6050	\$15
ECG Module	Sen0213	\$20
Microphone	Max4466	\$7
SD Card	-	\$4
SD Card Module	SPI	\$2
Microcontroller	ESP32	\$12
Battery	3.7V 500 mAh	\$5
Wet Disposal Electrodes	3M Red Dot	\$2
	Total =	\$67

Table 1 lists all the components that are used in this prototype implementation, as well as their respective costs. The total cost of the prototype is ~\$67. This device can be easily manufactured with off-the-shelf components and can be interfaced with any smartphone. The device is low-cost and can be used at home for long-term monitoring of heart health. By using a device strap or medical tape on the chest area, the user can wear the device for a long time without feeling uncomfortable. As future development progresses, data preprocessed by the prototype can be uploaded to the cloud, enabling medical professionals

to track patients' heart conditions from their phones or computers in real-time or after the recordings. Trained AI algorithms running on the cloud can similarly track heart conditions, as further described below.

2.4 Artificial Intelligence (AI) Processing Module

The AI processing module consists of a trained machine learning model, which takes the input data from the controller module and classifies the signals into a set of pre-defined classes, e.g., a signature of a known heart condition, normal heartbeat, etc. The machine learning model used in this module is Long Short-Term Memory (LSTM), which is an artificial recurrent neural network [68]. We chose this model because it has been proven to be well-suited for time series learning, and in particular, for certain cardiac conditions [69]. It can be directly applied to the analysis of ECG, PCG, and SCG signals as they are all-time series in nature. In addition, compared to image-based approaches, treating signals as time series requires fewer data preprocessing, leading to higher performance in real-time detection. The output of the AI processing module is a set of heart conditions detected in the signals.

2.5 Printed Circuit Board (PCB) Design

The PCB design both eliminates unnecessary cables and makes the device as small as possible. First, the wiring between the ESP32 and the sensors was done using the Eagle CAD application, as shown in Figure 17. Then, using the auto-router feature, the wiring process on the PCB provides the best routes for the PCB with the help of the algorithm (see Figure 18-A). These routes, which are made by using both the lower and upper parts of the PCB, not only reduce the complexity but also enable the creation of PCB designs with

maximum efficiency. The correct pins must match the wiring process. For example, when making the connection between the ESP32 and the ECG sensor, we have to make sure that the voltage-voltage, ground-ground, and analog out-35 pins of the ESP32 are connected. There is no overlap between the code and the connection. Figures 18B and 18C demonstrate the top and bottom views of the PCB design, respectively.

Figure 17

Schematic Wiring Design on Eagle CAD for ESP32 and Sensors Connections

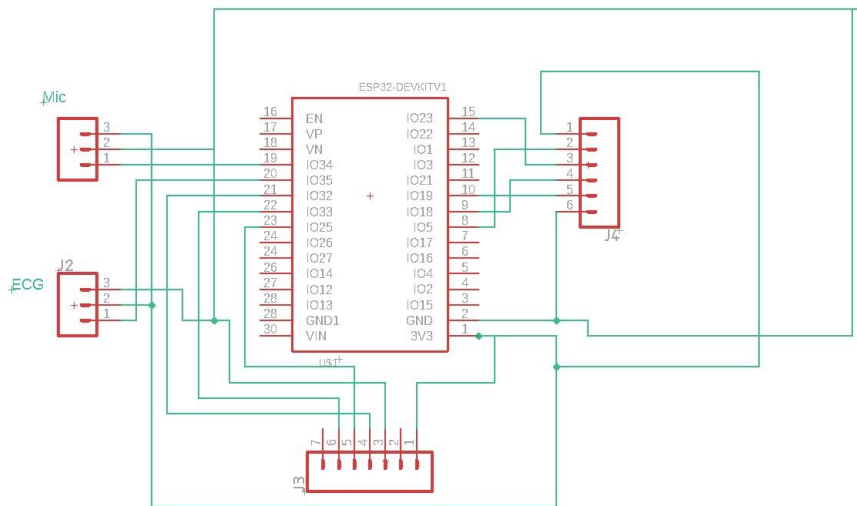
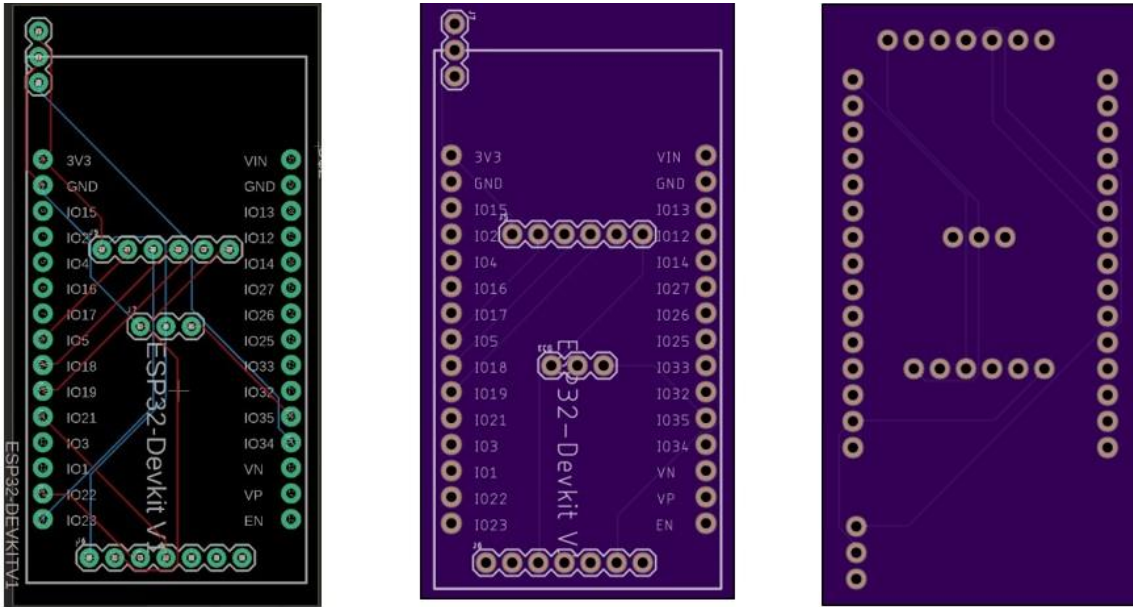


Figure 18

PCB Design Includes A) Wire Connection of the Board B) Top Look C) Bottom Look



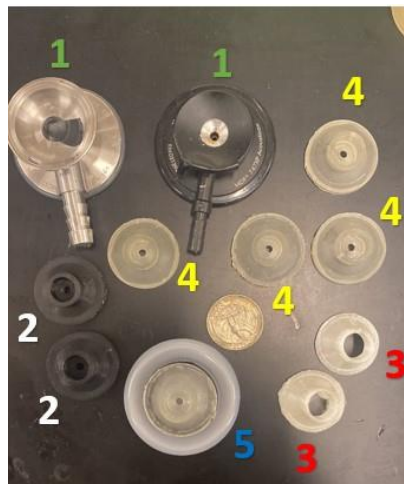
2.6 Stethoscope and Housing

The stethoscope is very important for increasing the received sound quality of the heart. For this reason, we have produced studies on different stethoscopes (see Figure 19). We produced different stethoscope designs using different materials. As a material, we tested metal, polylactic (PLA), thermoplastic polyurethane (TPU), and Formlabs elastic 50A resin. For the first design of stethoscopes for our design, we used a hospital type of aluminum stethoscope to amplify the PCG signal (Figure 19-1). Initially, we opened a hole the size of a microphone on the top of the stethoscope. Then microphone is placed on top of the stethoscope for the recording process. Although the collected signals were efficient, sometimes there could be a short circuit due to the connection between the microphone and the metal part of the stethoscope. Other than that, it was also not comfortable for wearable

designs because it was heavy, big, and bulky. After that, we first designed a stethoscope slightly larger than the quarter coin size, using PLA material (Figure 19-2). Although it was suitable for our expectations in terms of design and size, it was not suitable due to its rigidity. Also, this design made the user sweat and it could not amplify the sounds coming from the heart at the desired level. Then we tried the same design using the TPU material (Figure 19-3). The TPU material was advantageous because it was flexible and did not make the user sweat. At the same time, it gave slightly better results in sound quality than the PLA material. However, although our results were improved, they were not suitable for long-term recordings. For this reason, we obtained a similar design from an SLA printer using Formlabs elastic 50A resin (Figure 19-4). Due to its flexibility, this material is suitable for long-term use and does not make the user sweat. Overall, the quality of the received signal is very close to the signal received from a metal stethoscope. After making sure of the quality of the material and the efficiency of the stethoscope, we produced a certain number of them for testing.

Figure 19

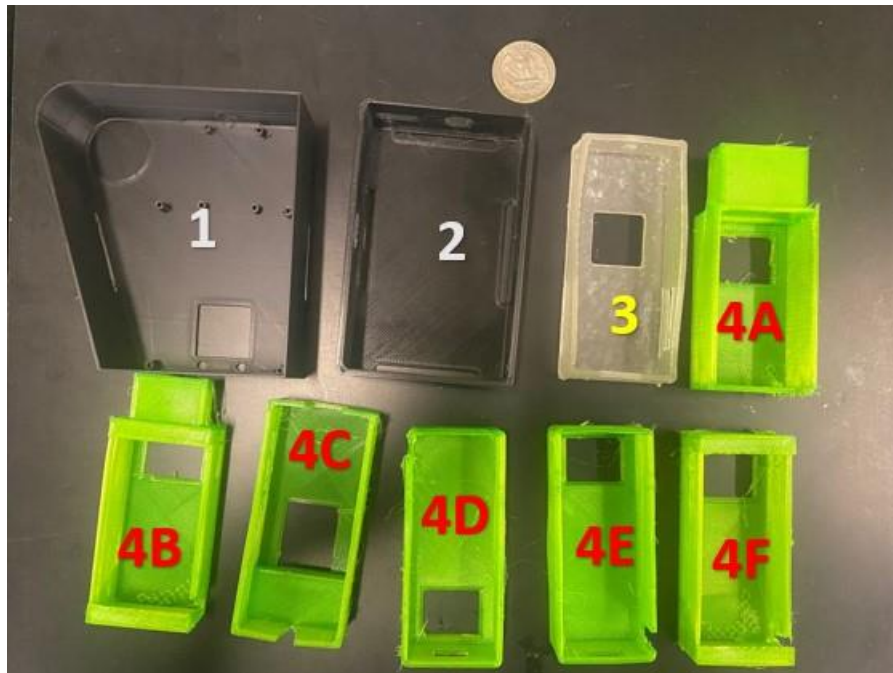
Stethoscope Designs Made with Different Materials



The housing design of the device, which will form the layer between the user's skin and the device, is important for the comfort and ergonomics of the user. The enclosure not only protects the device from external factors but also protects the user against problems that may arise from the device. At the same time, since the user aims to use the device for a long time, it will increase the efficiency of the housing made of comfortable, ergonomic, non-sweating, and non-itchy material. Figure 20 illustrates the housing designs made with different materials for the device. Considering the changes in the dimensions of the device, the smaller the device size, the smaller the housing design. First, we used PLA material for housing as shown in Figure 20-1 and Figure 20-2. PLA was not ergonomic because it was rigid, and it also causes sweating and itching. For this reason, instead of PLA, we tested the Formlabs elastic 50A resin, this material is durable, flexible, and ergonomic, and does not cause sweating and itching, with a printed housing shown in Figure 20-3. However, it is too expensive to produce for its wide deployment for device testing. For this reason, we 3D printed the designs using TPU, as shown in Figure 20- 4A, B, C, D, E and F. Similar to Formlabs elastic 50A, TPU is flexible, ergonomic, durable, and comfortable to wear. At the same time, it is suitable for cheap production. The housing model shown in Figure 20-4F is the design used for the final prototype. The shape of this model received the best evaluation of all designs based on user input. It allows the lid to be positioned correctly in a reliable and stable manner.

Figure 20

Housing Designs Made with Different Materials



Chapter 3

Data Acquisition

As mentioned in the previous chapter, the device acquires ECG, PCG, and SCG signals from the heart. To perform data acquisition, the device must be programmed to have the required functions. Apart from this, for the programmed device to collect data properly, it must be properly placed on the body as well. This section covers the programming of the device, proper placement on the body, data acquisition, real-time monitoring, and smartphone application.

3.1 Device Programming

3.1.1 *Arduino Programming for the Device*

An ESP32-based microcontroller is used as the “brain” of the whole prototype system. The ESP32 must be programmed to receive data from sensors and provide wired or wireless communication with external devices. The Arduino Integrated Development Environment (IDE) platform was used as a basis for programming the device using a C++ based software language. The full code of the final iteration of the prototype device is presented in Appendix 1.

First, libraries need to be installed on the Arduino IDE platform, so it can program the ESP32 microcontroller. These libraries ensure that the written code is properly transmitted to the ESP32 and that the ESP32 can run the given commands properly. "BLEDevice" library for Bluetooth communication, "RemoteXY" library for a phone application, "FS", "SD" and "SPI" libraries for the SD card, “Wire” and "MPU6050_tockn"

libraries for the MPU6050 sensor are all used in this code on the Arduino IDE platform to ensure proper communication between the ESP32 and the code.

After the libraries are defined, the baud rate and Bluetooth name of the device are defined in the setup section. In addition, the codes defined for the SD card are used to check whether the SD card is properly connected to the device. If the connection is correct, a new text file (.txt format) is opened on the SD card, and the collected data is stored in this file. If there is a file with the same name, a new text file will be opened automatically. To prevent problems that may occur with the device due to the battery, if the device loses power, the last data is automatically saved to the file in SD card. When the power is back on again, the new data is saved in a newly opened text file. In this way, the security of the collected data is ensured. Furthermore, this section contains the code for resetting and restarting the MPU6050 accelerometer to ensure that when the device is restarted, the axes of the accelerometer are properly aligned.

The code runs continuously in the Loop section. In this section, sensors are defined to the appropriate pins on the ESP32 and each pin represents a different sensor. Along with the commands from the code, ESP32 detects the data coming from the pins and transfers this data to be displayed in Arduino, LabVIEW, MATLAB and phone application. For example, in simplified terms, the ECG sensor is defined to pin 35 of the ESP32 with the command `"int a = analogRead (35);"`. For wired connections, `"Serial.print(a);"` command is used to write and transfer values from the existing ECG sensor. In this way, data can be viewed and tracked in a suitable format. (For example, 1/14/2022 13:45 ECG: 1453). `"SerialBT.println(a);"` command is used for Bluetooth transfer of this data to the computer and to display it in real-time. Finally, the data from the ECG sensor is written to the first

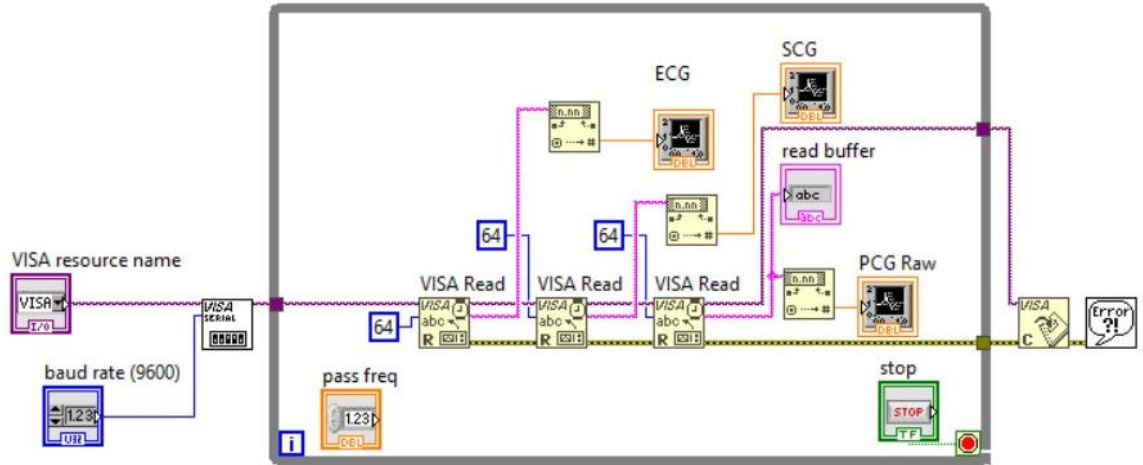
graph in the phone application with the command "RemoteXY.onlineGraph_1 = float (a);". In this way, the data can be tracked in real-time via graphs with the user's phone. Similar steps are done for PCG and SCG signals as well.

3.1.2 LabVIEW Programming for the Device

LabVIEW is a powerful platform for real-time signal monitoring, signal processing, and data tracking. Usually, the sensors are connected to LabVIEW compatible Data Acquisition (DAQ) devices, connected to a computer, and signals are observed on the screen of the computer running LabVIEW software. However, since our device is wearable, has remote communication, and uses ESP32, it would be very unreasonable to use an additional DAQ device. For this reason, a wired or wireless connection is established between the ESP32 and LabVIEW using the serial communication method. Figure 21 shows the schematic program to connect the ESP32 to the LabVIEW platform and display the ECG, PCG, and SCG signals. Visa serial command helps identify and screen available visa resources connected to the laptop. From the Visa Resource Name section, the port where the device is defined is selected. Then, the baud rate written in ESP32 is written to the baud rate tab in Visa Serial to ensure the baud rate match. Then a while loop is created that will keep the program running over and over until it is stopped. Visa Read commands are generated in the while loop and these commands allow LabVIEW to detect data read by the serial port. Each Visa Read command is associated with a different signal from a different sensor. Then graphics are created and connected with Visa Read commands. Thus, it is ensured that the signals are displayed individually or collectively on the graph. Figure 21 shows the schematic design for ESP32-LabVIEW communication.

Figure 21

Schematic Design for Using ESP32 Microprocessor with 3 Sensors on LabVIEW



3.2 Device Placement

For the device to perform long-term data collection, the device must be placed comfortably on the user's body. The placement of each sensor plays an important role in obtaining smooth and quality data from the three sensors. This device has a 3-electrode system for ECG and uses RA, LA, and LL electrodes (see Figures 3 and 16). To receive ECG data, the electrodes are placed on the user's body, and the leads are connected to these electrodes accordingly as shown in Figure 22.

Figure 22

ECG Lead-Electrode Connection



Note. Green represents LA, Red represents RA, and Yellow represents LL.

For a phonocardiogram, positioning the microphone close to the heart will improve the quality of the signal to be received. For this reason, the microphone is used with a stethoscope and is placed close to the heart with the help of medical tape. The stethoscope acts as an amplifier, increasing the quality and size of the received signal. In this way, the maximum amount of information is obtained from the heart sound before filtering the data. The accelerometer placed close to the sternum improves the quality of the received seismocardiogram signal of chest vibrations caused by heart vibrations. The position of the accelerometer plays a major role in the quality of the received signal (see Figure 10), as evidenced by the studies and tests of H. Ashouri and O. T. Inan on this subject [70].

3.3 Real-Time Monitoring

Displaying these three signals collectively in real-time plays an important role in monitoring the relationship between the signals, monitoring the quality of the signals, monitoring the abnormalities in the signals, and heart rhythm monitoring. In this thesis, two different methods were used for real-time monitoring. The first method is to use the Arduino IDE platform's own graphics system. The second method is to use ESP32 on the LabVIEW platform.

3.3.1 Real-Time Monitoring Using the Arduino IDE Platform

The Arduino IDE serial plotter is used for real-time monitoring of simple signals. It can give practical and meaningful results in a short-term display of signals. It is difficult to achieve a simultaneous high-quality display of three signals on this platform. This platform would not be useful as a primary monitoring environment, since both the timeline is fast and the data is difficult to track. Its use is primarily to test the device, monitor changes in coding, and make any on-the-fly changes. Figure 23 displays the raw ECG signal on the Arduino IDE platform.

Figure 23

ECG Signal Monitoring on Arduino Serial Plotter

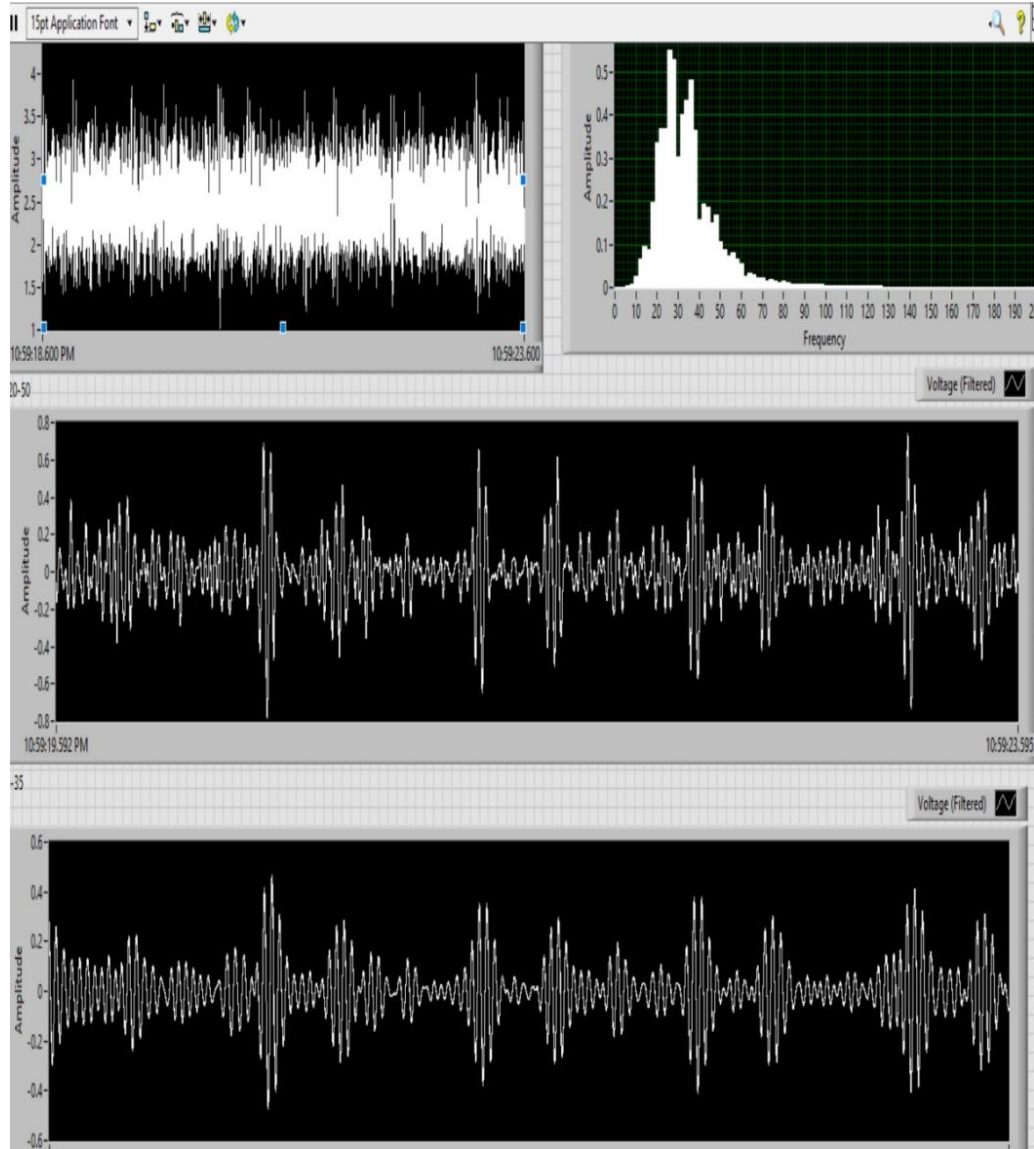


3.3.2 Real-Time Monitoring Using LabVIEW

Real-time monitoring using LabVIEW is comparatively advantageous. Not only raw signals but also frequency range and filtered signals can be displayed in real-time. This allows both real-time monitoring, recording of data, and also facilitates the detection of abnormalities in the signal. Figure 24 shows the monitoring of the PCG signal on LabVIEW. The first graph in the upper left shows the raw signal received from the microphone. The second graph at the top right shows the frequency range of the PCG signal determined from real-time fast Fourier transform (FFT). The third and fourth graphics show the filtered version of the raw signal using bandpass filters in different frequency ranges, as explained in the next chapter (Signal Processing) of this thesis.

Figure 24

Real-Time PCG Signal Monitoring on LabVIEW



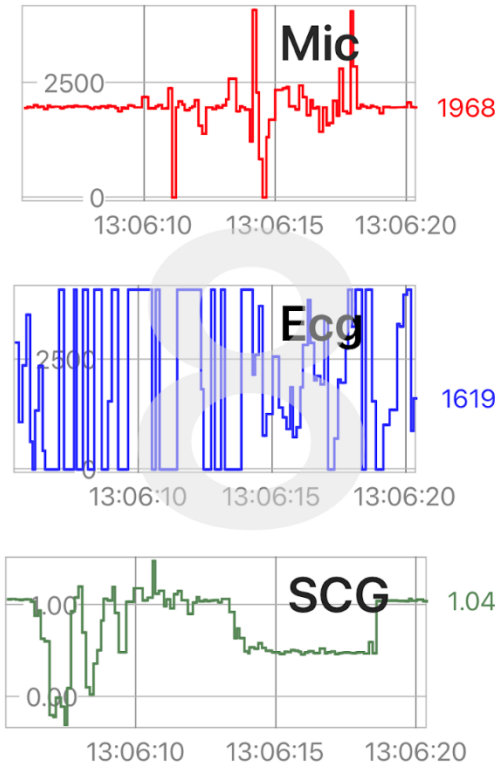
Note. First graph on the top left side displays original PCG signal, second graph on the top right side displays the frequency range of the PCG signal, the third and fourth graphs display the filtered PCG signals with different cut-off frequency ranges.

3.4 Phone Application

For a wearable health monitoring device, it is very important to be able to view and access the data from the computer as well as at least monitor the data on a smartphone. In this way, in an abnormal situation, the user can be aware of the situation early and doctors can intervene early before a problem occurs. Many companies and researchers are working on software that will enable communication between wearable devices and phones [71-73]. In this study, a simple application has been developed to exchange information, data, and commands between a phone and microcontroller over Bluetooth or Wi-Fi. This application is compatible with iOS or Android and is only responsible for transferring the data it receives from the sensor to the three graphics in its interface. In this way, the data can be followed in real-time from the user's phone. The application can be designed on websites such as Blynk or RemoteXY and the code can be generated for free. This phone app is suitable for all microcontrollers compatible with Arduino IDE. Figure 25 displays the real time monitoring using the RemoteXY phone application.

Figure 25

Real-time Monitoring Using the RemoteXY Phone Application



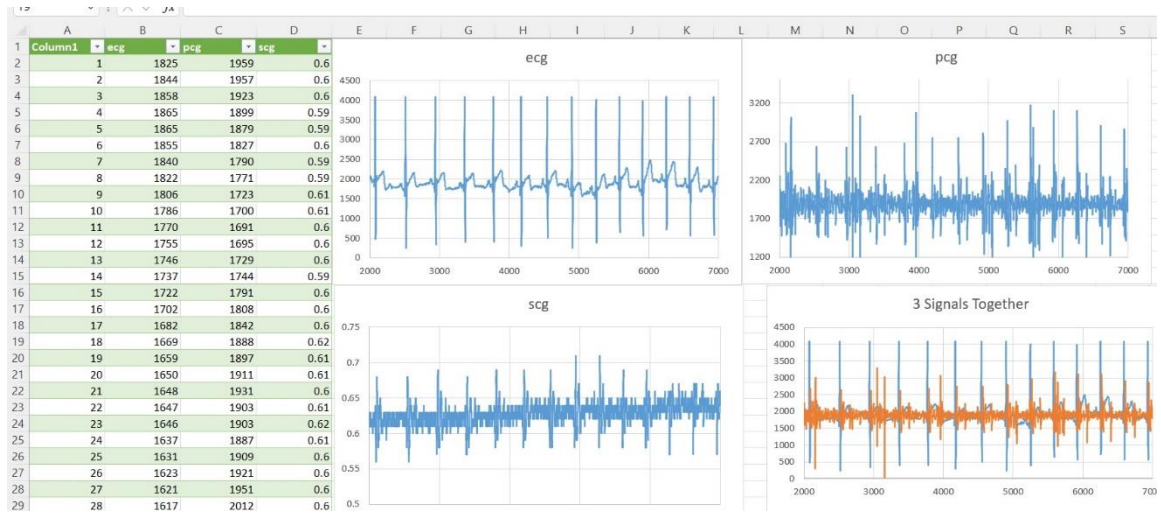
3.5 Data Harvesting from SD Card to Spreadsheet

Besides real-time data monitoring and data transfer, all data is simultaneously saved on an SD card to ensure data security. The data received from the sensors are written to the text file created on the SD card, on which this file can then be transferred to a computer. Information stored in the text file can then be processed using software such as Origin or Microsoft Excel. This process is usually very simple. First open a spreadsheet file using Microsoft Excel then click on Data tab. Then click on the Get Data tab and select the text file that needs to be examined on the SD card. After the data is determined in the window that opens, the process is terminated by using the transfer data command.

The transferred data can be visualized with the help of graphs. Figure 26 shows data on the SD card exported to Excel and graphed. The graphs of ECG, PCG, and SCG signals are shown on the right side of the figure as well as their relationships with each other.

Figure 26

Transferred Raw Data from the SD Card to Excel Spreadsheet



Note. Column 1 represents the number of samples, column 2 represents the magnitude of ECG signal, column 3 represents the magnitude of PCG signal, and column 4 represents the magnitude of SCG signal. First graph on the top left side displays the raw ECG signal, second graph on the top right side displays the original PCG signal, third graph on the bottom left side displays the original SCG signal, and fourth graph on the bottom right side displays the correlation between three signals.

Chapter 4

Signal Processing

Signals received from sensors often contain noise, which can be caused by environmental effects, electromagnetic fields, the quality of the cable used, or the sensor, among other factors. Although noisy signals often contain the desired information, the information is difficult to understand, interpret and monitor. Therefore, the signal is de-noised using signal processing methods. There are many methods to complete signal processing, only some of which are introduced in this chapter. Signals can be physically or digitally processed (or both). In this thesis, signals were processed in the digital environment.

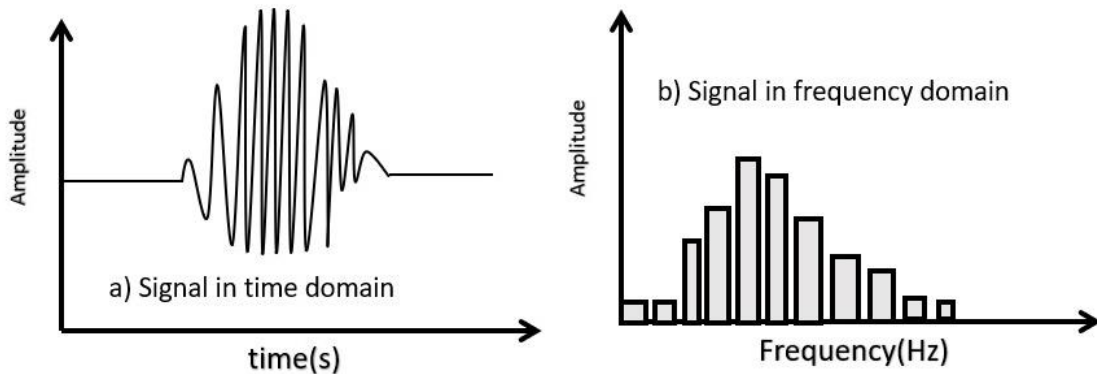
Certain steps are required for cardiac electro/mechanical signal processing. First, it is necessary to determine the frequency range of the received signal that contains most of the meaningful information content. Although there are many methods for this, one of the most known and used methods is the fast Fourier transform (FFT). After the frequency range of the signal is determined, filtering is applied to remove the noise from the signal. Thus, the signal can a cleaner form.

4.1. Fast Fourier Transform (FFT)

The primary use of FFT in research is to transform time-domain signals into frequency-domain signals and vice versa (see Figure 27) [74]. This method is quite useful for calculating the modal parameters of frequency components. If the system generates noise, the noise can be recorded in a digital wave file and used for further processing [75].

Figure 27

Schematic of a) Signal in the Time Domain and b) Signal in the Frequency Domain Used to Explain FFT



There are several advantages to digital signal transmission over analog signal transmission. Digital technologies encode information into a discrete signal, whereas analog technologies employ continuous signals [76]. Such changes are quickly computed by factorizing the Discrete Fourier Transform (DFT) matrix into a product of sparse (mainly zero) elements [76, 77]. The FFT is an efficient algorithm for computing the DFT, where the compute time reduces from the order of N^2 to $N\log_2 N$ and N is the number of samples of the discrete signal. For large N , this means enormous computational time savings for the FFT compared to the elementary DFT.

It is critical to review the FFT results before and after filtering. Performing the FFT of the ECG signal on LabVIEW can play an important role in both real-time and post-processing. Increasing the sampling rate and sampling frequency of the device will also increase the frequency domain quality. For this reason, spectral measurement features or

FFT commands are used in the program. The received line signal is coupled to the block box of the spectral measurements. Then, as seen in Figure 28 in the spectral measurements section, Magnitude (Peak) is selected for the measurement option, and Linear is selected for the Result option. A chart is then created and linked to the results from the spectral measurements. Figure 29 shows 6-7 seconds of raw ECG signal and frequency domain. As the frequency domain shows, information in the signal mostly lies between 0.1 and 65 Hz. However, we see that the actual desired signal is mostly between 0.2 and 35 Hz. In the next section, we will use these values in the filtering process, and we will talk about the details there. Figures 30 and 31 show 5-6 seconds of raw PCG signal and its frequency domain.

Figure 28

Fast Fourier Transform (FFT) Set up on LabVIEW

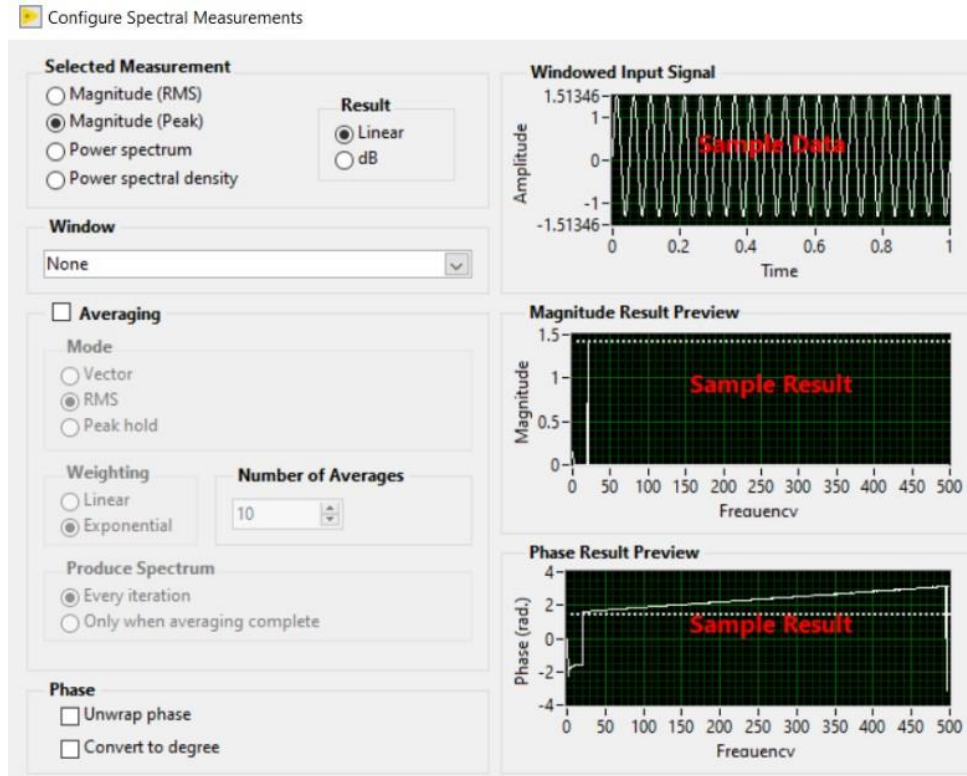


Figure 29

Raw ECG Signal in Time Domain and Frequency Domain

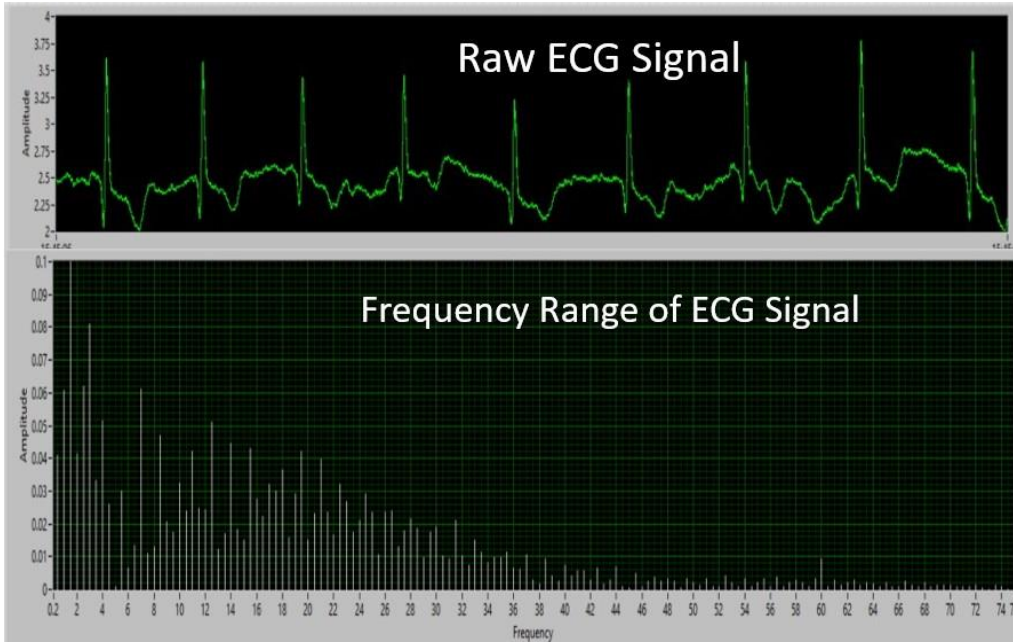


Figure 30

Raw PCG Signal in Time Domain

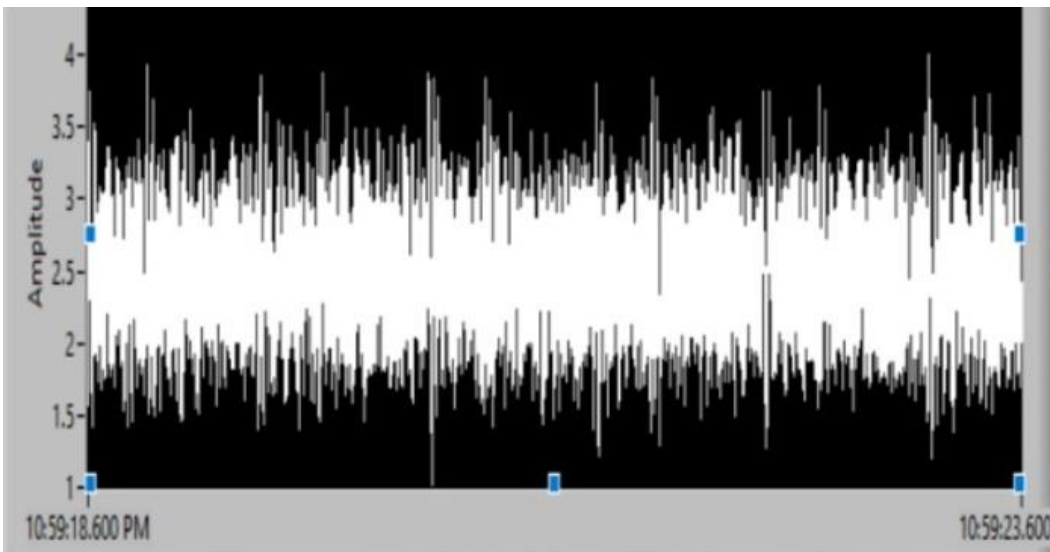
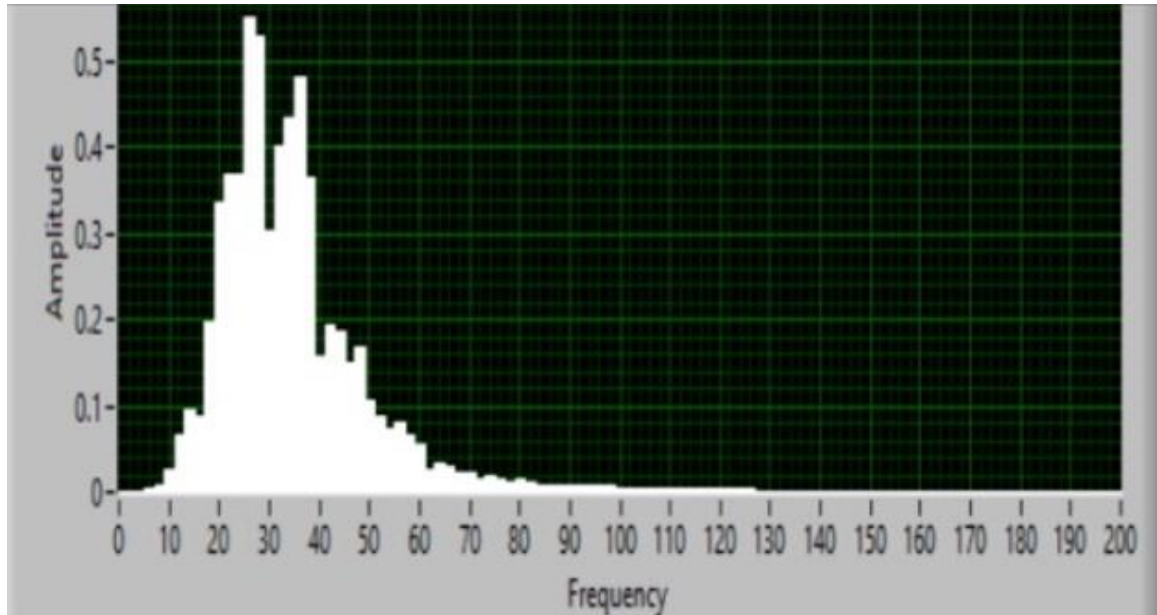


Figure 31

PCG Signal in Frequency Domain

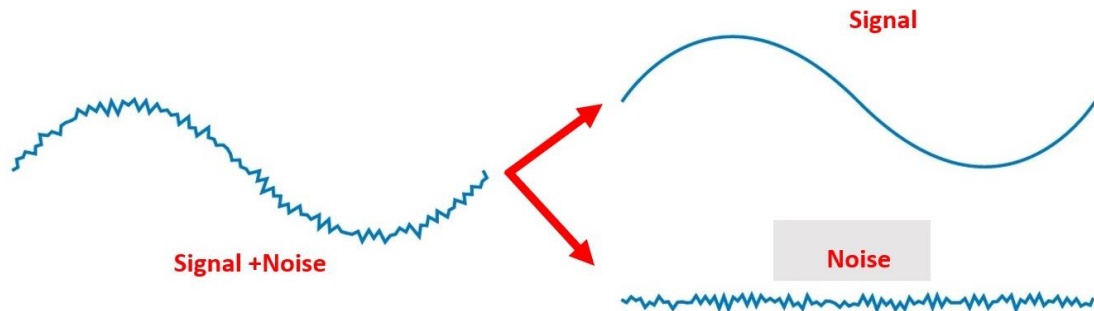


4.2 Filter

One of the most important tools for signal processing is filtering. Collected noisy signals from sensors are often difficult to understand and appear complex because of the noise they contain (see Figure 32). One of the easiest ways to fix this is to filter the signal based on the frequency range of the signals to remove noise. In this way, the signal is clear and suitable for working in machine learning algorithms. Since digital filters are generally much more flexible and easier to use, the work described in this thesis uses digital filtering. As described below, the passband contains frequencies that are allowed to pass, whereas the stopband contains frequencies that are not allowed to pass. The transition band is located in between.

Figure 32

Schematic of Noise Isolation from the Signal

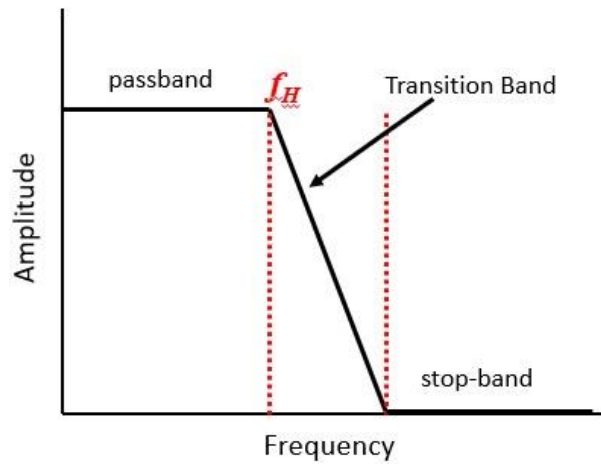


4.2.1 Low-Pass Filter

A low-pass filter is a filter that allows signals with frequencies lower than a certain high cutoff frequency to pass while attenuating signals with frequencies greater than the cutoff frequency. The frequency response of the filter is determined by its design. In audio applications, the filter is also known as a high-cut filter or treble-cut filter. It is not possible to create a perfect low pass filter in the real world, but we can create a very close-to-perfect low pass filter by using the digital filtering method. Figure 33 shows the effect of a typical low pass filter on signal components at different frequencies.

Figure 33

Schematic of a Low-Pass Filter

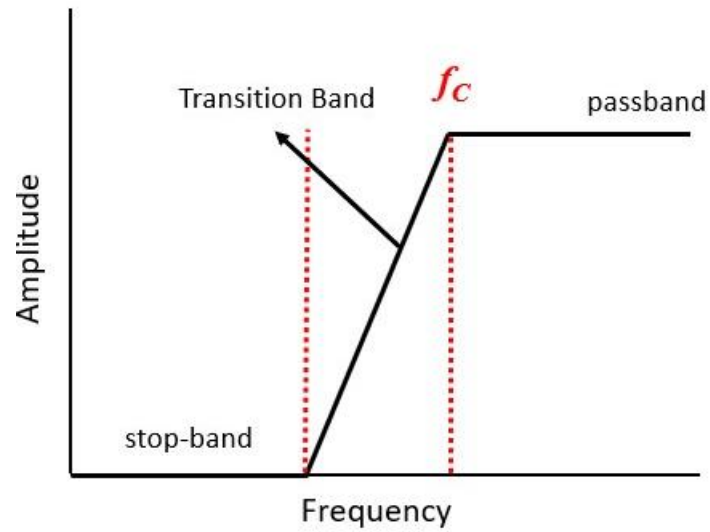


4.2.2 High-Pass Filter

A high-pass filter is, in some way, the opposite of a low-pass filter and allows high-frequency signals to pass while blocking low frequencies. A high pass filter attenuates frequencies below a cutoff frequency (stopband) while allowing signals above a low cutoff frequency to pass (passband) as shown in Figure 34. The amount of attenuation is controlled by the design of the filter. High-pass filters are often used to remove low-frequency patterns from time-series data while highlighting high-frequency trends.

Figure 34

Schematic of a High-Pass Filter

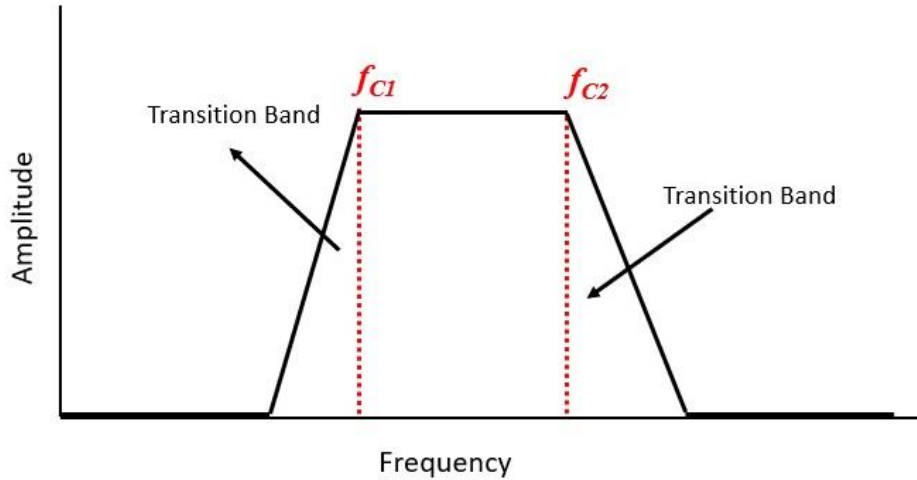


4.2.3 Band Pass Filter

The band-pass filter is designed to only allow a certain range of frequencies to pass. The frequencies within the band, between a low cut-off frequency and a high cut-off frequency, can pass the filter while frequencies outside this band will be stopped. As a result, a signal can be filtered for a certain frequency range, as shown in Figure 35.

Figure 35

Schematic of a Band-Pass Filter

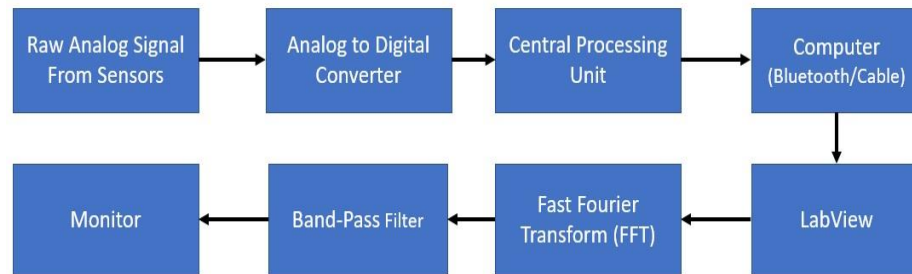


4.2.4 Real-Time Filtering Using LabVIEW

Figure 36 shows the signal processing steps from the raw signal received from the sensor to the final version with the filtering process applied. The frequency range of the data imported into the computer is determined primarily by using FFT. Then, noise is removed by applying band-pass filtering. To filter the signal from noise at a maximum efficiency, filtering with different frequency ranges was tested.

Figure 36

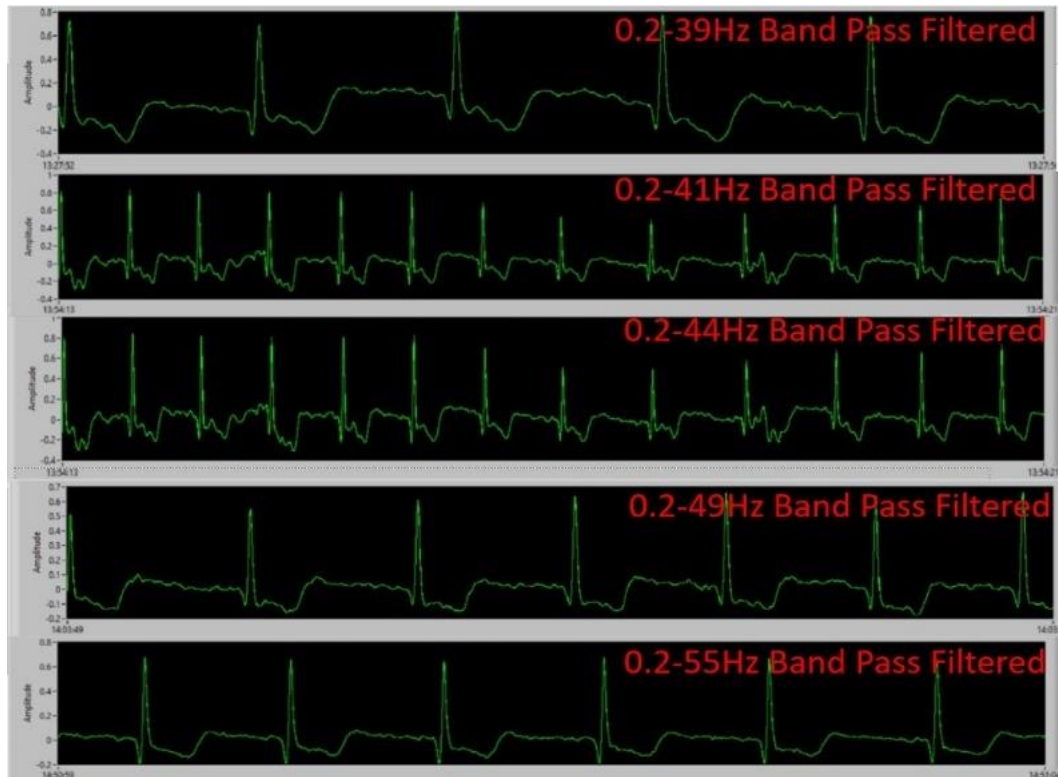
Block Diagram for the Signal Filtering Process



LabView is a powerful program for real-time signal filtering. It performs multiple filtering operations simultaneously in real-time, providing the user with the opportunity to monitor all filtering operations at the same time. In this way, we can find the most suitable cut-off frequency range. Figure 37 below shows the different filtering processes in the 0.2-55 Hz range of the ECG signal. As the frequency range changes, serious changes occur in its structure. While decreasing the range, important information is missing from the signal, while increasing the range excessively, noise reappears on the signal. As a result of all the tests, as shown in the next section, we determined the most efficient cutoff frequency range for the ECG signal as 0.2-36/38 Hz. Figure 38 demonstrates the filtered PCG signals with different cut off frequency ranges.

Figure 37

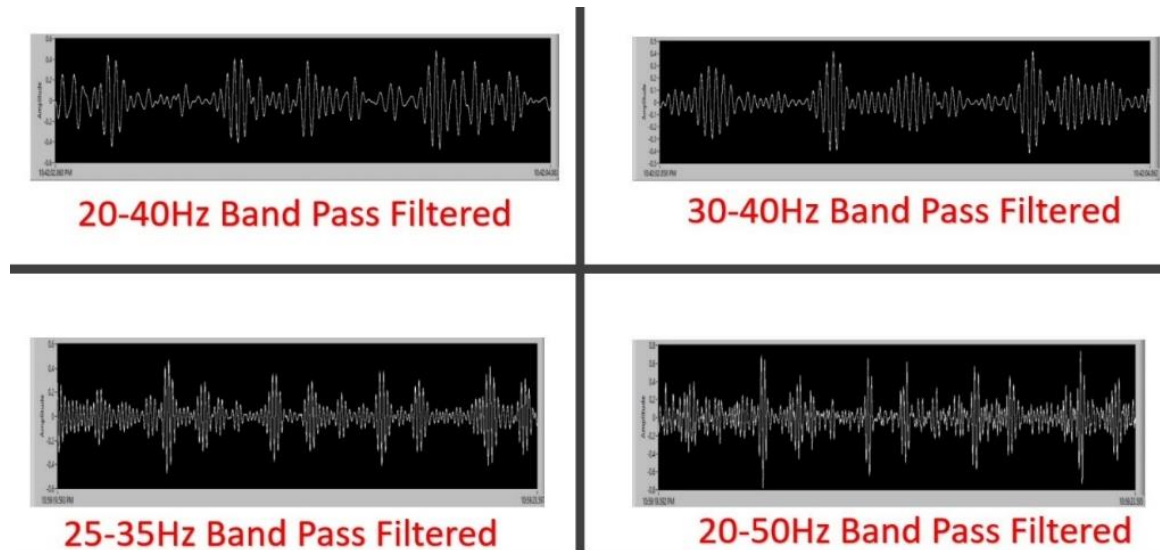
Filtered ECG Signals Acquired in Real Time Using a Band-pass Filter Using Different Cutoff Frequency Ranges



Note. Due to recording constraints, the time duration of each recording differs; however, the effect of band pass filter smoothing should be evident when comparing among plots.

Figure 38

PCG Signal is Filtered in Real-Time by Using a Band-Pass Filter Using Different Cutoff Frequency Ranges Selected Regarding Figure 31



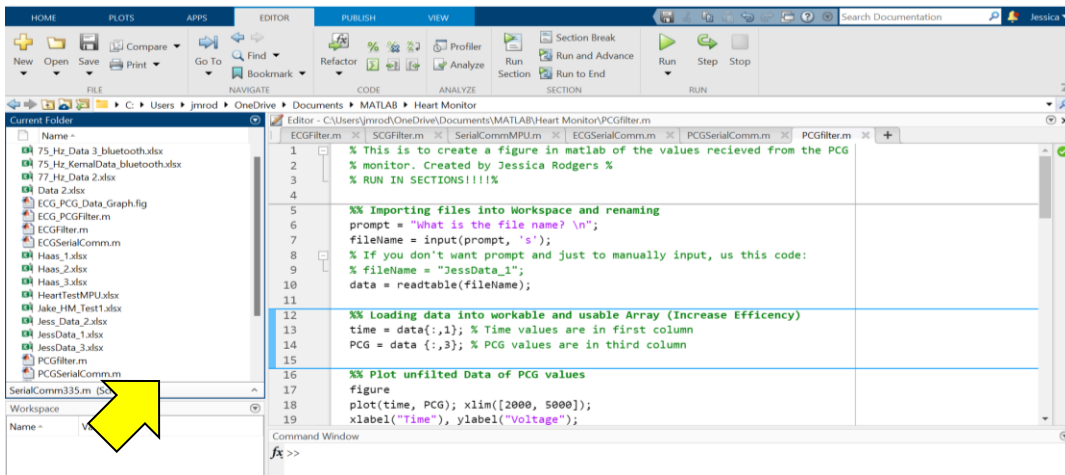
4.3 MATLAB Program for Signal Processing

Filtering operations made via MATLAB are also powerful, but not in real-time. Our work on real-time filtering with MATLAB is still in progress. The data saved on the SD card or directly on the computer can be filtered in different frequency ranges via MATLAB. We have developed special programs for ECG, PCG, and SCG for this process. Thus, the desired filtering process of the desired signal can be performed. The code consists of 9 different tabs and each tab is complementary to the next. While executing the code, instead of running the entire code at once, it is run piecemeal to make sure that the filtering process proceeds correctly. The code of this program can be found at the end of the thesis as an Appendix 2. Directions to run the program:

- 1) Ensure all files that are going to be utilized are within the same file as your scripts, so they can be seen in your “Current Folder” in MATLAB, shown here (see Figure 39):

Figure 39

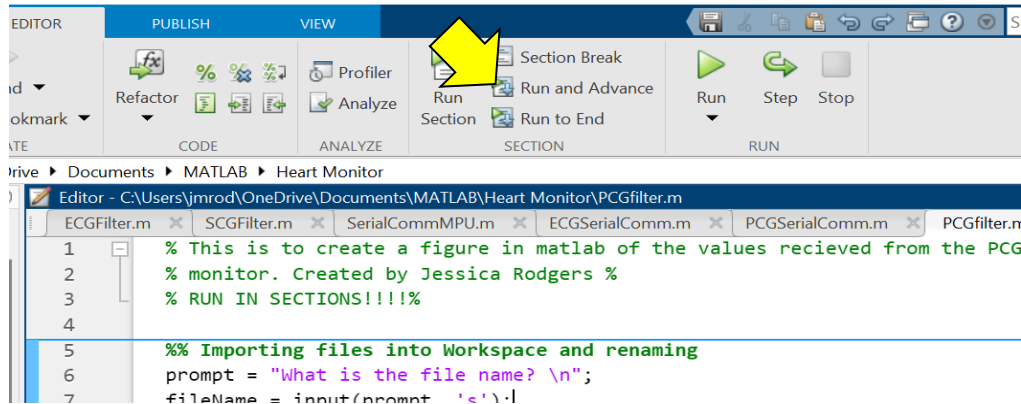
Step 1 for Preparing Filtering Code



- 2) Run The section titled, “Importing Files into Workspace and renaming”. To run a single section, click your mouse anywhere into that specific section, which is defined by the bolded section title and the next bolded section title. Click “Run and Advance”, shown in Figure 40, this will run the current section clicked into, and then prep for the next run by moving your cursor into the next section.

Figure 40

Step 2 for Preparing Filtering Code



- 3) This will prompt the user in the command window with “What is the file name?”
Type in the command window the name of the file, excluding the file type. For example, if the entire file name in the folder is, “Data1.xlsx” the user will type, “Data1”. It will then prompt you for the specification sheet in the excel sheet, type the name of the sheet in the command window. For example, if the excel sheet says “ECG1”, type “ECG1”.
- 4) Click “Run and Advance” this will run the next section titled “Loading data into workable arrays” and will separate the excel columns into usable arrays.
- 5) Click “Run and Advance” this will run the “Plot unfiltered Data...” section, which will show you the unfiltered data on a graph.
- 6) Click “Run and Advance” this will run the “Transform Unfiltered Data...” section, this will transform the data into the frequency domain instead of the time domain.

- 7) Click “Run and Advance” this will run the “Plot frequency domain values” section, this will prompt you to input the sampling frequency of this data, and type in the integer into the command window. It will then graph the values in the frequency domain alongside the original data unfiltered. This way you can analyze the two graphs to help determine what values to filter out.
- 8) Click the “Run and Advance” button, this will run the “Create Frequency Filter” section. This will prompt you with a pop window to design a filter, as shown below.
- 9) Once the correct values are inputted, hit the “Design Filter” button at the bottom of the filter designer window, shown below. Then, go to “File”, and click “Export”, as shown Figure 41.

Figure 41

Step 9 for Preparing Filtering on MATLAB

Current Filter Information

Structure: Direct-Form FIR
Order: 50
Stable: Yes
Source: Designed

Store Filter ...
Filter Manager ...

Filter Specifications

Mag. (dB)

0

F_{pass} F_{stop} $F_s/2$ f (Hz)

A_{pass} A_{stop}

Response Type

Lowpass

Highpass

Bandpass

Bandstop

Differentiator

Design Method

IIR Butterworth

FIR Equiripple

Filter Order

Specify order: 10

Minimum order

Options

Density Factor: 20

Frequency Specifications

Units: Hz

Fs: 48000

Fpass: 9600

Fstop: 12000

Magnitude Specifications

Units: dB

Apass: 1

Astop: 80

Current Filter Information

Structure: Direct-Form FIR
Order: 50
Stable: Yes
Source: Designed

Store Filter ...
Filter Manager ...

Filter Specifications

Mag. (dB)

0

F_{stop1} F_{pass1} F_{pass2} F_{stop2} $F_s/2$ f (Hz)

A_{stop1} A_{pass} A_{stop2}

Response Type

Lowpass

Highpass

Bandpass

Bandstop

Differentiator

Design Method

IIR Butterworth

FIR Equiripple

Filter Order

Specify order: 10

Minimum order

Options

Density Factor: 20

Frequency Specifications

Units: Hz

Fs: 48000

Fstop1: 7200

Fpass1: 9600

Fpass2: 12000

Fstop2: 14400

Magnitude Specifications

Units: dB

Astop1: 60

Apass: 1

Astop2: 80

Design Filter

File Edit Analysis Targets View Window Help

New Session Ctrl+N

Open Session... Ctrl+O

Save Session Ctrl+S

Save Session As...

Store Filter...

Import Filter from Workspace Ctrl+I

Export... Ctrl+E

Generate MATLAB Code >

Print Preview

Print... Ctrl+P

Print to Figure

Close

Filter Manager ...

Filter Specifications

Mag. (dB)

0

F_{stop1} F_{pass1} f

A_{stop1}

Response Type

Lowpass

Highpass

Filter Order

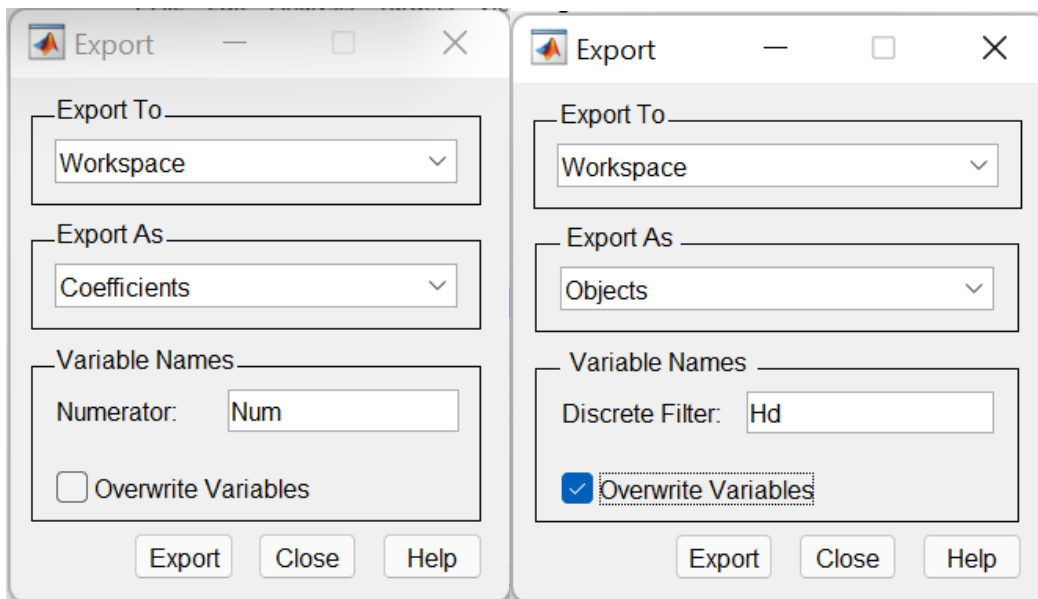
Specify order: 10

Units: Hz

10) Another window will pop up, asking how you want to export to the workspace, as shown in Figure 42. Click under the drop-down menu “Export As” and click “Objects”. Each time to use the filter designer, make sure the box that says, “Overwrite Variables” is Checked off, as shown on the right side below. Then click “Export”. The original window is shown on the left, what it should look like before hitting “Export” is on the right. Once the filter has been exported, you can run the next section, titled “Create Filtered Signal” by clicking “Run and Advance”.

Figure 42

Step 10 for Preparing Filtering on MATLAB



11) The next two sections create graphs, both in the time domain, which is what we look at when looking at a signal, and the frequency domain, which shows which frequencies

are found in our signal, each is described by their section titles. You can run both or either of these by running each separately by clicking on the section you wish to run and hitting the “Run Section” button, shown below.

4.3.1 Signal Filtering Using MATLAB

Datasets were obtained by subject 1, who participated in the study voluntarily. He was asked to sit in a quiet room during the recording period, and he was recommended not to move to minimize the noise from the environment. The sampling rate used with these sets is all equal to 760 Hz. About 5 minutes of real-time data were collected from him for ECG, PCG, and SCG. The following sections explain the application of filtering on this raw data acquired from the sensor hardware described in previous chapters.

4.3.1.1 ECG Signal Filter. Although the original ECG data contains a small amount of noise, the signal is largely free from noise thanks to the analog filtering system onboard the ECG sensor. Residual noise is removed from the signal using the filtering process. Figure 43 shows the original ECG signal filtered in the range of 0.2-36 Hz. Figures 44 and 45 show the original signal and its filtered and zoomed state in the 0.2-38 Hz range. As it is understood after the filtering process, the 0.2-35/38 Hz range will give the best results for the signals received from the ECG sensor. For the ECG signal, the signal quality is successful and the filtering result gives the ECG signals closest to the optimal. Also, P, Q, R, S, and T peaks can be easily seen and identified on the signal.

Figure 43

Original ECG Signal and 0.2-36 Hz Band-Pass Filtered Form

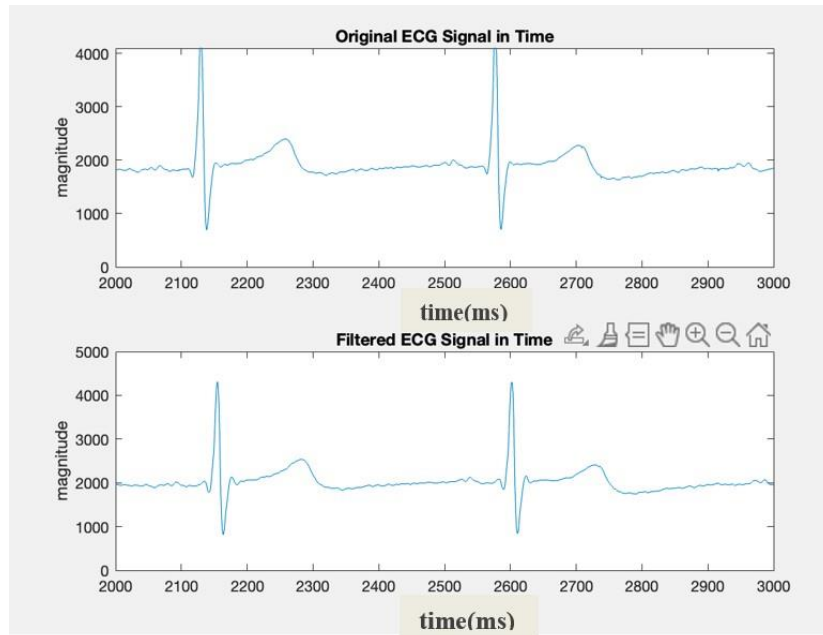


Figure 44

Zoomed in Version of Original ECG Signal and 0.2-36 Hz Band-Pass Filtered Form

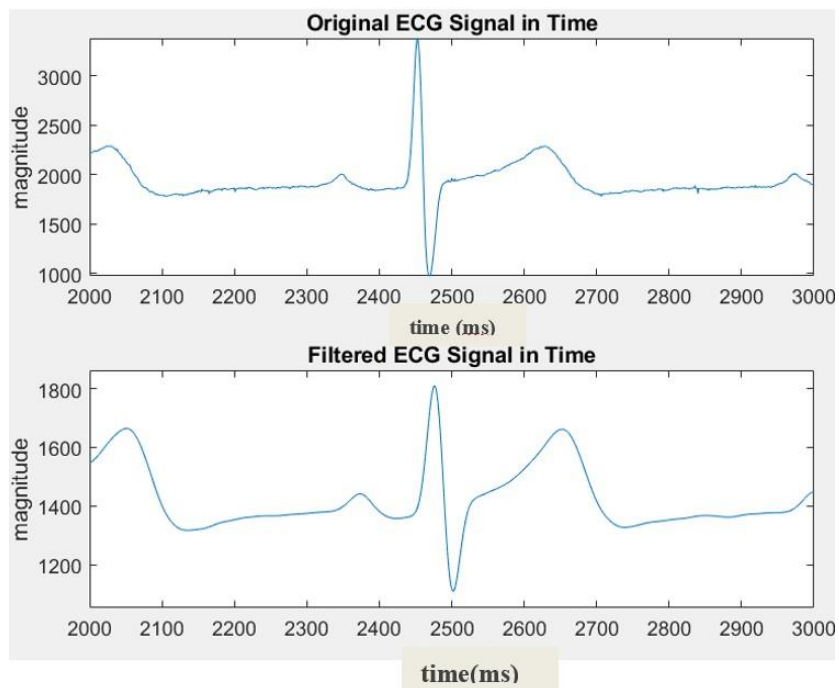
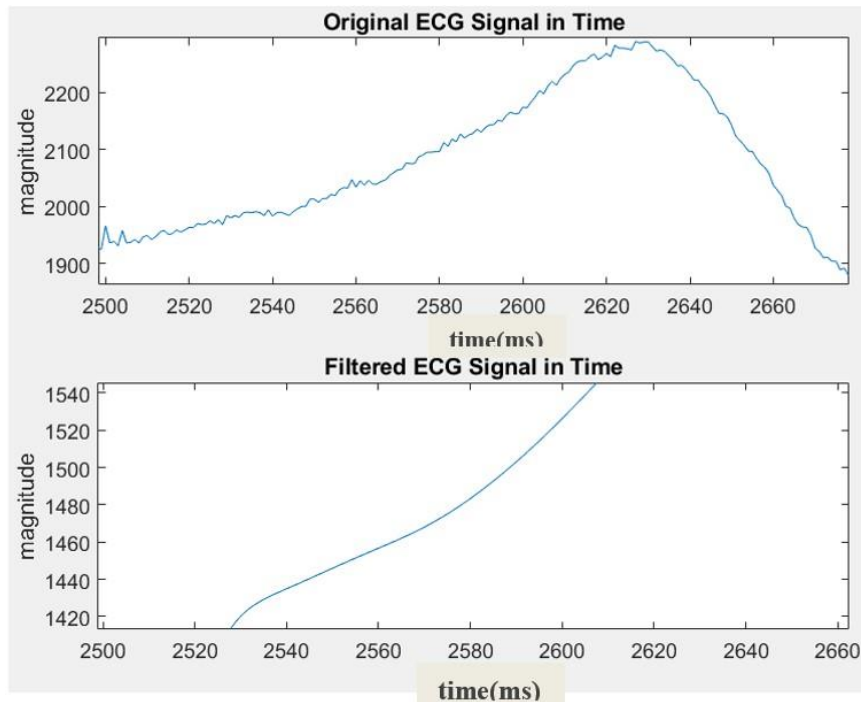


Figure 45

Zoomed in Version of the Original ECG Signal and 0.2-36 Hz Band-Pass Filtered Form



Note. Filter removes DC bias from original ECG signal, reducing apparent Y axis range after filter is applied.

4.3.1.2. PCG Signal Filter. The original PCG data contains some noise and can be expected to have more if the subject is moving or is otherwise active. The heart-focused recording benefits from using a stethoscope, which specifically amplifies heart-related sounds. Other noise can be removed from the signal as much as possible using the filtering process. Figure 46 is the original PCG signal and its filtered version of these signals in the 25-35 Hz range. Figure 47 displays the original signal and filtered in the 10-45 Hz range. Figure 48 illustrates the original signal and filtered in the 20-40 Hz range. As can be understood after the filtering process, the 25-35Hz range will give the best results for the

signals received from the PCG sensor. Although the signal quality for the original PCG signal is not very good, with the filtering result, it is made intelligible. S1 and S2 peaks can be easily seen on the signal, and this plays an important role in our understanding of the “Lub-Dub” phenomenon.

Figure 46

Original PCG Signal and 25-35 Hz Band-Pass Filtered Form

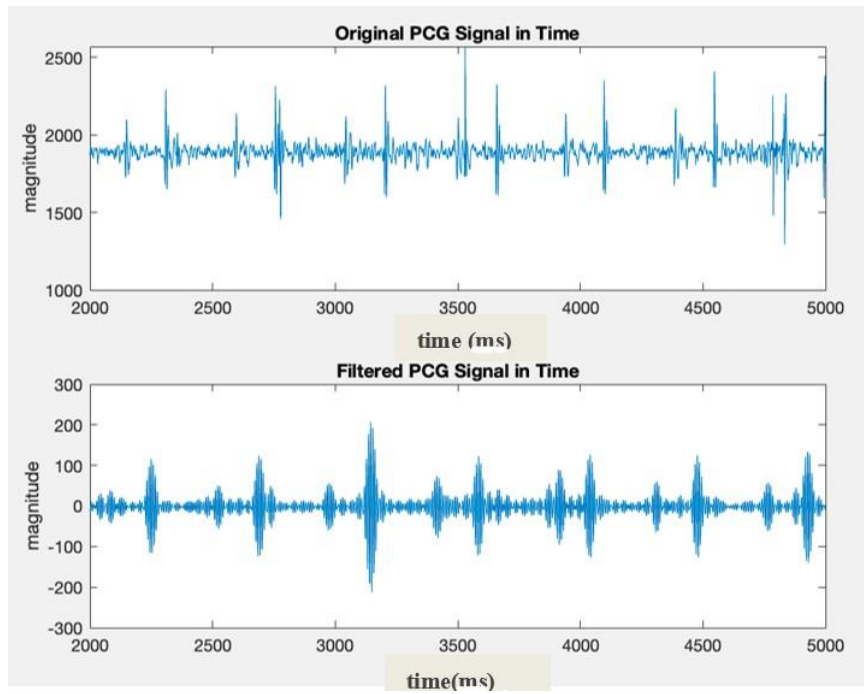


Figure 47

Original PCG Signal and 10-45 Hz Band-Pass Filtered Form

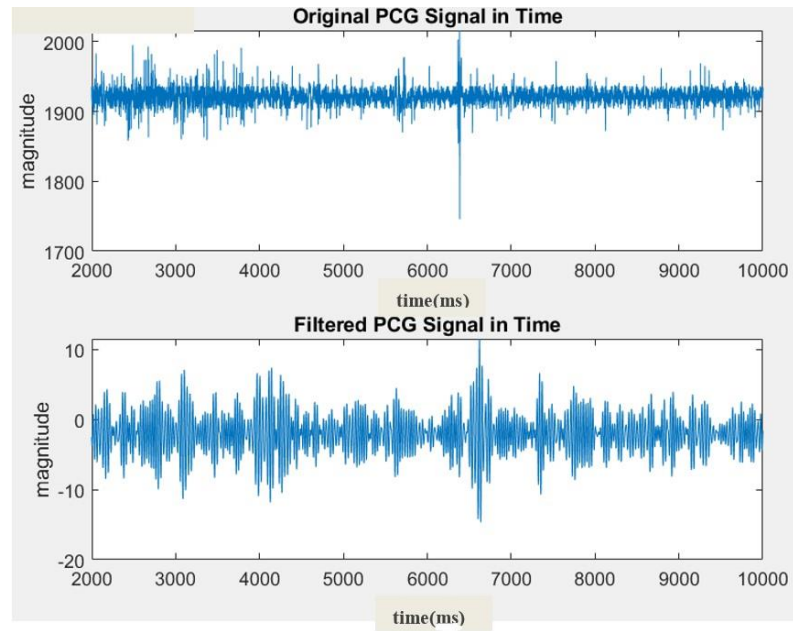
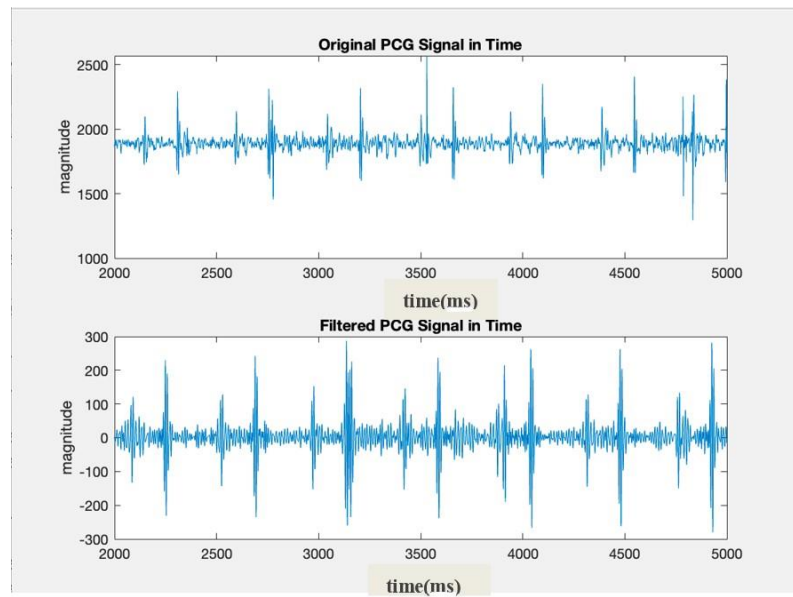


Figure 48

Original PCG Signal and 20-40 Hz Band-Pass Filtered Form



4.3.2 Peak Detection and Heart Rate Calculation using MATLAB

Detection of heart rhythm plays an important role in the detection of important heart diseases such as arrhythmia. Detection of abnormal conditions in heart rhythm can play an important role in early diagnosis [78]. Although there are many ways to detect heart rhythm, the most used method is by taking the R peak of the QRS complex as a reference and measuring the distance between the next R peaks, that distance is also known as the R-R interval. In order to do all these, R peak detection must be carried out successfully and the maximum efficient result must be obtained with the help of an algorithm.

When we look at the stages of the algorithm mathematically, firstly, the signal is put into the denoising process to get rid of the noise. Many methods for the denoising process have been done by researchers before [79, 80]. Some of them are morphological filtering, digital filtering, and decomposition-based denoising methods [81, 82]. If we use the decomposition-based denoising method, which is one of the most effective methods, we can decompose the signal in this way and convert the signal to a series of modes [83]. Then we can remove the noises by setting these modes to 0. Thus, we can detect a lot of noise, identify it, and remove it from the signal. For this, the signal is converted from time domain to frequency domain using FFT.

The R peak must be preserved while other frequencies must be suppressed. For this, the bandpass filtering method that we explained in the previous section is used. By using the wavelet transform method, the signal is transferred to a different frequency band, thus the higher scales (low frequency) and lower scales (high frequency) of the ECG signal are eliminated. Then signal is transferred back into the time domain again. It is aimed to get

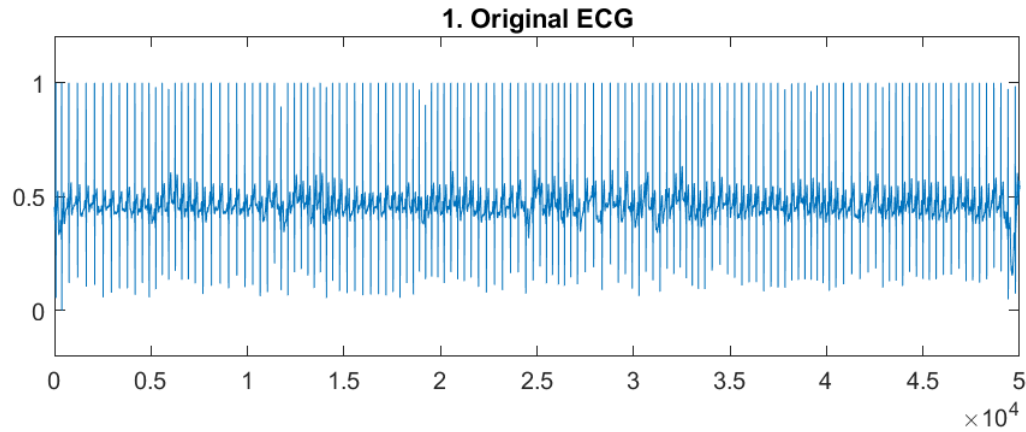
the best result by performing this process once or twice, then finding the local maxima using the windowed filter, and then removing the small values and storing the significant ones. After these steps, the peaks are determined by the program. Since the ECG signal contains many R-R intervals, the optimal distance needs to be calculated to find the average distance between two peaks. For that, this process is repeated once again, and the finality of the result is assured. Then the distance between the first and the last peaks is calculated. Then the distance between these two peaks is divided by the total number of peaks to find the average distance between two neighboring peaks. To calculate the average heart rhythm in one minute, the sampling rate is multiplied by 60 seconds and then divided by the average distance of R-R peaks.

Subject 2 volunteered to collect the data by sitting for 5 minutes without making sudden movements. The originally collected data is shown in Figure 49. The first chart shows all data tabs together. First, this data is purified from signal noise by applying the filtering process as it mentioned above. Figure 50 shows the noise-free version of the total data set. As it is understood at first glance, there is a serious improvement in the total dataset. If we take a closer look at the given data, as shown in Figure 51, the top left side of the figure shows the zoomed-in version of 10000-15000 numbers of samples of the original ECG signal, which is noisy, and the baseline is not stable as well as peaks are up and down. The top right side of the figure shows the zoomed-in filtered version to 10000-15000 numbers of the sample of the ECG signal. As is seen Filtered ECG Signal graph, most of the noise we see in the Original ECG graph has been removed. Figure52 shows the detected R peaks are properly placed on the original ECG signal. As a result of the collected

data of subject 2, his heart rhythm was determined as **82.1** beats per minute (BPM). This is a normal result for a healthy adult.

Figure 49

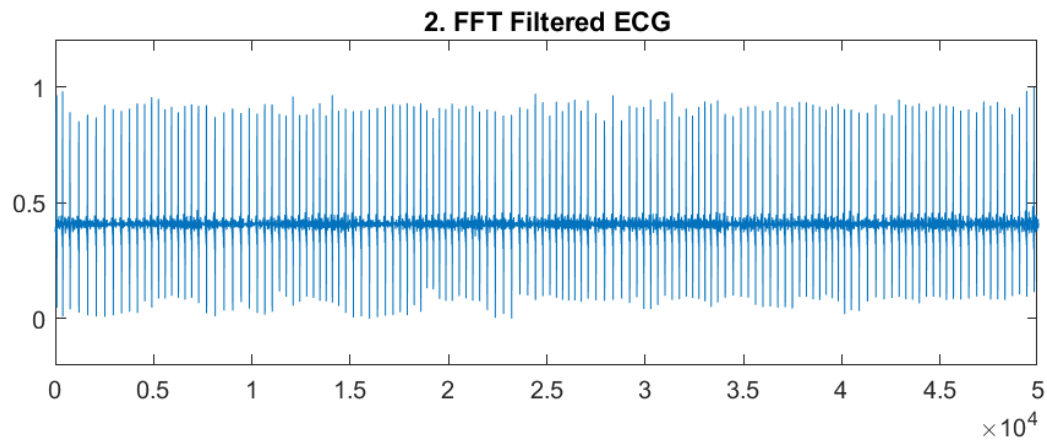
Original ECG Signal Obtained from Subject 2



Note. X axis measured as number of sampled at 500 Hz, Y measured in arbitrary units.

Figure 50

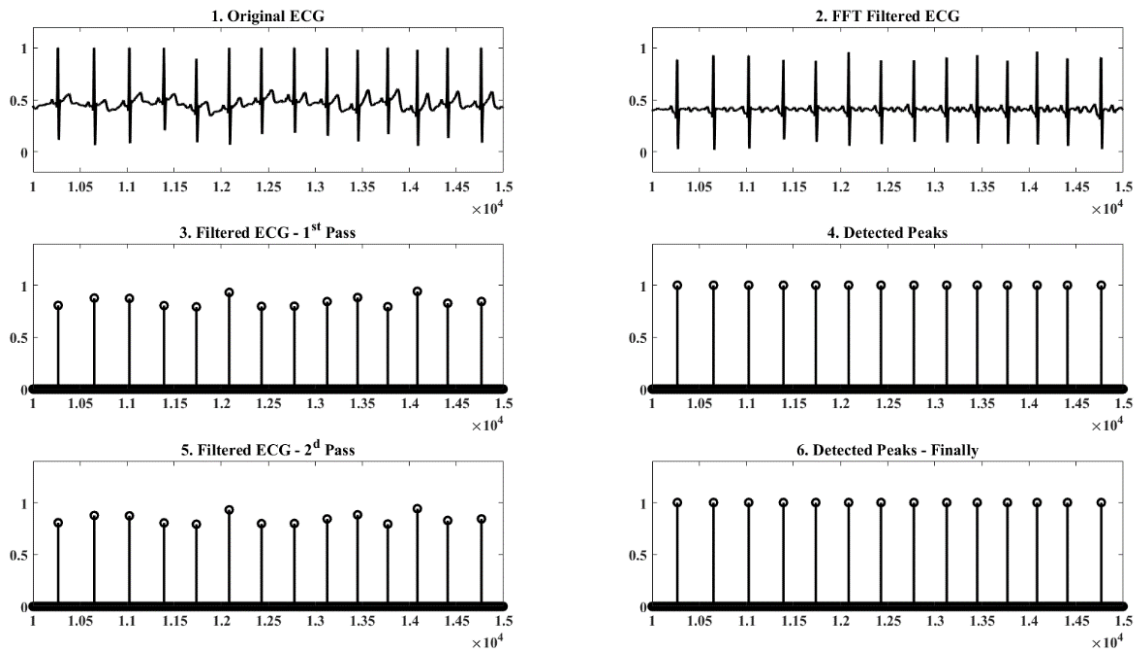
FFT Filtered ECG Signal Obtained from Subject 2



Note. X axis measured as number of sampled at 500 Hz, Y measured in arbitrary units.

Figure 51

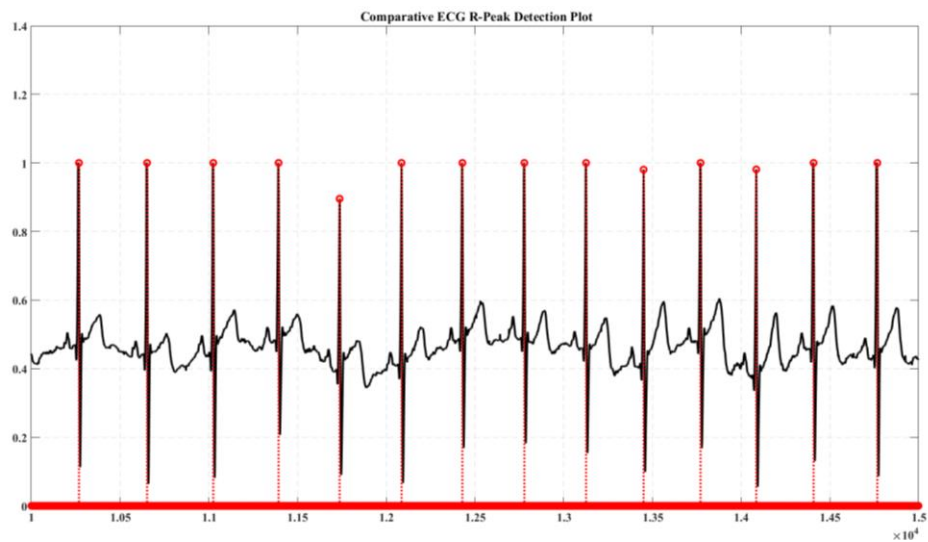
Steps of Detecting R Peaks from the ECG Signal Obtained from Subject 2



Note. X axis measured as number of sampled at 500 Hz, Y measured in arbitrary units.

Figure 52

Detected R Peaks are Placed on the Original ECG Signal Obtained from Subject 2

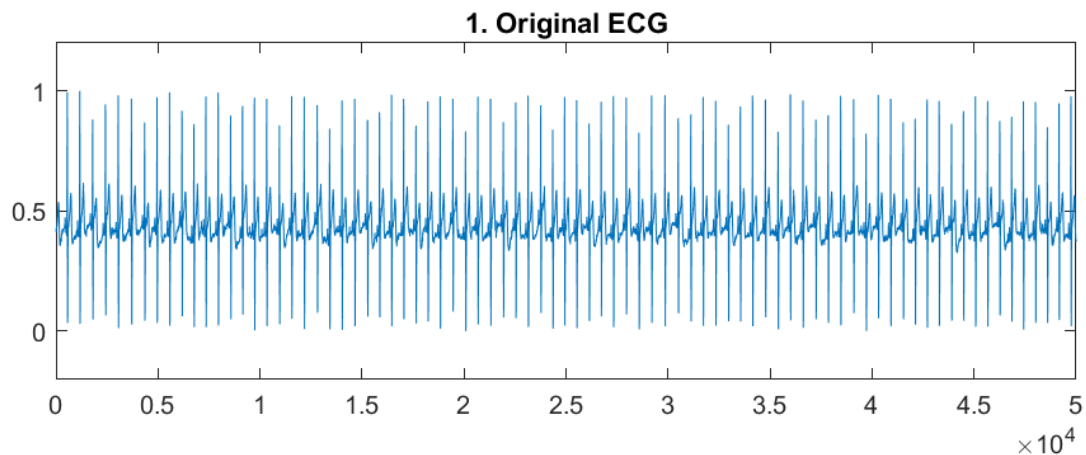


Note. X axis measured as number of sampled at 500 Hz, Y measured in arbitrary units.

We decided to process a recording from another volunteer to ensure that the peak detection and heart rhythm program works accurately. For this reason, subject 1 volunteered to collect data by sitting for 4 minutes without sudden movements. The original data collected from subject 1 is shown in Figure 53. First, this data is purified from noise by applying the bandpass filtering process. Figure 54 shows the filtered version of the total dataset. As it can be understood at first glance, there is a serious improvement in the total dataset. Major noise we see in the Original ECG graph have been cleared as seen in the Filtered ECG signal graph (see Figures 54 and 55). Figure 56 shows that the detected R peaks are properly placed in the original ECG signal. As a result of the data collected from subject 1, his heart rhythm was determined as **75.9** beats per minute (BPM). Similar to the conclusion for subject 1, this is also a normal result for a healthy adult.

Figure 53

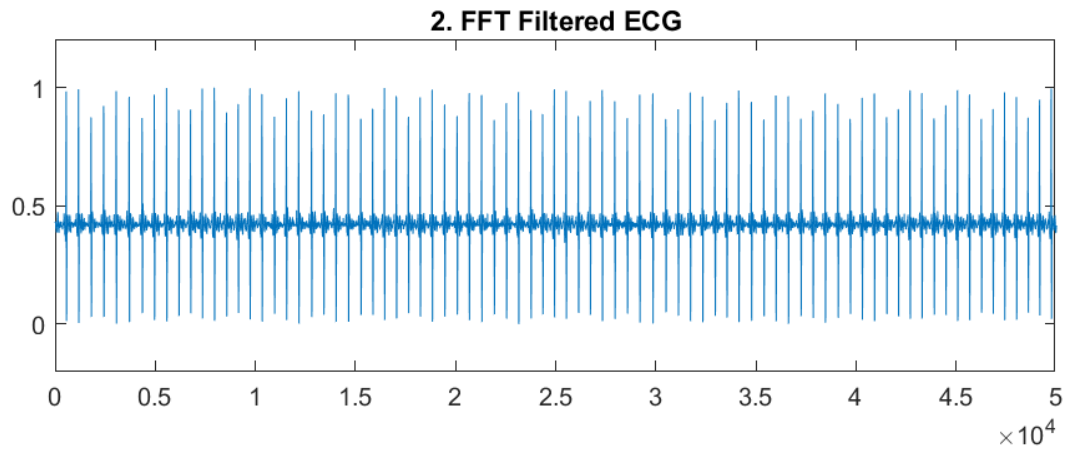
Original ECG Signal Obtained from Subject 1



Note. X axis measured as number of sampled at 760 Hz, Y measured in arbitrary units.

Figure 54

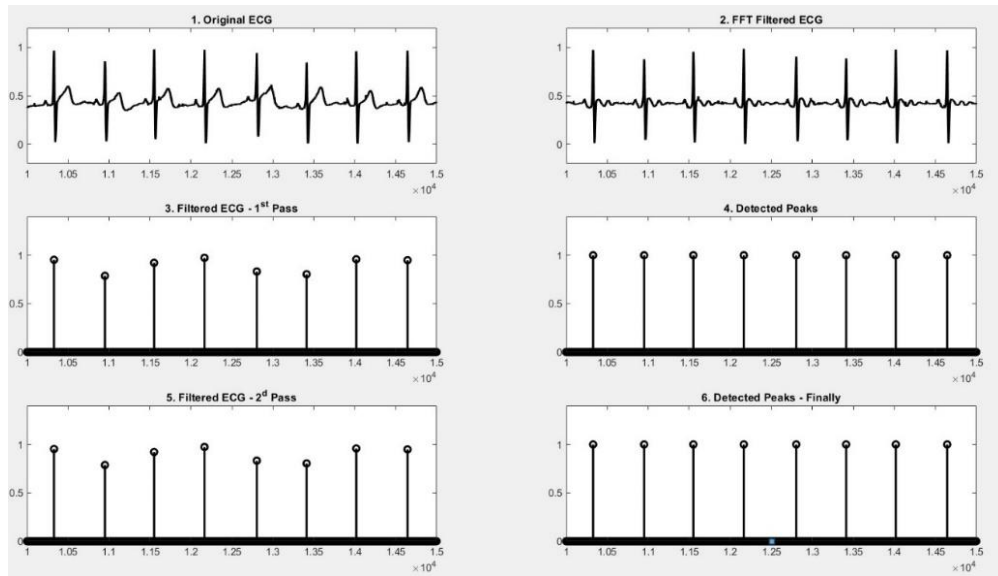
FFT Filtered ECG Signal Obtained from Subject 1



Note. X axis measured as number of sampled at 760 Hz, Y measured in arbitrary units.

Figure 55

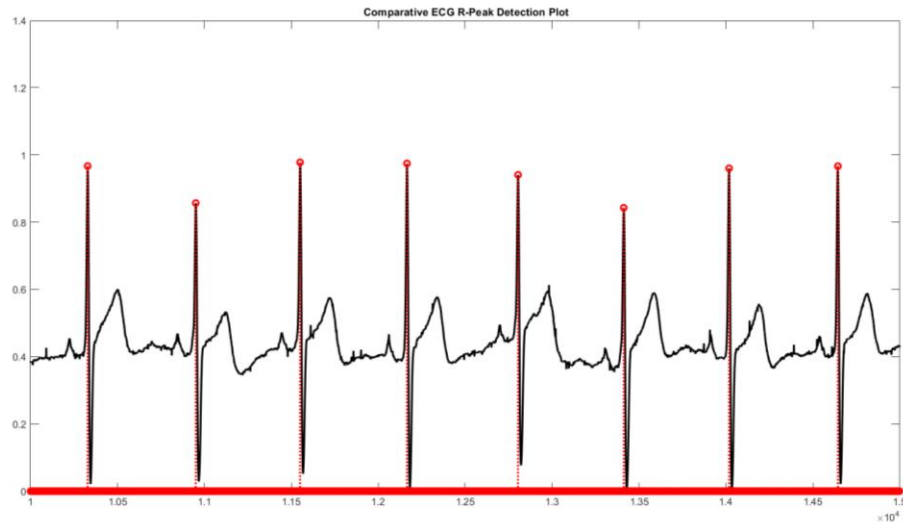
Steps of Detecting R Peaks from the ECG Signal Obtained from Subject 1



Note. X axis measured as number of sampled at 760 Hz, Y measured in arbitrary units.

Figure 56

R Peaks are Properly Placed on the Original ECG Signal Obtained from Subject 1



Note. X axis measured as number of sampled at 760 Hz, Y measured in arbitrary units.

Chapter 5

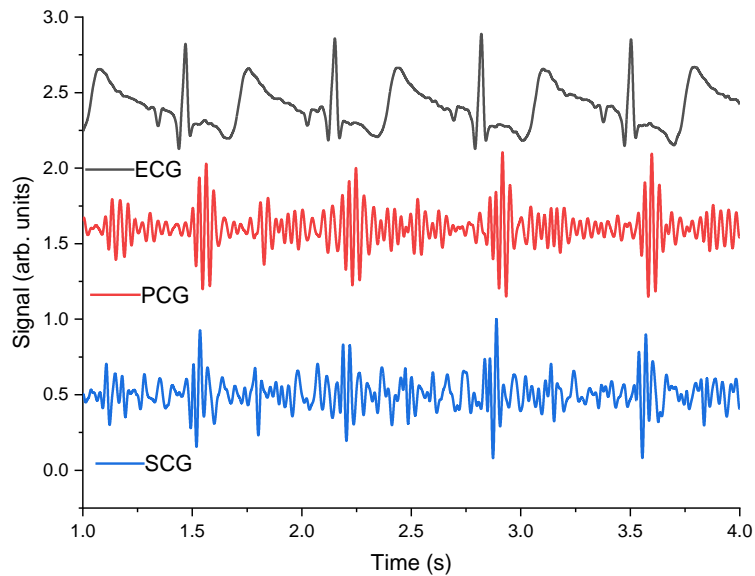
Device Performance and Machine Learning

5.1 Device Performance

Figure 57 shows a representative 3-second-long window of simultaneously recorded, filtered ECG, PCG, and SCG signals acquired with the prototype described in earlier chapters. Filter parameters were set through an initial frequency-domain analysis of raw biophysical signals, which identifies a cutoff for rejecting high-frequency noise, as discussed in the preceding chapter. These real signals reaffirm the correlation among biophysical signals schematically illustrated in Figure 12 and are also representative of those sent to the AI module for diagnostic processing.

Figure 57

Simultaneous ECG, PCG, and SCG Signals were Recorded by the Prototype Heart Health Monitor



Raw, simultaneous, real-time signals recorded using a 500 Hz sampling rate from a healthy individual are presented in the following several figures. Note that no filtering process was used to identify the presented correlation among the signals. Figure 58 shows the ECG signal in 6 seconds (out of 10 minutes) recording from subject 2. The peaks of the ECG signal are so clear that they can be easily identified. Figure 59 demonstrates the PCG signal in 6 seconds (out of 10 minutes) of recording. The S1 and S2 heart sound signals are visible, and they can be easily identified. Figure 60 illustrates the SCG signal in 6 seconds (out of 10 minutes) of recording. Signal quality suffers from low signal-to-noise ratio, which could be improved using a filtering process. Nevertheless, the signal is still useful

in identifying important peaks. When we look at the graphs individually, peaks of the ECG, PCG, and SCG occur at nearly the same times.

Figure 58

Representative 6 Seconds of 10 min Recording of ECG Signal

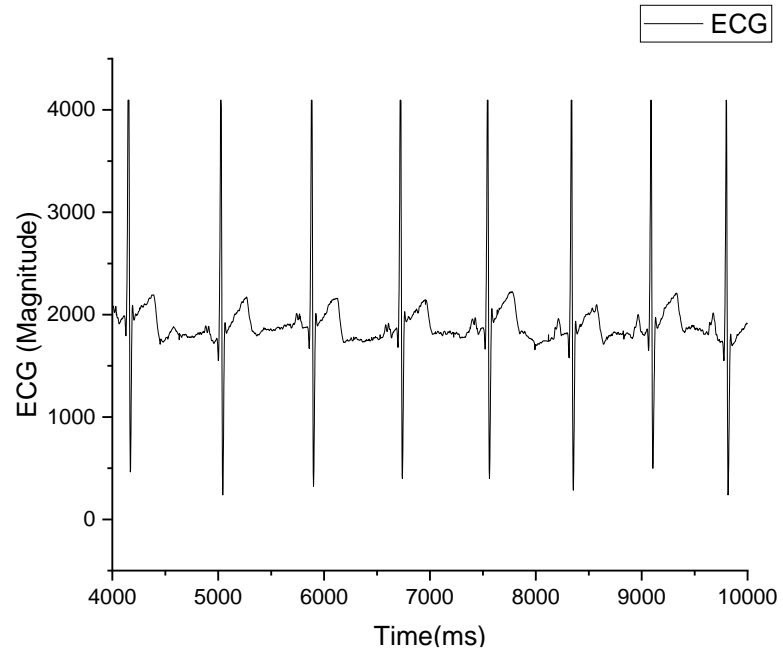


Figure 59

Representative 6 Seconds of 10 min Recording of PCG Signal

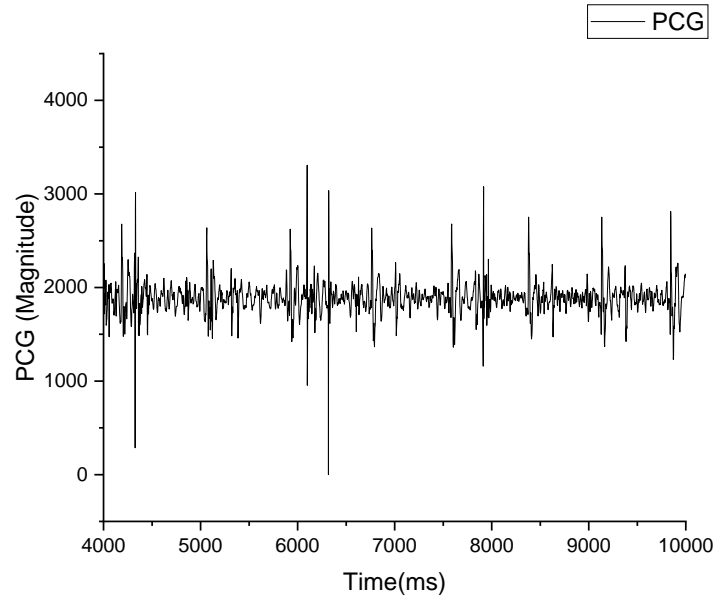
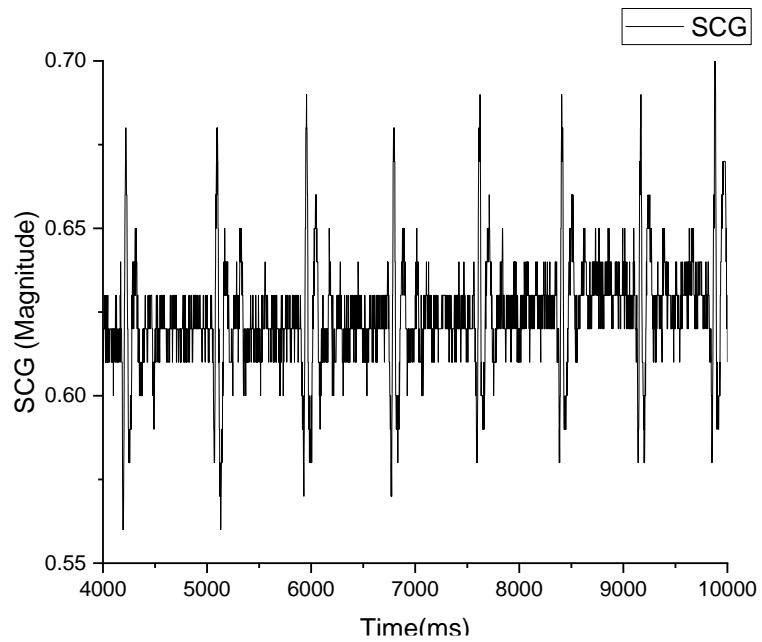


Figure 60

Representative 6 Seconds of 10 min Recording SCG Signal



Taking a closer look at these signals together, such as the ECG and PCG (see Figure 61), it is clear that the R peaks of the ECG signal and S1 peaks of the PCG signal, and the T peak of the ECG signal and S2 of the PCG signal have some correlation. As described earlier, such correlation is expected regarding important cardiac events. As is shown in Figure 62, the ECG and SCG signals also have a meaningful correlation with each other. Peaks of ECG and SCG signals follow each other and this can be used for identifying heartbeats, detecting abnormalities in heartbeats, and more. Last but not least, when we look at these 3 signals together in one graph as shown in Figure 63, we can easily see that ECG, PCG, and SCG have an important relationship. By looking at these three signals at once in real-time, we can identify abnormalities, important cardiac events, heart conditions, and more.

Figure 61

Correlation Between the ECG and PCG Signals

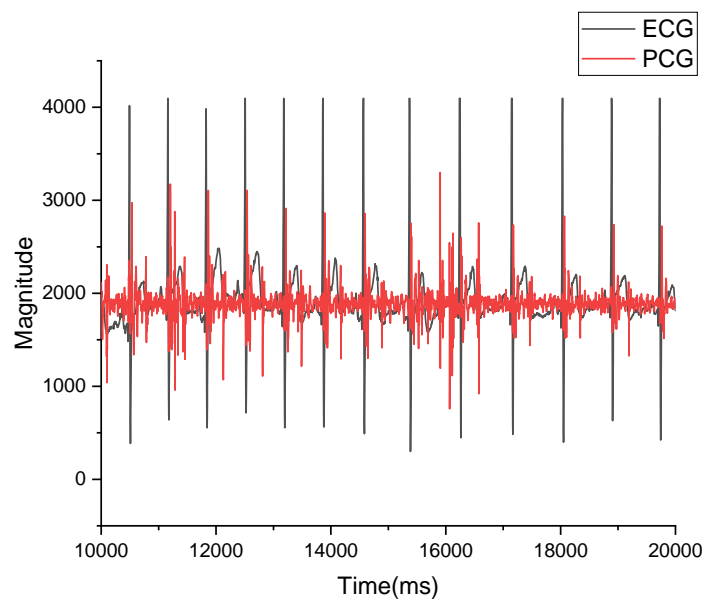


Figure 62

Correlation Between the ECG and SCG Signals

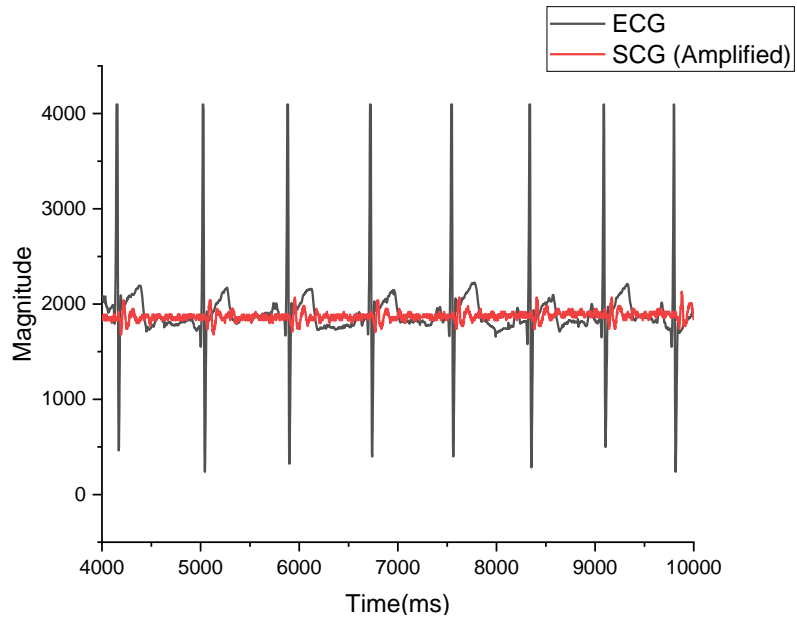
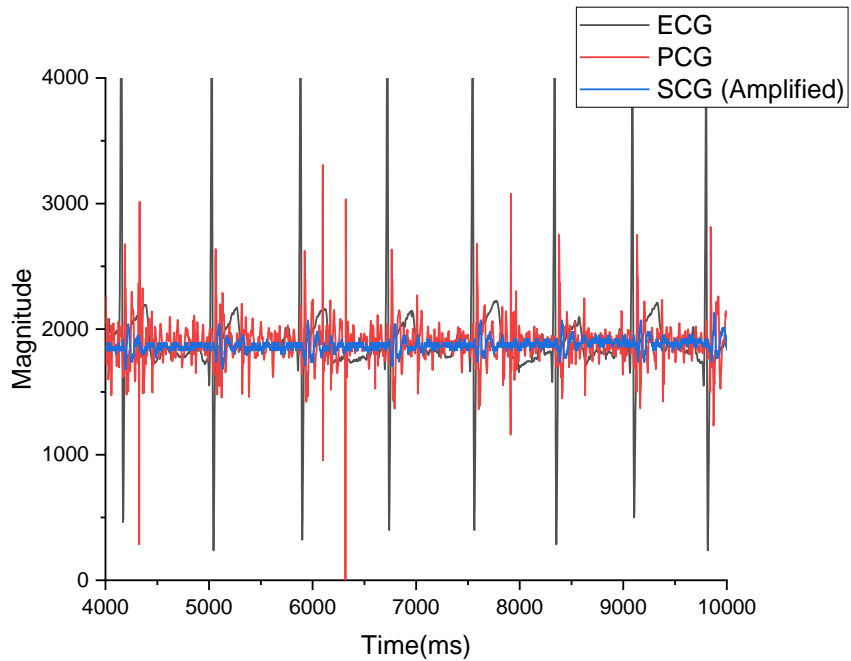


Figure 63

Correlation Between the ECG, PCG, and SCG Signals



5.2 Training LSTM

Our initial effort in using the long short-term memory (LSTM) model developed by collaborators at Washington State University – Vancouver to process the collected signals is focused on ECG data due to the wide availability of labeled ECG datasets in online databases. To train the LSTM model, the MIT BIH Arrhythmia database [84] was used. This contains 48 labeled records of different individuals, with varying ages and medical conditions. Each record includes a 30-minute ECG dataset recorded in two channels at a rate of 360 Hz. In addition, each record includes a list of annotations and their corresponding locations on the ECG. Table 2 shows a summary of the medical conditions annotated in the training dataset, along with the total number of samples for each label.

Table 2

Labels in Training Dataset, from [84]

Label	Description	Total	Label	Description	Total
N	Normal	18686	r	R on T premature ventricular contraction	0
L	Left bundle branch block	2019	F	Fusion of ventricular and normal	202
R	Right bundle branch block	1814	e	Atrial escape	5
B	Bundle branch block	0	j	Nodal escape	58
A	Atrial premature	637	n	Supraventricular escape	0
a	Aberrated atrial premature	39	E	Ventricular escape	28
J	Nodal premature	22	/	Paced	906
S	Supraventricular premature or ectopic	0	f	Fusion of paced and normal	66
V	Premature ventricular contraction	1782	Z	Non-beat or unclassifiable	758

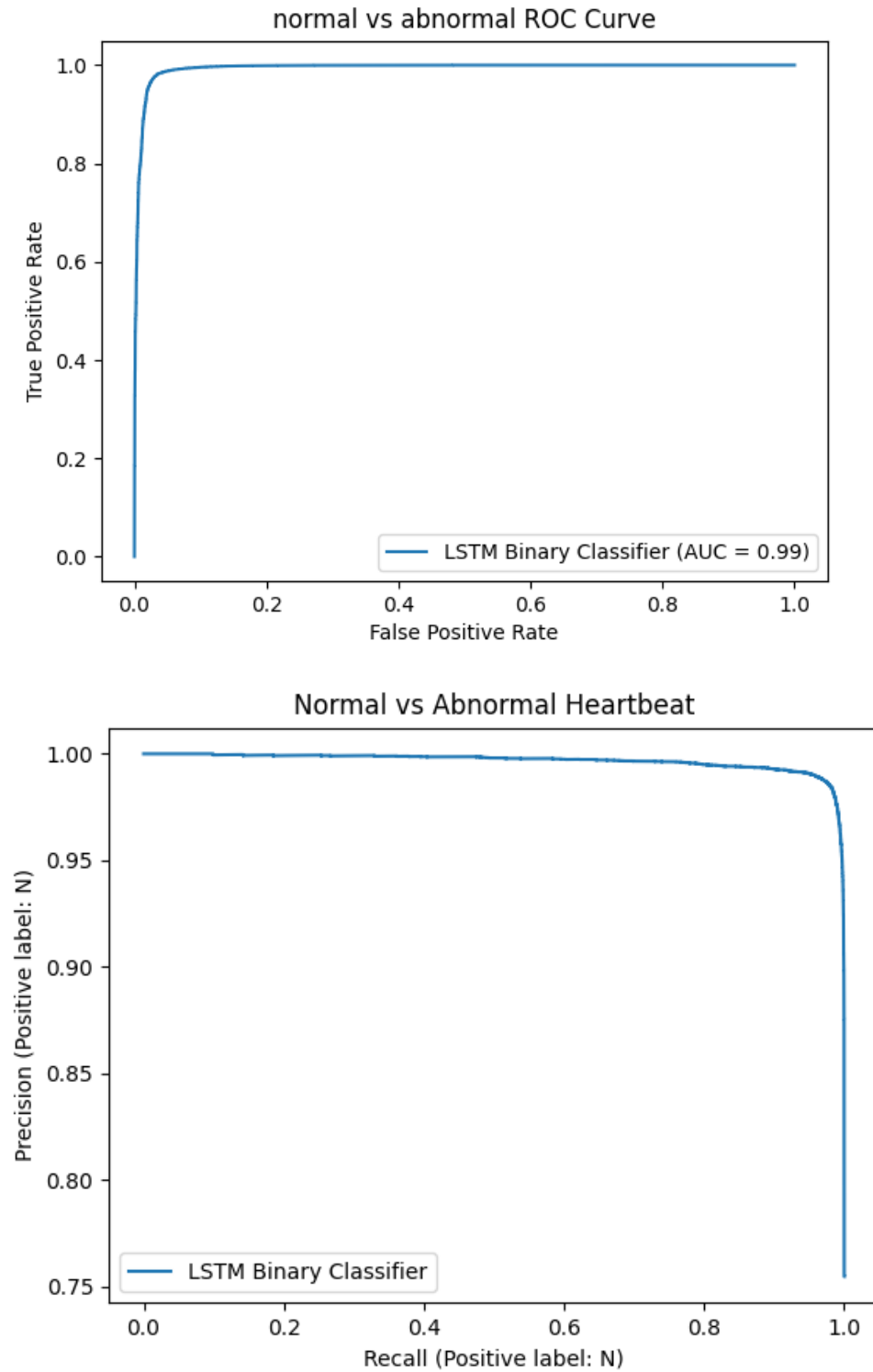
To prepare the dataset for training, the annotated QRS complexes were used to extract individual heartbeats into 1-second-long windows centered on the complex. Each annotated beat window has a 360 entry-long array of ECG millivolt readings. After all of the windows were extracted, they were split into testing and training datasets (25% and 75%, respectively), and also stratified by annotation type to guarantee evenly distributed labels. This type of dataset splitting results in both groups of data having the same distribution of classification types.

The present LSTM model is made up of a layer of 90 Dense nodes, a layer of 45 LSTM nodes, and an output layer of 18 Dense nodes with SoftMax activation to produce a probability matrix for each classification type. The model was trained using a 600 ms window around each annotation, divided into 200 ms before and 400 ms after the annotation location. This results in 216 input features given the MIT BIH Arrhythmia training data frequency of 360 Hz. Each sample was filtered with a 5th order Butterworth bandpass filter [85] with a passband between 0.5 Hz and 40 Hz to reject low-frequency artifacts caused by respiration and high-frequency artifacts caused by electrical noise.

After training the LSTM model for 50 epochs, the MIT BIH testing dataset was used to evaluate its accuracy. Figure 64 shows the receiver operating characteristic curve (area under curve (AUC) = 0.99) and the Precision-Recall plot for the LSTM model in classifying normal (label N) and abnormal (all non-N labels) signals. It has been demonstrated that the Precision-Recall plot is more informative than the ROC curve in evaluating binary classifiers on imbalanced datasets [86]. The results suggest that the LSTM model can classify heartbeats with an accuracy of 97-98%.

Figure 64

ROC Curve and Precision-Recall Curve of The LSTM Model for Classifying Normal and Abnormal Signals



5.3 System Evaluation

To evaluate the entire prototype system, we have tested the whole workflow. This involves signal collection from the human body, signal transmission, data pre-processing, and finally, classification using the trained LSTM model. Specifically, we set the variable system frequency of the prototype to collect signals at 360 Hz from a healthy test subject. This frequency is consistent with the MIT BIH training dataset. The collected data were transmitted to the AI processing module, where the signals were segmented into 1-second windows, each of which was centered by the peak of the QRS. Here, we used a widely adopted QRS detection algorithm to detect the peaks. After pre-processing, these signals were fed into the training LSTM model for classification. The detected conditions and their occurrence counts are shown in Table 3.

Table 3

Detected Conditions on Data Collected by the System

Conditions	N	A	j	Other
Counts	73	2	1	0
Percentage	96.1%	2.6%	1.3%	0%

As shown in the results, among the total 76 QRS complexes, 73 were classified as normal (N), 2 were classified as atrial premature (A), and 1 was classified as a nodal escape (j). No other conditions were detected in the data. While it is currently not possible to verify

these classifications as the data has not been reviewed by a cardiologist, the results appear to be close to what would be expected from a healthy individual.

In addition to the classification accuracy, running performance is also an important metric, especially if the system will be used for real-time detection of abnormal heart conditions. To this end, the AI processing module was evaluated on two types of hardware: a computer using an NVIDIA GTX 1080 GPU, and a Raspberry Pi 4. The average classification time per QRS complex on the computer is 0.010 seconds, while on the Raspberry Pi 4, the average classification time is 0.052 seconds. These results show that the AI Processing module is highly efficient, even when running on a small, portable device such as the Raspberry Pi. Given that a normal heart rate is usually under 180 beats per minute (BPM), the running performance of our system demonstrates great potential for real-time heart monitoring and anomaly detection. For future work, we will develop a multimodal learning algorithm that can learn from multiple data sources, so that the SCG and PCG signals can be leveraged in the learning process.

Chapter 6

Conclusion

6.1 Thesis Summary

The number of deaths from heart disease continues to increase. Heart disease is not only deadly but also extremely expensive to treat. Early diagnosis of heart conditions is very important in order to avoid these consequences. For this reason, many studies have been carried out towards tools and techniques for the early diagnosis of heart diseases. One of the most commonly used methods for the diagnosis of heart conditions is the electrocardiogram. However, since the electrocardiogram only receives electrical signals from the heart, it is not a method that permits detection of all abnormalities that may occur in the heart. Every beat of the heart provides sound and vibration resulting from the initial electrical activity. If these three signals – electrical, acoustic, and vibrational – are monitored simultaneously, there is a chance of catching important findings missed by using ECG alone. This project presents a wearable device that could potentially detect abnormal cardiovascular function by sensing electrical (ECG), acoustic (PCG), and vibrational (SCG) changes in heart performance. The prototype device developed as part of this thesis shows that it can record ECG, PCG, and SCG signals simultaneously.

The first aim of this thesis is to produce a device that can receive ECG, PCG, and SCG signals together. Thus, it was necessary to create a system in which the sensors and microcontrollers would work in harmony. First of all, sensors with which ECG, PCG, and SCG signals can be acquired were determined. Then, an ESP32 microcontroller was selected, which could simultaneously collect the data from these sensors and transfer the

collected data, both wired and wirelessly. After testing the compatibility of sensors and microcontrollers, a PCB was designed to host all these components. In addition, in order to ensure data security and not to lose information in any possible situation, the data was collected using an SD card system. This recorded data is saved to the SD card while also being transmitted wired/wirelessly.

The second purpose of this thesis is to design a stethoscope adapter that will minimize the noise in the PCG signal and to design a housing to effectively contain all the previously described components. The microphone, when used alone, picked up too much noise from the environment, making it difficult to detect some of the important signals from the heart. For this reason, we produced a stethoscope using different materials and different designs. For the final prototype, we printed a stethoscope using an SLA printer with Formlabs elastic 50A resin material. This stethoscope was preferred because it is ergonomic and flexible, significantly reduces the noise coming from the outside, and does not make the user sweat or cause itchiness. After the stethoscope design was provided, a housing design was made to accommodate the whole system and protect it from external impacts. In addition, since the user is expected to wear this system for long-term recordings, soft-bodied 3D prints were made with TPU material, which is a flexible material that will not make the user sweat. Then, a strap system was created that will allow the system to stay on the patient's chest for a long time without discomfort.

The third aim of this thesis was to create a platform where we can monitor the ECG, PCG, and SCG signals simultaneously. For this, we have set up different systems suitable for wired and wireless communication. First, using the LabVIEW platform, a program was for simultaneous monitoring of these three signals and signal processing. Later, a system

was established to enable communication between LabVIEW and the ESP32 board. In this way, there is no need to use intermediate DAQ devices. The data obtained from our device were monitored simultaneously via the LabVIEW platform, either wired or wirelessly. Afterward, an application was designed to enable the tracking of data from smartphones. The application is not suitable for signal processing, but it provides simultaneous wireless tracking of the user's data from the sensors.

The fourth purpose of this thesis is to eliminate the noise in the collected signals. Two different programs were created for the signal filtering process. First of all, the LabVIEW system, where real-time filtering would be performed, was established. By using the FFT feature, the frequency ranges of the primary information content were determined; possible noise in the signal was filtered to boost the signal-to-noise ratio. The LabVIEW platform permitted simultaneous visualization of raw and filtered signals, aiding in filter design. Later, since LabVIEW is, comparatively, not an easy-to-access application, a MATLAB program was created for filtering. As mentioned in Chapter 4, the filtering process was successful. Then, an algorithm and a program that can perform peak detection were developed. This program can detect the R peaks of the ECG signal and calculate the user's heart rate. Data collected from different volunteers were evaluated in the filtering and peak detection programs, and the collected results were successful.

The final purpose of this thesis is to process the collected data through an AI machine learning algorithm to detect abnormalities. For this, we worked with Washington State University and assessed our data in the machine learning algorithm they designed. They compared data acquired by the prototype described in this thesis with an LSTM

model trained using the MIT BIH training dataset. In essence, this demonstrates key aspects of end-to-end functionality of the heart monitor platform as introduced in Figure 16.

6.2 Future Work

More volunteers providing biophysical data to further optimize the prototype device is desirable. The deficiencies in the system can be minimized by processing different data sets collected from more, diverse volunteers who may demonstrate physiological variability or otherwise test the limits of device performance. For this reason, permission from the Rowan Institutional Review Board (IRB) will be required to test the device on an expanded set of different volunteers who are not otherwise associated with this work. With the permission obtained, it is planned for our team to collect 5-minute data sets from male and female volunteers from different age groups in various positions such as sitting, laying down, standing, walking, and running.

Although the data collected by the device for the SCG signal gives data from the heart, it creates problems in long-term recordings because the data suffer from a low signal-to-noise ratio. In order to solve these technical problems, future work should be focused on testing the device for a long time with different sensors and finding the most suitable SCG sensor and filtering combination. Once the quality of the SCG signal is assured, it can be tested in the already-developed peak detection algorithm. ECG and SCG should provide generally correlated heart rhythm results in the short term. Should the correlation drift over longer monitoring periods, the possibility of a problem in the heart within the scope of obtaining different results can be considered.

Real-time filtering is very important. For this reason, to the project should plan on establishing a system that can monitor abnormalities by performing real-time filtering on the phone application or a computer. In this way, the user can see data representations which isolate meaningful signals from the noise. In addition, monitoring algorithms can find problems more easily in noise-free signals, and in this way, can warn the user quickly in case of problems. In addition to the algorithm used only for ECG, it is suggested that similar algorithms for PCG and SCG signals should be developed. For this, we need to collect more data first.

Although the size of the device has already been reduced from its original designs, it would be desirable to further reduce its size to that of a coin. The PCB board developed in this thesis includes an SD card module, ESP32 microcontroller development board, Sen0312 development board, microphone module, and MPU6050 accelerometer development board. The fact is that all these components have separate development boards and they take up a lot of space. In addition, these boards all have unnecessary components that are not used in our application. The size of the device can be reduced to a minimum by designing a system in which only the key components are combined. For this, optimization and miniaturization of the device should be pursued by working with electronics engineers.

References

- [1] C. W. Tsao *et al.*, "Heart Disease and Stroke Statistics—2022 Update: A Report From the American Heart Association," *Circulation*, 2022, doi: 10.1161/CIR.0000000000001052.
- [2] C. D. Fryar, T.-C. Chen, and X. Li, *Prevalence of Uncontrolled Risk Factors for Cardiovascular Disease: United States, 1999-2010* (no. 103). US Department of Health and Human Services, Centers for Disease Control and Prevention, 2012.
- [3] A. S. Prasad and N. Kavanashree, "ECG Monitoring System Using AD8232 Sensor," in *2019 International Conference on Communication and Electronics Systems (ICCES)*, 2019: IEEE.
- [4] A. K. Roy, A. Misal, and G. Sinha, "Classification of Pcg Signals: A Survey," vol. 975, 2014.
- [5] H. Boudoulas, Y. H. Sohn, W. O'neill, R. Brown, and A. M. Weissler, "The QT>QS2 Syndrome: A New Mortality Risk Indicator in Coronary Artery Disease," *The American Journal of Cardiology*, vol. 50, no. 6, 1982.
- [6] J. Moini, *Anatomy and Physiology for Health Professionals*, Third ed. Jones & Bartlett Learning.
- [7] B. J. Aehlert, *ECGs Made Easy*. Elsevier Health Sciences, 2015.
- [8] Wapcaplet. "Diagram of the Human Heart." Wikimedia.
[https://commons.wikimedia.org/wiki/File:Diagram_of_the_human_heart_\(cropped\).svg](https://commons.wikimedia.org/wiki/File:Diagram_of_the_human_heart_(cropped).svg).
- [9] R. Drake, A. W. Vogl, and A. W. Mitchell, *Gray's Anatomy for Students* Elsevier Health Sciences, 2009.
- [10] W. F. Boron and E. L. Boulpaep, *Medical Physiology*. Elsevier Health Sciences, 2016.
- [11] M. Rubart, "Genesis of Cardiac Arrhythmias: Electrophysiological Considerations," *Heart disease: A textbook of cardiovascular medicine*, pp. 659-699, 2001.
- [12] W. Lederer, "Cardiac Electrophysiology and the Electrocardiogram," *Medical physiology*, pp. 504-528, 2017.
- [13] T. Kurian, C. Ambrosi, W. Hucker, V. V. Fedorov, and I. R. Efimov, "Anatomy and Electrophysiology of the Human AV Node," *Pacing and Clinical Electrophysiology*, pp. 754-62, 2010.

- [14] A. Goldberger, *Goldberger's Clinical Electrocardiography*. Elsevier, 2018.
- [15] S. Saksena and A. J. Camm, *Electrophysiological Disorders of the Heart*. Elsevier Health Sciences, 2011.
- [16] A. Davies and A. Scott, *Starting to read ECGs: A Comprehensive Guide to Theory and Practice*. Springer, 2014.
- [17] H. B. Geiter Jr, *EZ ECG Rhythm Interpretation*. FA Davis, 2006.
- [18] B. Surawicz, R. Childers, B. J. Deal, and L. S. Gettes, "AHA/ACCF/HRS Recommendations for the Standardization and Interpretation of the Electrocardiogram," *Circulation*, 2009.
- [19] L. Goldman and A. I. Schafer, *Goldman's Cecil Medicine* Elsevier Health Sciences, 2011.
- [20] E. A. Amsterdam *et al.*, "2014 AHA/ACC Guideline for the Management of Patients With Non-ST-Elevation Acute Coronary Syndromes," *Circulation*, 2014.
- [21] P. M. Rautaharju *et al.*, "AHA/ACCF/HRS recommendations for the standardization and interpretation of the electrocardiogram: part IV: the ST segment, T and U waves, and the QT interval: a scientific statement from the American Heart Association Electrocardiography and Arrhythmias Committee, Council on Clinical Cardiology; the American College of Cardiology Foundation; and the Heart Rhythm Society. Endorsed by the International Society for Computerized Electrocardiology," 2009.
- [22] D. Ewing, D. Borseley, F. Bellavere, and B. Clarke, "Cardiac Autonomic Neuropathy in Diabetes: Comparison of Measures of RR interval Variation," *Diabetologia*, pp. 18-24, 1981.
- [23] K. K. Kim, J. S. Kim, Y. G. Lim, and K. S. Park, "The Effect of Missing RR-Interval Data on Heart Rate Variability Analysis in the Frequency Domain," *Physiological Measurement*, no. 10, p. 1039, 2009.
- [24] J. Brouwer, M. P. Van Den Berg, D. E. Grobbee, J. Haaksma, and A. A. Wilde, "Diagnostic performance of various QTc interval formulas in a large family with long QT syndrome type 3: Bazett's formula not so bad after all...", *Annals of Noninvasive Electrocardiology*, vol. 8, no. 4, pp. 269-274, 2003.
- [25] S. M. Al-Khatib, N. M. A. LaPointe, J. M. Kramer, and R. M. Califf, "What Clinicians Should Know About the QT Interval," *JAMA*, vol. 289, no. 16, pp. 2120-2127, 2003, doi: 10.1001/jama.289.16.2120.
- [26] T. E. o. E. Britannica, "Phonocardiography," *Encyclopedia Britannica*, 11 Feb. 2019.

- [27] R. J. Matthews, *Cardiology*.
- [28] E. F. Gomes and E. Pereira, "Classifying heart sounds using peak location for segmentation and feature construction," in *Workshop Classifying Heart Sounds*, 2012, pp. 480-92.
- [29] A. Raza, A. Mehmood, S. Ullah, M. Ahmad, G. S. Choi, and B.-W. On, "Heartbeat sound signal classification using deep learning," *Sensors*, vol. 19, no. 21, p. 4819, 2019.
- [30] R. F. Rushmer, "Cardiovascular Dynamics," *Academic Medicine*, p. 742, 1961.
- [31] S. McGee, *Evidence-based physical diagnosis e-book*. Elsevier Health Sciences, 2021.
- [32] P. Gupta, "High precision accelerometer contact microphones for detection of mechano-acoustic cardiopulmonary signals," Georgia Institute of Technology, 2020.
- [33] A. Pomerance, "Pathological and clinical study of calcification of the mitral valve ring," (in eng), *J Clin Pathol*, 1970.
- [34] K. Munck, K. Sørensen, J. J. Struijk, and S. E. Schmidt, "Multichannel seismocardiography: an imaging modality for investigating heart vibrations," *Physiological Measurement*, vol. 41, no. 11, p. 115001, 2020.
- [35] P. Mounsey, "Praecordial Ballistocardiography," *Br Heart J*, pp. 259-71, 1957.
- [36] B. S. Bozhenko, "[Seismocardiography--a new method in the study of functional conditions of the heart]," (in rus), *Ter Arkh*, vol. 33, pp. 55-64, Sep 1961.
- [37] J. M. Zanetti and D. M. Salerno, "Seismocardiography: a technique for recording precordial acceleration," in *Computer-Based Medical Systems-Proceedings of the Fourth Annual IEEE Symposium*, 1991: IEEE Computer Society, pp. 4, 5, 6, 7, 8, 9-4, 5, 6, 7, 8, 9.
- [38] M. Di Rienzo *et al.*, "A Wearable System for the Seismocardiogram Assessment in Daily Life Conditions," in *2011 Annual International Conference of the IEEE Engineering in Medicine and Biology Society*, 2011: IEEE, pp. 4263-4266.
- [39] D. M. Salerno *et al.*, "Exercise seismocardiography for detection of coronary artery disease," *American journal of noninvasive cardiology*, vol. 6, pp. 321-330, 1992.
- [40] O. T. Inan *et al.*, "Novel wearable seismocardiography and machine learning algorithms can assess clinical status of heart failure patients," *Circulation: Heart Failure*, vol. 11, no. 1, p. e004313, 2018.

- [41] M. Paukkunen, M. Linnavuo, and R. Sepponen, "A portable measurement system for the superior-inferior axis of the seismocardiogram," *J. Bioeng. Biomed. Sci*, vol. 3, pp. 1-4, 2013.
- [42] C. Glaros and D. I. Fotiadis, "Wearable Devices in Healthcare," in *Intelligent Paradigms for Healthcare Enterprises*, B. G. Silverman, A. Jain, A. Ichalkaranje, and L. C. Jain Eds. Berlin, Heidelberg: Springer Berlin Heidelberg, 2005, pp. 237-264.
- [43] F. Sana, E. M. Isselbacher, J. P. Singh, E. K. Heist, B. Pathik, and A. A. Armoundas, "Wearable Devices for Ambulatory Cardiac Monitoring: JACC State-of-the-Art Review," (in eng), *J Am Coll Cardiol*, vol. 75, no. 13, pp. 1582-1592, Apr 7 2020, doi: 10.1016/j.jacc.2020.01.046.
- [44] Y. Sun *et al.*, "Wearable pulse wave monitoring system based on MEMS sensors," *Micromachines*, vol. 9, no. 2, p. 90, 2018.
- [45] H. Kudo, T. Sawada, E. Kazawa, H. Yoshida, Y. Iwasaki, and K. Mitsubayashi, "A flexible and wearable glucose sensor based on functional polymers with Soft-MEMS techniques," *Biosensors and Bioelectronics*, vol. 22, no. 4, pp. 558-562, 2006.
- [46] A. K. Basu, A. Basu, S. Ghosh, and S. Bhattacharya, "Introduction to MEMS in Biology and Healthcare," 2021.
- [47] I. Sheikh, M. Imadeldin, E. Du, M. A. Leavitt, and A. Waseem, "Advances in healthcare wearable devices," *NPJ Flexible Electronics*, vol. 5, no. 1, 2021.
- [48] B. G. Silverman, L. C. Jain, A. Jain, and A. Ichalkaranje, *Intelligent paradigms for healthcare enterprises: systems thinking*. Springer Science & Business Media, 2005.
- [49] E. K. Chung, *Ambulatory electrocardiography: holter monitor electrocardiography*. Springer Science & Business Media, 2013.
- [50] A. B. Martin, M. Hartman, D. Lassman, A. Catlin, and N. H. E. A. Team, "National Health Care Spending In 2019: Steady Growth For The Fourth Consecutive Year: Study examines national health care spending for 2019," *Health Affairs*, vol. 40, no. 1, pp. 14-24, 2021.
- [51] C. Buttorff, T. Ruder, and M. Bauman, *Multiple Chronic Conditions in the United States*. Santa Monica, CA: RAND Corporation, 2017.
- [52] J. P. DiMarco and J. T. Philbrick, "Use of ambulatory electrocardiographic (Holter) monitoring," *Annals of internal medicine*, vol. 113, no. 1, pp. 53-68, 1990.

- [53] A. Mubarik and A. M. Iqbal, "Holter monitor," in *StatPearls [Internet]*: StatPearls Publishing, 2022.
- [54] H. Ozkan, O. Ozhan, Y. Karadana, M. Gulcu, S. Macit, and F. Husain, "A portable wearable tele-ECG monitoring system," *IEEE Transactions on Instrumentation and Measurement*, vol. 69, no. 1, pp. 173-182, 2019.
- [55] D. Lo Presti, F. Santucci, C. Massaroni, D. Formica, R. Setola, and E. Schena, "A multi-point heart rate monitoring using a soft wearable system based on fiber optic technology," *Scientific reports*, vol. 11, no. 1, pp. 1-10, 2021.
- [56] M. Di Rienzo, G. Rizzo, Z. M. Işıl, and P. Lombardi, "SeisMote: A Multi-Sensor Wireless Platform for Cardiovascular Monitoring in Laboratory, Daily Life, and Telemedicine," (in eng), *Sensors (Basel)*, vol. 20, no. 3, Jan 26 2020, doi: 10.3390/s20030680.
- [57] Y. Cotur, M. Kasimatis, M. Kaisti, S. Olenik, C. Georgiou, and F. Güder, "Stretchable composite acoustic transducer for wearable monitoring of vital signs," *Advanced functional materials*, vol. 30, no. 16, p. 1910288, 2020.
- [58] T. Choudhary, L. Sharma, and M. K. Bhuyan, "Heart Sound Extraction From Sternal Seismocardiographic Signal," *IEEE Signal Processing Letters*, vol. 25, no. 4, 2018.
- [59] E. A. Thomson *et al.*, "Heart rate measures from the Apple Watch, Fitbit Charge HR 2, and electrocardiogram across different exercise intensities," *Journal of sports sciences*, vol. 37, no. 12, pp. 1411-1419, 2019.
- [60] S. Ummadisetty, B. K. Biswal, and S. S. Ray, "A Portable System for Simultaneous Acquisition of ECG and PCG in Real Time," in *2014 International Conference on Power, Control and Embedded Systems (ICPCES)*, 2014: IEEE, pp. 1-4.
- [61] P. K. Jain, A. K. Tiwari, and O. L. Bhagat, "Seismocardiography: An Alternate Method to Estimate Electro-mechanical Window," in *2016 International Conference on Systems in Medicine and Biology (ICSMB)*, 2016: IEEE.
- [62] N. Cameron, "ESP32 microcontroller features," in *Electronics Projects with the ESP8266 and ESP32*: Springer, 2021, pp. 641-682.
- [63] S. H. Ali, A. Akhtar, M. A. Khan, and M. Bilal, "Detection of Parkinson's Tremor in Real Time Using Accelerometers," in *2021 IEEE 7th International Conference on Smart Instrumentation, Measurement and Applications (ICSIMA)*, 2021: IEEE, pp. 5-9.
- [64] M. I. M. Ismail *et al.*, "A review of vibration detection methods using accelerometer sensors for water pipeline leakage," *IEEE access*, vol. 7, pp. 51965-51981, 2019.

- [65] G. Raghu and A. S. Ponraj, "Remote Safety Assistance and Health Monitoring System," *Indian Journal of Science and Technology*, vol. 9, no. 45, pp. 1-6, 2016.
- [66] M. Bravo-Zanoguera, D. Cuevas-González, M. A. Reyna, J. P. García-Vázquez, and R. L. Avitia, "Fabricating a Portable ECG Device Using AD823X Analog Front-End Microchips and Open-Source Development Validation," (in eng), *Sensors (Basel)*, vol. 20, no. 20, Oct 21 2020, doi: 10.3390/s20205962.
- [67] S. Briginets, A. Volkov, G. Martinov, and A. Veselkov, "Development of a mobile heart monitor based on the ECG module AD8232," in *AIP Conference Proceedings*, 2018, vol. 2015, no. 1: AIP Publishing LLC, p. 020014.
- [68] K. Greff, R. K. Srivastava, J. Koutník, B. R. Steunebrink, and J. Schmidhuber, "LSTM: A Search Space Odyssey," *IEEE Transactions on Neural Networks and Learning Systems*, vol. 28, no. 10, 2016.
- [69] T. Petty *et al.*, "Evaluating Deep Learning Algorithms for Real-Time Arrhythmia Detection," in *2020 IEEE/ACM International Conference on Big Data Computing, Applications and Technologies (BDCAT)*, 2020: IEEE.
- [70] H. Ashouri and O. T. Inan, "Automatic Detection of Seismocardiogram Sensor Misplacement for Robust Pre-Ejection Period Estimation in Unsupervised Settings," (in eng), *IEEE Sens J*, vol. 17, no. 12, pp. 3805-3813, Jun 15 2017, doi: 10.1109/jsen.2017.2701349.
- [71] H. Rashid, S. Shekha, S. M. T. Reza, I. U. Ahmed, Q. Newaz, and M. Rasheduzzaman, "A low cost automated fluid control device using smart phone for medical application," in *2017 International Conference on Electrical, Computer and Communication Engineering (ECCE)*, 16-18 Feb. 2017 2017, pp. 809-814, doi: 10.1109/ECACE.2017.7913014.
- [72] E. Agu *et al.*, "The Smartphone as a Medical Device: Assessing Enablers, Benefits and Challenges," in *2013 IEEE International Workshop of Internet-of-Things Networking and Control (IoT-NC)*, 2013, pp. 48-52.
- [73] C. Stamate *et al.*, "The cloudUPDRS app: A medical device for the clinical assessment of Parkinson's Disease," *Pervasive and Mobile Computing*, vol. 43, pp. 146-166, 2018/01/01/ 2018, doi: <https://doi.org/10.1016/j.pmcj.2017.12.005>.
- [74] M. T. Heideman, D. H. Johnson, and C. S. Burrus, "Gauss and the history of the fast Fourier transform," *Archive for history of exact sciences*, pp. 265-277, 1985.
- [75] E. O. Brigham, *The fast Fourier transform and its applications*. Prentice-Hall, Inc., 1988.

- [76] T. Harčarik, J. Bocko, and K. Masláková, "Frequency Analysis of Acoustic Signal using the Fast Fourier Transformation in MATLAB," *Procedia Engineering*, vol. 48, pp. 199-204, 2012/01/01/ 2012, doi: <https://doi.org/10.1016/j.proeng.2012.09.505>.
- [77] C. Van Loan, *Computational frameworks for the fast Fourier transform*. SIAM, 1992.
- [78] M. S. Rahman, C. Choi, Y.-p. Kim, and S. Kim, "A Simple and Robustness Algorithm for ECG R-peak Detection," *Journal of Electrical Engineering and Technology*, vol. 13, no. 5, pp. 2080-2085, 2018.
- [79] G. Ott, E. A. Costa, S. J. Almeida, and M. B. Fonseca, "IIR filter architectures with truncation error feedback for ECG signal processing," *Circuits, Systems, and Signal Processing*, vol. 38, no. 1, pp. 329-355, 2019.
- [80] M. Blanco-Velasco, B. Weng, and K. E. Barner, "ECG signal denoising and baseline wander correction based on the empirical mode decomposition," *Computers in biology and medicine*, vol. 38, no. 1, pp. 1-13, 2008.
- [81] X. Hu, Z. Xiao, and N. Zhang, "Removal of baseline wander from ECG signal based on a statistical weighted moving average filter," *Journal of Zhejiang University SCIENCE C*, vol. 12, no. 5, pp. 397-403, 2011.
- [82] S. K. Salih, S. Aljunid, S. M. Aljunid, and O. Maskon, "Adaptive filtering approach for denoising electrocardiogram signal using moving average filter," *Journal of Medical Imaging and Health Informatics*, vol. 5, no. 5, pp. 1065-1069, 2015.
- [83] P. Lynn, "Online digital filters for biological signals: some fast designs for a small computer," *Medical and Biological Engineering and Computing*, vol. 15, no. 5, pp. 534-540, 1977.
- [84] A. L. Goldberger *et al.*, "PhysioBank, PhysioToolkit, and PhysioNet: components of a new research resource for complex physiologic signals," *Circulation*, vol. 101, no. 23, 2000.
- [85] S. Daud and R. Sudirman, "Butterworth Bandpass and Stationary Wavelet Transform Filter Comparison for Electroencephalography Signal," in *2015 6th International Conference on Intelligent Systems, Modelling and Simulation*, 2015: IEEE.
- [86] T. Saito and M. Rehmsmeier, "The Precision-Recall Plot is More Informative Than the ROC Plot When Evaluating Binary Classifiers on Imbalanced Datasets," *PloS one*, vol. 10, no. 3, 2015.

Appendix A

Arduino Code for ESP32

```
#include "FS.h"

#include "SD.h"

#include <SPI.h>

#define SD_CS 5

#include "BluetoothSerial.h"

#if !defined(CONFIG_BT_ENABLED) ||
    !defined(CONFIG_BLUEDROID_ENABLED)

#error Bluetooth is not enabled! Please run `make menuconfig` to and enable it

#endif

BluetoothSerial SerialBT;

String c;

String a;

String b;

String d;

String k;

String y;

double f;

double g;

String dataMessage;

double myTime;

void setup() {

    Serial.begin(2000000);

    SerialBT.begin("ESP32test"); //Bluetooth device name
```

```

Serial.println("The device started, now you can pair it with bluetooth!");

// Initialize SD card
SD.begin(SD_CS);

if (!SD.begin(SD_CS)) {
    Serial.println("Card Mount Failed");
    return;
}

uint8_t cardType = SD.cardType();

if (cardType == CARD_NONE) {
    Serial.println("No SD card attached");
    return;
}

Serial.println("Initializing SD card...");

if (!SD.begin(SD_CS)) {
    Serial.println("ERROR - SD card initialization failed!");
    return; // init failed
}

File file = SD.open("/data.txt");

if (!file) {
    Serial.println("File doesn't exist");
    Serial.println("Creating file...");
    writeFile(SD, "/data.txt", "ESP32 and SD Card \r\n");
}

else {
    Serial.println("File already exists");
}

```

```

    }
    file.close();
}

void loop() {
    RemoteXY_Handler ();
    mpu6050.update();
    RemoteXY_Handler ();
    RemoteXY.onlineGraph_1 = float (analogRead(35)) ;
    RemoteXY.onlineGraph_2 = float (analogRead(34)) ;
    RemoteXY.onlineGraph_3 = float (mpu6050.getAccZ()) ;
    int a = analogRead(35);
    int b = analogRead(34);
    Serial.print("ecg : ");
    Serial.print(a);
    Serial.print("\tpcg : ");
    Serial.print(b);
    Serial.print("\taccZ : ");
    Serial.println(mpu6050.getAccZ());

    SerialBT.print("ecg : ");
    SerialBT.print(a);
    SerialBT.print("\tpcg : ");
    SerialBT.print(b);
    SerialBT.print("\taccZ : ");
}

```

```

    SerialBT.println(mpu6050.getAccZ());
}

// Write the sensor readings on the SD card

void logSDCard() {
    dataMessage = " Mic= " + String(c) + " " + " ECG = " + String(a) + " SCG = " +
String(g) + "\n";

    Serial.print("Save data: ");

    Serial.println(dataMessage);

    appendFile(SD, "/data.txt", dataMessage.c_str());
}

// Write to the SD card (DON'T MODIFY THIS FUNCTION)

void writeFile(fs::FS &fs, const char * path, const char * message) {

    Serial.printf("Writing file: %s\n", path);

    File file = fs.open(path, FILE_WRITE);

    if (!file) {

        Serial.println("Failed to open file for writing");

        return;

    }

    if (file.print(message)) {

        Serial.println("File written");

    } else {

        Serial.println("Write failed");

    }

    file.close();
}

```

```
// Append data to the SD card (DON'T MODIFY THIS FUNCTION)
void appendFile(fs::FS &fs, const char * path, const char * message) {
    Serial.printf("Appending to file: %s\n", path);
    File file = fs.open(path, FILE_APPEND);
    if (!file) {
        Serial.println("Failed to open file for appending");
        return;
    }
    if (file.print(message)) {
        Serial.println("Message appended");
    } else {
        Serial.println("Append failed");
    }
    file.close();
}
```

Appendix B

MATLAB Code for Filtering

```
% This is to create a figure in matlab of the values recieved from the
% ECG monitor. %
% RUN IN SECTIONS !!! %

%% Importing files into Workspace and renaming
prompt = "What is the file name? \n";
fileName = input(prompt, 's');
prompt = "What is the sheet name? \n";
sheetName = input(prompt, 's');
% If you don't want prompt and just to manually input, us this code:
% fileName = "Data_1";
data = xlsread(fileName, sheetName);
%% Loading data into workable and usable Array (Increase Efficiency)
%time = data(:,1); % Time values are in first column
ECG = data(:,1); % ECG values are in second column

%% Plot the unfiltered Data of ECG Values
figure
plot(ECG); xlim([2000, 5000]);
xlabel("Time"), ylabel("Voltage");
title("ECG Monitor Values");

%% Transform Unfiltered Data into frequency domain
% fft func transforms signals from time to frequency
ECGf = fft(ECG);

%% Plot new frequency domain values
prompt = "What is the sampling frequency? \n";
Fs = input(prompt); % set frequency sampling rate
fECGv = linspace(0,Fs,length(ECG));
% create vector for plotting
% points for each signal value in original ECG data

% Plot ECG values on figure in time and frequency for comparison
figure
subplot(2,1,1)
plot(ECG); xlim([2000, 3000]);
xlabel("Time"), ylabel("Voltage");
title("ECG Monitor Values");

subplot(2,1,2)
plot(fECGv, abs(ECGf)); xlim([0.75, Fs]);
```

```

xlabel("Frequency (Hz)", ylabel("Magnitude");
title("Frequency Graph of ECG Signal");
%% Create Frequency Filter
filterDesigner % Allows creation of frequency filter

%% Create filtered signal
filteredECG = filter(Hd, ECG);

% Transform filter in frequency domain
filtECGf = fft(filteredECG);

%% Compare signals

figure
subplot(2,1,1);
plot(ECG); xlim([2000, 3000]);
title('Original ECG Signal in Time');
xlabel('time (s)'); ylabel('magnitude');

subplot(2,1,2);
plot(filteredECG); xlim([2000,3000]);
title('Filtered ECG Signal in Time');
xlabel('time (s)'); ylabel('magnitude');

%% See difference in frequency domain

figure
subplot(2,1,1);
plot(fECGv, abs(ECGf));
title('Original ECG Signal in Frequency'); xlim([0.75,Fs]);
xlabel('Frequency (Hz)'); ylabel('magnitude');

subplot(2,1,2);
plot(fECGv,abs(filtECGf));
title('Filtered ECG Signal in Frequency'); xlim([0.75, Fs]);
xlabel('Frequency (Hz)'); ylabel('magnitude');

```